TAMPEREEN TEKNILLINEN YLIOPISTO
TAMPERE UNIVERSITY OF TECHNOLOGY

Sanja Pöyry

Computational Modelling of Membranes Rich in Cardiolipin and Sterols

Julkaisu 1110 • Publication 1110

Tampere 2013

Tampereen teknillinen yliopisto. Julkaisu 1110
Tampere University of Technology. Publication 1110

Sanja Pöyry

Computational Modelling of Membranes Rich in Cardiolipin and Sterols

Thesis for the degree of Doctor of Science in Technology to be presented with due permission for public examination and criticism in Sähkötalo Building, Auditorium S1, at Tampere University of Technology, on the 25th of January 2013, at 12 noon.

Tampereen teknillinen yliopisto - Tampere University of Technology
Tampere 2013

Doctoral candidate

Sanja Pöyry, M.Sc
Biological Physics and Soft Matter Group
Department of Physics
Tampere University of Technology

Supervisor

Ilpo Vattulainen, Prof.
Biological Physics and Soft Matter Group
Department of Physics
Tampere University of Technology

Pre-examiners

Maria Sammalkorpi, D.Sc
Department of Chemistry
Aalto University

Himanshu Khandelia, PhD
MEMPHYS, Center for BioMembrane Physics
University of Southern Denmark

Opponent

Ünal Coskun, PhD
Max-Planck Institute of Molecular Cell Biology
and Genetics

ISBN 978-952-15-3006-7 (printed)
ISBN 978-952-15-3011-1 (PDF)
ISSN 1459-2045

ABSTRACT

TAMPERE UNIVERSITY OF TECHNOLOGY
SANJA PÖYRY : Computational modelling of membranes rich in cardiolipin and sterols

This work focuses on the properties of model membranes rich in two lipids: cholesterol and cardiolipin. Despite being structurally very different, the biological significance of both of these lipids is partly related to their ability to promote order in lipid membranes. The studies presented here explore the function of these two lipids in membrane environments by use of atomic-scale molecular dynamics simulations.

The first study concentrates on the properties of cholesterol and related sterols. The question as to whether the structure of cholesterol could be optimized by removing certain methyl groups is tackled by examining the effect of several modified sterols on general lipid bilayer properties. The results indicate an important role for the methyl groups and speak against calling them molecular fossils.

The studies involving cardiolipin comprise three parts. At first, the influence of salt on general properties of cardiolipin-rich membranes is described. The field of research is subsequently broadened to include the interplay of cardiolipin with membrane-associated proteins: a membrane-embedded protein complex and a membrane-attacking antimicrobial peptide.

The results show that cardiolipin amplifies some of the effects that salt has on membranes, particularly through restricting the dynamics of the other lipids' head groups. More generally, the presence of salt seems to mainly affect the dynamic properties of the bilayer, whereas changes in the structural properties are rather small. In the case of the protein embedded in a cardiolipin-rich membrane, three cardiolipin molecules are observed to freely diffuse to locations near the active sites of the protein. Notably, the locations are similar to those seen in crystal structures. When located in these spots, cardiolipin may participate in the proton uptake of the complex. The evidence supports the integral role of cardiolipin in the structure and function of this membrane protein. Finally, in the study involving antimicrobial peptides, the cardiolipin-rich membrane is observed to respond to the peptide attack by increasing membrane curvature. Notably, the bilayer structure is never broken, i.e. no lysis is observed. This may indicate a possible mechanism with which cardiolipin would be able to protect microbial membranes against the attacks of antimicrobial peptides.

In summary, this work provides novel views on the functions of two vital lipids, cholesterol and cardiolipin, with use of atomic-scale molecular dynamics simulations.

ACKNOWLEDGEMENTS

This work has been carried out in the Biological Physics and Soft Matter Group of the Department of Physics at Tampere University of Technology (TUT). FICS graduate school, Vilho, Yrjo and Kalle Väisalä Foundation and Pirkanmaa Regional Fund are acknowledged for funding the thesis work. The computational resources were provided by the HorseShoe supercluster computing facility at the University of Southern Denmark, CSC−IT Centre for Science Ltd (Espoo, Finland), and the Australian National Facility (NCI). Special thanks go to TUT for providing the G-wing coffee room and for TUT, the Finnish Cultural Foundation, and Vilho, Yrjo and Kalle Väisalä Foundation for travel funding.

I wish to thank professor Ilpo Vattulainen for supervising my work, and especially for being always so incredibly positive and encouraging. I am also grateful to all other members of the group for creating a great working atmosphere and for all the valuable discussions and advice. Special extra-thanks go to Tomasz Róg, Samuli Ollila, Timo Vuorela, Anette Hall, Pekka Postila, Oana Cramariuc, Karol Kaszuba, Otto Pulkkinen, Sami Paavilainen, Matti Javanainen, Juha Järvinen, and Hector Martinez-Seara. The work of all co-authors not yet mentioned is greatly appreciated.

The coffee room is surely like an oasis of the G-wing. I wish to thank Matti Viitala, Tapio Rantala, Jouko Nieminen, Matti Lindroos, Eeva Niemi, Mikael Kuisma, Sampo Kulju, and all other people for making it so. Several people at the physics department have been very helpful, thanks especially to Petri Kaukasoina, Ari Laitinen, Jaana Saaristo, and Taina Meriläinen.

I am grateful to professor Alan Mark for the opportunity to work in his group. Thanks also to other people working there, especially Signe Teuber Seger, Moritz Winger, Pramod Nair, Rong Chen and David Poger, for making the visit both fun and highly useful. Thanks also for all friends outside Uni.

The pre-examiners of this thesis, Dr. Himanshu Khandelia and Dr. Maria Sammalkorpi, provided a number of excellent comments that greatly helped with improving this thesis. I thank also Dr. Ünal Coskun for agreeing to be my opponent.

Finally, my deepest gratitude goes to my friends and family, in equal amounts to everyone (plus some extra to Saku).

Tampere, January 2012

Sanja Pöyry

CONTENTS

LIST OF PUBLICATIONS

This thesis consists of the following articles:

I S. Pöyry, T. Róg, M. Karttunen and I. Vattulainen. The significance of cholesterol methyl groups. J. Phys. Chem. B, **112** (10), 2922 -2929, (2008).

II S. Pöyry, T. Róg, M. Karttunen and I. Vattulainen. Mitochondrial membranes with mono- and divalent salt: Changes induced by salt ions on structure and dynamics. J. Phys. Chem. B **113**, 15513-21 (2009).

III S. Pöyry, O. Cramariuc, P. Postila, K. Kaszuba, M. Sarewicz, A. Osyczka, I. Vattulainen and T. Róg. Atomistic simulations indicate cardiolipin to have an integral role in the structure of the cytochrome bc1 complex. Submitted to BBA Bioenergetics (2012).

IV S. Pöyry, A. Mark and I. Vattulainen. Cardiolipin protects charged membranes against the antimicrobial peptide aurein. Submitted to BBA Biomembranes (2012).

The models in articles **I** and **II** were constructed by Tomasz Róg. The simulations, major part of the analysis and paper writing were carried out by the author. The model and simulations in paper **III** were made by Karol Kaszuba and the analysis and writing were done by the author (for the major part), Oana Cramariuc, and Pekka Postila. Finally, in paper **IV** the author carried out all model building, analysis and writing.

LIST OF ABBREVIATIONS

PC	Phosphatidylcholine
PE	Phosphatidylethanolamine
PI	Phosphatidylinositol
CL	Cardiolipin
ATP	Adenosine triphosphate
DNA	Deoxyribonucleic acid
IM	Inner mitochondrial membrane
OM	Outer mitochondrial membrane
MD	Molecular dynamics
NMR	Nuclear magnetic resonance
NpT	Constant number of particles, pressure and temperature
sn	Stereospesific numbering
$\alpha, \beta, \gamma, \phi$	Angle between two vectors
Δt	Timestep
δ_{ij}	Kronecker delta
ϵ_0	Permittivity of vacuum
e	Elementary charge
$\vec{F_i}$	Force acting on particle i
θ_{ijk}	Angle between two consecutive bonds between particles i, j and k
θ^0_{ijk}	Equilibrium angle between two consecutive bonds
k_B	Boltzmann constant
k^b_{ij}	Force constant for bond stretching
k_ϕ	Force constant for dihedrals
k^θ_{ijk}	Force constant of the angle potential between two consecutive bonds
m_i	Mass of particle i
N	Number of particles
p	Pressure
q_i	Charge of particle i
Q	Berendsen pressure coupling strength parameter
r	Distance
$\vec{r}_i$	Position vector of particle i
r_{ij}	Distance between particles i and j

$\vec{r}_{ij}$	Vector from particle i to j
$\sigma_{ij}, \epsilon_{ij}$	Lennard-Jones parameters for particles i and j
t	Time coordinate
τ	Berendren temperature coupling time constant
T	Temperature
T_0	Reference temperature
ϕ_{ijkl}	Dihedral angle describing the rotation of bond $i-j$ around $j-k$ with respect to $k-l$, i.e. it is the angle between planes ijk and jkl, defined by the particles i, j, k and l.
ϕ_s	Equilibrium angle for a dihedral angle
$\mathbf{v}_i$	Velocity of particle i
V	Potential
$V(\mathbf{r}_1, ..., \mathbf{r}_N)$	Potential energy as a function of particle positions r_i, i.e. the force field
V_b	Bond stretching contributions to the potential energy in the force field
V_a	Bond angle contributions to the potential energy in the force field
V_d	Dihedral angle contributions to the potential energy in the force field
V_{C}	Coulomb interaction contributions to the potential energy in the force field
V_{LJ}	Van der Waals contributions to the potential energy in the force field described by the Lennard-Jones potential
x, y, z	Cartesian coordinates
S_{ij}	Order parameter tensor
S_{CD}	Deuterium order parameter tensor
Φ	Electrostatic potential
ρ	Particle density
rdf	Radial distribution function
g_{AB}	Radial distribution function for particle types A and B
ρ_A	Density of particles A
$\langle \rho_A \rangle$	Average density of particles A
C_2	Second rank correlation function
P_2	Second rank Legendre polynomial
$\hat{\mu}$	Unit vector
D_{T}	Lateral tracer diffusion coefficient
MSD	Mean Square Displacement
CM	Center of mass

1. OVERVIEW

Fats are by no means something you should only stay away from. In fact, you would not be able to. All living organisms consist for a large part of fats, which in science are called *lipids*. The central feature of lipids is their ability to form *membranes*, thin sheets that surround cells and divide them into compartments. We are all packed with these structures, indeed in total the membranes in one human being have been estimated to cover an outstanding surface area of around 100 km^2 (1). Furthermore, these structures exhibit a large variety: there are hundreds of differend lipids and consequently the membranes formed by them have different properties. To make the matter even more complex, the lipids work together with proteins, affecting their function and vice versa.

This work focuses on two lipids whose biological significance is partly related to their ability to promote order in lipid membranes: cholesterol and cardiolipin. These two lipids are known to be vital for the proper function of certain biological membranes and thus make up an important research topic. Interestingly, the distribution of both cholesterol and cardiolipin in animal cells is highly uneven but opposite: almost all of the cell's cholesterol is located in the plasma membrane, whereas cardiolipin resides almost exclusively inside cells in organelles called mitochondria.

In this work, the properties of cholesterol and cardiolipin are explored in various settings by using a computational modeling approach called molecular dynamics. Molecular dynamics simulation has proved to be a powerful yet fantastically simple method to examine the properties of biological systems. It can be used both to complement experiments by elucidating the atomic-scale mechanisms underlying some phenomenon and to give predictions for cases not considered through experiments.

The thesis is structured as follows. The necessary biological background information, namely general properties of lipids and more specific details about cholesterol

and cardiolipin and their interactions with other biomolecules, is reviewed in Chapter 1. Chapter 2 describes the used research methods, including the basics of molecular dynamics, analysis methods, and a few words about comparing simulation results with experimental data. Chapters 3–6 introduce and discuss briefly the most interesting results of this work. While Chapter 3 focuses on cholesterol and certain other sterols, Chapters 4–6 describe the results concerning mainly cardiolipin.

Chapter 3, which is based on *Paper I*, addresses the question as to whether the structure of cholesterol could be optimized by removing certain chemical groups from its structure. The question is tackled by examining the effect of several modified sterols on general lipid bilayer properties. Chapter 4, based on *Paper II*, describes the influence of salt on general properties of cardiolipin-rich membranes and particularly the role of cardiolipin in the matter. The interactions of cardiolipin with proteins are described in chapters 5 and 6, based on *Papers III* and *IV*, respectively. More specifically, we observe evidence about cardiolipin's integral role in the function of a respiratory protein complex and a possible mechanism with which cardiolipin may protect membranes against antimicrobial peptides.

2. BACKGROUND

All living matter comprises essentially four different carbon-rich building blocks: *sugars*, *amino acids*, *nucleotides* and *fatty acids* (1), see Fig. 2.1. When combined, sugars and nucleotides form chains called *polysaccharides* and *polynucleotides*, respectively. Polysaccharides have various functions in cell structure and energy storage, whereas polynucleotides serve e.g. as carriers of genetic information. *Proteins*, which are combinations of amino acids, will be discussed briefly. The last group is related to molecules called *lipids*, on whose properties this work focuses.

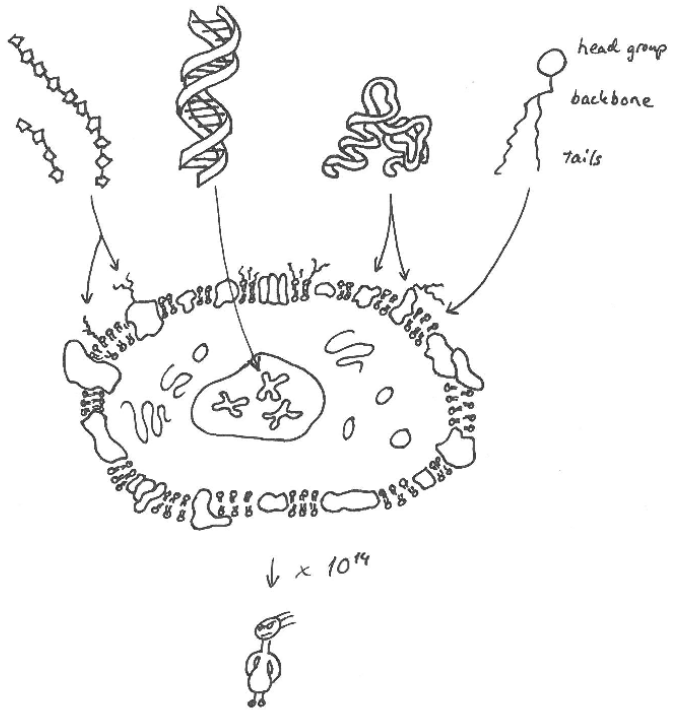

Figure 2.1: The four components of life which form cells (shown in the middle) and finally complex organism (shown on the bottom). On the top row from left to right: polysaccharides (sugar chains), polynucleotides (e.g. DNA), proteins and lipids (fats). The arrows indicate a couple of examples of places where these compounds can be found in cells. It should be noted that the locations indicated are only examples, for example proteins, lipids and sugars are also found inside the cell in great amounts. When roughly 10^{14} cells (1) work in collaboration, they may form a human being (an artist's view).

2.1 Lipids and membranes

Fatty acids and their derivatives, and substances related biosynthetically or functionally to these compounds, are called lipids (according to a definition put forward by W. W. Christie (2)). Lipids are small, amphiphilic molecules with numerous biological functions in connection with energy storage, cell structures and signaling.

All lipids considered in this work belong to glycerolipids and steroids (for structures see Fig. 2.2). The wider lipid family, however, includes a variety of other kinds of structures as well, such as waxes, sphingolipids and eicosanoids. The most important feature of lipid structure, which should be kept in mind when reading the following paragraphs, is the amphiphilicity, meaning that they contain both water-hating and water-loving parts. As clarified later, this gives rise to an intriguing ability for the lipids to self-assemble into various structures (see Fig. 2.1 and 2.3).

All lipids are either derived from or otherwise related to fatty acids. Fatty acids are hydrocarbon chains with a carboxyl group attached to one end. The hydrocarbon chain can either be *saturated*, meaning that there are no double bonds between the carbons, or *unsaturated* with one or several double bonds. To identify a certain fatty acid, we need four pieces of information: the number of carbon atoms and the number, position, and conformation (*cis* or *trans*) of double bonds. The simplest notation, which is also used in this work, is to write the number of carbon atoms followed by the number of double bonds, e.g. 18:2 for linoleic acid (see Fig. 2.2b). Other fatty acids that are linked to the lipids used in this study include palmitic acid (16:0) (Fig. 2.2a) and oleic acid (18:1) (Fig. 2.2d). When being part of a lipid structure, fatty acids are commonly referred to simply as *tails* (see also Fig. 2.1).

Fatty acids can be linked to a *backbone* (glycerol in this work) by ester (or ether) bonds. The sites where they are bound in the glycerol are called sn-1 and sn-2. The third site, sn-3, is attached to a polar *head group*, in membrane lipids most commonly via a phosphate group (3). This work focuses on these so-called *phospholipids* (excluding cholesterol), the most abundant of the membrane lipid types. Attached to the phosphate group is another polar group, in this work either choline (most common head group in most cell membranes (3)), ethanolamine (phosphatidylethanolamine is one component of e.g. the mitochondrial membranes) or

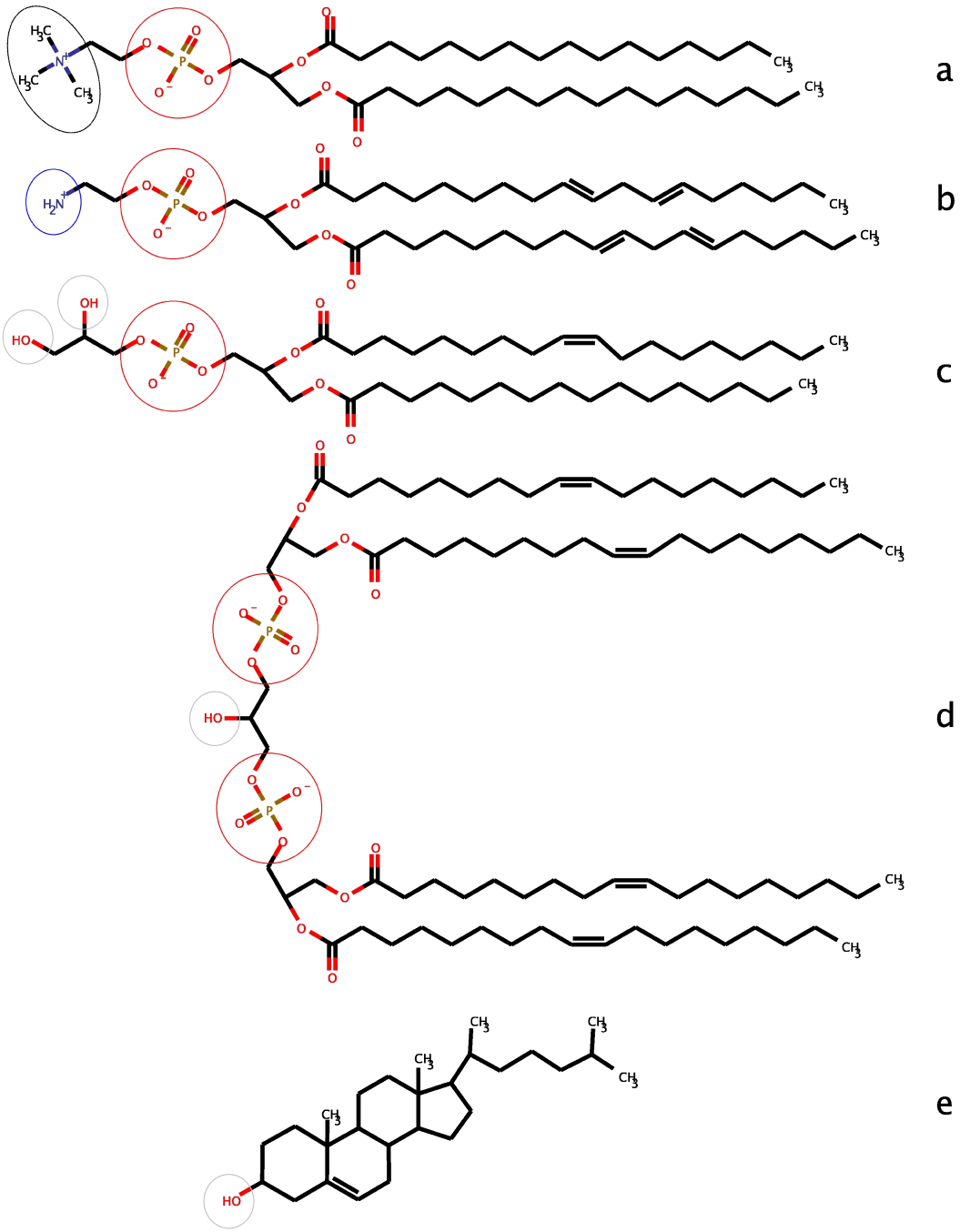

Figure 2.2: The structures of (a) DPPC (dipalmitoylphosphatidylcholine), (b) DLPE (dilauroylphosphatidylethanolamine), (c) POPG (palmitoyloleylphosphatidylglycerol), (d) cardiolipin (tetraoleylcardiolipin), (e) cholesterol. Some important functional groups are circled: choline (black), amine (blue), phosphate groups (red), and hydroxyl groups (gray).

glycerol (phosphatidylglycerol is found, among other places, in bacterial and cancer cell membranes), see Fig. 2.2.

Steroids in turn are based on a structure of four attached carbon rings. The one used in this work, cholesterol, has a small hydroxyl head group and a short carbon chain attached to the opposite ends of the ring system. The ring system and the tail serve as the hydrophobic part of the molecule, see Fig. 2.2e.

2.1.1 Water drives lipids into various structures

The non-polar carbon chains of fatty acids are not able to participate in the hydrogen bonding network of water. Consequently, the nearby water molecules are coerced to partly align around the chains, increasing order and thus decreasing entropy (4). Thus the acyl chains tend to avoid being in touch with water as much as possible, while the polar heads attempt to be hydrated by water (4). Driven by this so-called hydrophobic effect (4), lipids assemble themselves into a variety of structures when immersed in water.

The structures that a certain lipid species tends to form, can, at least to some extent, be predicted based on the effective shape of a single lipid molecule. This basically refers to the compatibility between the head group and the hydrocarbon tail sizes (1). Notably, the effective shape depends also on the surrounding conditions, such as ionic strength. A couple of different basic effective shapes and the corresponding aggregates formed in aqueous environments are shown in Fig. 2.3. As seen from the picture, the cylindrical shape implies a bilayer with zero curvature, whereas a cone-like and an inverted cone shapes correspond to a micelle and inverted hexagonal (H_{II}) phases, respectively. Some other possible structures, such as the hexagonal (H_I) and the cubic phase, are not shown in the picture.

The lamellar bilayer, which will be addressed in more detail in the following section, is of particular interest in this work, indeed, all studies performed during this work are centered on its properties. Furthermore, the inverted hexagonal (H_{II}) structure is important due to the propensity of cardiolipin (CL), one key lipid in this work, to form this kind of structures under certain conditions, and thus crucially affect the properties of cardiolipin-containing membranes.

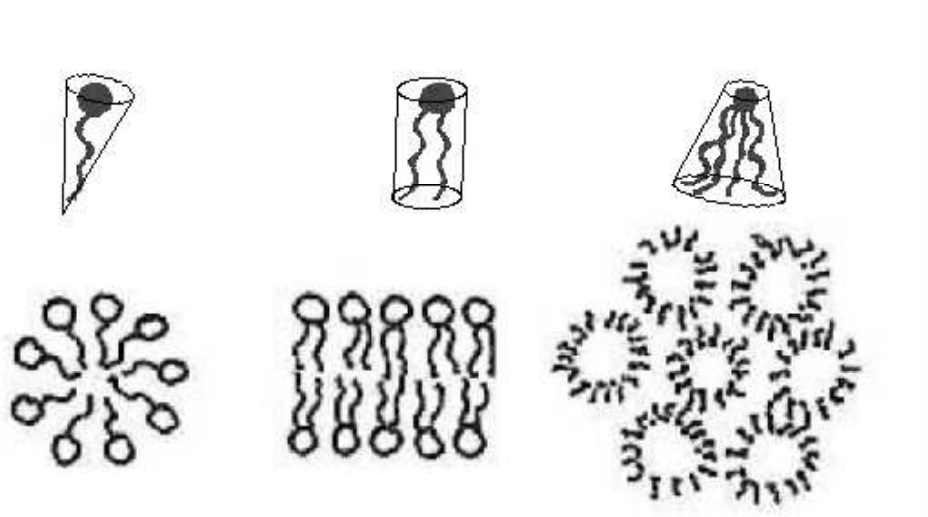

Figure 2.3: Schematic illustrations of some selected lipid effective shapes (the cone, cylinder, and inverted cone sketched on top of the lipids) and the corresponding phases in aqueous environments. From left to right: micelle, lamellar bilayer and inverted hexagonal phases (an artist's view). It should be noted that the surrounding conditions have an effect on the effective shape of the lipid, that is, the same lipid may for different kinds of aggregates in different confitions.

2.1.2 Membranes are more than passive barriers

The most obvious purpose of lipid membranes is to form a barrier between the cell and its surroundings. This particular membrane is called the cell membrane. There are, however, membranes also inside the cells, where they divide the cell into compartments with different functions. Instead of merely being passive barriers, the lipid membranes operate as active interfaces through which the cell interacts with its environment. All material exchange between the cell, its environment and different compartments happens with the assistance of membranes (5). Moreover, membranes provide a site of action for various embedded membrane proteins (see for example the Nobel prize in chemistry 2012 for studies of G-protein-coupled receptors).

When seen from the physics point of view, a model lipid bilayer behaves essentially like a two-dimensional fluid, meaning that the lipid molecules are able to move in the plane of the membrane by diffusion. Moreover, lipids rotate around their long axis and occasionally flip from one monolayer to another in a process called flip-flop (1). Considering the biological functions of a cell, maintaining the proper fluid-like state of its membranes is vital. Besides affecting cell growth, reproduction and

membrane fusion, fluidity also allows the rapid diffusion of membrane-associated proteins, important in cell signaling (5).

Besides changing their morphological state as discussed in the previous section, model lipid membranes can also undergo phase transitions induced by temperature. The different phases are defined by the degree of order present in the system. There are basically two types of order relevant for the model systems studied here, namely positional order (order related to the positions of the lipid molecules) and conformational order (order related to the orientation of the lipid molecules or parts of them). At low temperatures, the model bilayer remains in a *solid ordered* phase. Here *solid* refers to the regular crystalline-like positional order and (*ordered*) refers to a high degree of conformational order of the acyl chains. This phase is commonly referred to as the (*gel phase*). As the temperature increases, the bilayer undergoes the *main phase transition* from the *solid ordered* phase to the *liquid disordered* phase at a transition temperature T_{m} characteristic for a given lipid. T_{m} is generally higher for lipids with longer and saturated acyl chains. In the same manner as above, the *liquid* now refers to low positional order and *disordered* refers to low conformational order. Interestingly, when incorporated into a model bilayer, cholesterol molecules are simultaneously able to both break the positional order of the solid ordered phase and retain the conformational order of the acyl chains, resulting in a phase whose properties lie between the solid ordered and liquid disordered. Hence the new phase is called the *liquid ordered* phase, owing as well to its translational disorder as to the considerable degree of conformational order. Thus, despite allowing a relatively rapid movement of the lipids in the membrane plane, cholesterol induces tighter packing of the tails, thickening the bilayer (1).

2.1.3 Cholesterol has many effects on membrane properties

Real cell membranes consist of numerous different lipids, whose distribution in the membrane plane is not necessarily homogeneous. One particularly vital lipid for the cell membranes is cholesterol (Chol). It was first discovered in 1815 by a French chemist M.E. Chevreul, who extracted it from human gall stones (6). Consequently, he named the molecule cholesterine, chole for bile and stereos for solid (6). In

discovering cholesterol structure, Heinrich Wieland did most of the pioneering work (6).

As other lipids, cholesterol comprises both hydrophobic and hydrophilic parts, see Fig. 2.2e. The hydroxyl group acts as a small hydrophilic head of the molecule. The rest of the molecule, a rigid tetracyclic ring system with an attached 8-carbon chain, is hydrophobic. Notably, the ring system is asymmetric about the ring plane, an important feature for cholesterol function. The 'rough' side (β-face) has two methyl groups 18 and 19 pointing out of the plane, while the 'smooth' α-face has no substituents.

Cholesterol accounts for up to 50 percent of the bilayer lipids, in some cases even more (7). Minor amounts of cholesterol reside in intracellular membranes, a great majority is found in the plasma membrane surrounding the cell (8). Cholesterol modulates the bilayer properties by increasing the ordering of the phospholipid acyl chains. This effect has been observed both experimentally with NMR (see e.g. (9, 10)) as well as with computational methods (see e.g. (11–14)). In line with the increased acyl chain order, X-ray diffraction and osmotic stress studies have indicated condensation of the bilayer in the presence of cholesterol (15). Moreover, cholesterol increases the mechanical strength of the membrane, as observed with laser-induced ultrasonic probes (16). Experimental permeability studies have revealed a decrease in passive permeation through a membrane rich in cholesterol (17). As mentioned earlier, cholesterol is also associated with maintaining the proper fluidity of the bilayer. Cholesterol has been associated with domain formation (so-called *lipid rafts*) and signaling (18). It is also an important metabolite and precursor for bile salts, some vitamins, and adrenal, pituitary and sex (steroid) hormones (5). Both excess cholesterol and lack of properly structured cholesterol can lead to serious conditions. As an example, a rare condition called desmosterolosis occurs when the body is unable to convert desmosterol into cholesterol (19), resulting in hindered development and impaired cognition (20).

Another feature suggesting an important role for cholesterol is the laborious process of synthesizing them. The complicated and energetically expensive biosynthetic pathways require numerous steps (8), beginning with transformation of squalene, a

linear molecule, into a typical steroid ring structure (21). The first sterol intermediate is lanosterol, from which cholesterol is synthesized through almost 20 different intermediate forms (8). There are two optional routes for the pathway according to when the tail's double bond is removed. If this occurs in the last reaction, the immediate precursor of cholesterol will be desmosterol, and the route is called the Bloch pathway according to its discoverer Konrad Bloch (8). Otherwise, in the case of early reduction, the last step is 7-dehydrocholesterol (Kandutsch-Russell pathway) (8).

Prokaryotes, such as archaebacteria and eubacteria, do not generally require cholesterol (22). These species evolved at a time when molecular oxygen, which is required for the cyclization of squalene, was practically absent. Once the oxygen concentration in the atmosphere increased to a sufficient level, also the eukaryotic diversity began to emerge. Simultaneously, the synthesis of cholesterol became possible and indeed all eukaryotic species require cholesterol. Thus, cholesterol and related sterols have been suggested to have had a crucial role in the proliferation of eukaryotic life (1). Once feasible, the evolution of cholesterol from lanosterol was driven by improvements in the sterol's functions. Compared to lanosterol, cholesterol is more effective in restricting the leakage of glucose from phosphatidylcholine vesicles (23), whose microviscosities were also higher. These and other factors led Bloch to conclude that cholesterol seemed to function most effectively, lanosterol least effectively and the intermediate, only partly demethylated steps lie somewhere in between (23). In other words, the evolutionary process can be seen as an optimization of cholesterol's effects on certain physical properties of membranes by removal of its excess methyl groups from the α-face, 'smoothening' the structure (22, 24, 25). Indeed, both experimental and computational studies show decreased interactions between sterol molecules and acyl chains when methyl groups are present. Consequently, near the smooth α-face acyl chains ordering is higher (26) and packing of chain atoms more tight (27) compared to the rough β-face. The smooth structure of cholesterol may also explain why its ordering effects on lipid hydrocarbon chains are most pronounced in saturated lipid bilayers (13). In membranes comprised of unsaturated lipids, the effects of cholesterol are considerably weaker and similar to

the effects of other sterols (13).

2.1.4 Cardiolipin is a double lipid

Like cholesterol, cardiolipin (CL) also promotes order in the lipid membranes. These two lipids do, however, have quite a different structure and generally do not reside in the same membrane environments. While usually located in membranes which have coupled electron transport and phosphorylation, namely bacterial plasma membranes, chromatophores, chloroplasts and mitochondria (28), CL has also been found in e.g. plasma lipoproteins (29). Inside mitochondria, CL is primarily localized in the inner leaflet of the inner membrane (30). Considering its prevalence in mitochondria and various different eubacteria, it seems likely that CL occurred already in the rather early stages of evolution (30).

CL is a unique 'double-lipid' with a total of four acyl chains, whereas phospholipids normally only have two, see Fig. 2.2. The central glycerol group connects the two negatively charged phosphatidyl moieties, giving the lipid a double anionic charge. Notably, compared to the otherwise bulky structure, CL only has a tiny hydroxyl head group attached to the central glycerol. The relatively rigid dimeric structure combined with the small head group has indeed been suggested to be the defining feature in CL function. It may largely explain the physical characteristics of CL bilayers, including the sensitivity to interactions with the buffer, formation of nonlamellar phases, and enhanced structural integrity (31), as explained in more detail below.

The rigid structure of CL has been suggested to impair the headgroup's capability to participate in the intra- and intermolecular interactions with other phosphate groups, diminishing the shielding of the two negative charges (31). Consequently, the phosphate groups would become more susceptible to interactions with the surrounding solution (31). Together with the geometry of the CL molecule, this feature presumably induces greater cohesion in the interfacial region of CL membranes, resulting in greater structural integrity of the bilayer (31). Generally speaking, these properties imply that the presence of CL might stabilize the membrane and enhance its barrier properties (30). This would be vital e.g. for the proper function of cell res-

piration, which requires maintaining a proton gradient across a CL-rich membrane, or for organisms under the attack of antimicrobial peptides or some other adverse conditions. Indeed, there is some evidence of CL-rich membranes being resistant to some antimicrobial peptides and of some organisms increasing the CL content of their membranes in case of resource depletion and halophilic stress (31).

Another intriguing feature arising from CL's structure is its ability to form inverted hexagonal phases when neutralized by divalent cations, such as Ca^{2+} and Mg^{2+} (28). This is thought to be relevant e.g. for their participation in the formation of contact sites between mitochondrial membranes (30). Moreover, it has been shown that in bacteria CL microdomains gather to regions of high negative curvature (32).

A multitude of mitochondrial proteins have been shown to interact with CL (30). In fact, CL appears to be a prerequisite for the proper function of several pivotal proteins, such as some carriers and respiratory chain complexes, one of which will be discussed later in greater detail. There is also evidence indicating that CL has a key role in the higher order organization of the components of the respiratory chain, literally gluing the chain together (33). CLs operate either at the interface between a protein and its surroundings or between the subunits within a complex, possibly inducing conformational changes affecting the protein's activity (30). Some proteins necessitate a definite number of CL molecules associated with them, often bound to specific binding sites in the quaternary structure. Moreover, the association is often so strong that the dissociation of CL from the protein requires denaturing conditions and leads to disintegration (30). In addition to the effects on protein structure, CLs have been suggested to act as source of protons for the respiratory complexes (34). The acidic headgroups of CL are also able to carry out intramembrane proton transfer, possibly contributing to the direct coupling between the respiratory chain and the ATP synthase (30).

The above observations have led various studies to propose that CL is vital for mitochondrial bioenergetics (30). Presumably, however, CL is not absolutely indispensable for the mitochondrial activity, but rather optimizes oxidative phosphorylation and increases tolerance against adverse conditions. To some extent, CL can be

substituted by other phospholipids, such as phosphatidylglycerol, while preserving mitochondrial function (30).

2.1.5 Ions modulate membrane properties

By associating with membrane lipids, ions contribute to several essential activities, such as membrane fusion, phase transitions and transport across membranes (35). Moreover, great amounts of energy can be stored by establishing ion gradients across lipid membranes and subsequently utilized by the cell for usefull work (5, 36).

The proximity of ions greatly affects the physical properties of bilayers, altering among others the electrostatics and fluidity of the membrane (37). NaCl and $CaCl_2$ have been experimentally shown to increase the order within a lipid bilayer, subsequently decreasing the membrane elasticity and altering the main phase transition temperature (38). The effect was observed mainly with high salt concentrations and was more noticeable in the presence of Ca^{2+}. Simulations have produced similar results, as NaCl appears to increase the order parameter (35, 39, 40), thus shrinking the area per lipid (35, 40–42) and increasing the bilayer thickness (35). A simulation study indicated possible spatial restrictions on the carbonyl oxygens and water (39), imposed by Na^+ ions interacting with the lipids. Sodium ions have been also suggested to assemble lipids to form small complexes with limited mobility (35). In addition to the intrabilayer modifications, the interactions between neighboring bilayers are also affected. The effect has been demonstrated by multilamellar vesicle swelling in salt solution, driven principally by the attenuation of the van der Waals interactions and observed with X-ray diffraction (43).

Lipid headgroups are naturally most affected by the presence of ions. Although the ion is stripped of its surrounding water molecules upon binding (39), the hydration of the headgroups remains rather stable (40). Salts are, however, able to crucially change the conformations and dynamics of the dipolar phosphatidylcholine (PC) headgroups, as seen in studies utilizing NMR (44–47), neutron diffraction (45), osmotic stress and X-ray diffraction (48), fluorescent dyes (49) and simulations (50). The adjacency of ions has a marked but local influence on the headgroup tilt, although the global average tilt remains roughly unaffected (50, 51). Lipid dipole

reorientation and altered polarization of the water molecules generally counterbalance the effects on the electrostatic potential (35). The headgroup dipole has been suggested to act like a voltmeter, the tilt following the changes in the electrostatic potential (52, 53).

2.2 Membrane-associated proteins

Proteins are essential building blocks of cell structures, indeed, they constitute most of the cell's dry mass (3). Moreover, proteins have countless numbers of other functions such as promoting chemical reactions, controlling transport across membranes, signaling and acting as molecular motors.

Short amino acid chains are called *peptides* and longer ones are called proteins. The chain folds into a three-dimensional shape, dictated by noncovalent interactions. These folded chains can further join together to form larger complexes.

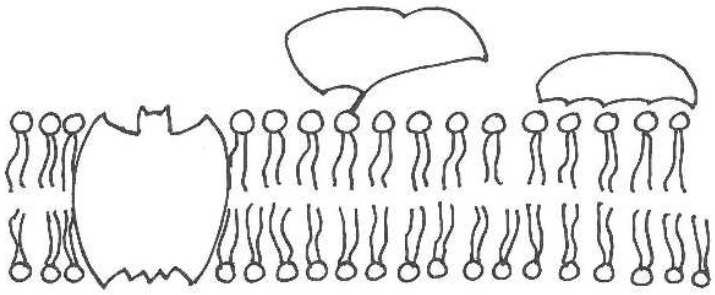

Figure 2.4: Examples of the three types of membrane proteins (from left to right): an integral membrane protein, a lipid-anchored protein and a peripheral protein (an artist's view).

2.2.1 Membrane proteins are anchored into lipid bilayers

Lipid membranes typically contain a number of attached proteins that act for example as receptors, channels and pumps. In fact, biological membranes are virtually crowded mixes of proteins and lipids (54). The proteins can either be temporarily associated with the membrane (peripheral proteins), anchored straight to the lipids or embedded into the membrane (integral membrane proteins), see Fig. 2.4.

Notably, the surrounding lipids not only provide a passive medium for the embedded proteins, but also seem to affect their structure and function, and vice versa. There are large amounts of evidence supporting the importance of lipid-protein interactions, however, many questions remain unanswered, see for example (54–57). The research on this topic is hindered for example by the limited number of available membrane protein structures. Indeed, only 2 % of the known high-resolution protein structures are those of membrane proteins, while the share of all genes encoding membrane proteins is approximately 20–30 % (58, 59).

Perhaps most obviously, the surrounding lipids may influence the organization of membrane proteins: the stability of their structures, folding and assembly (56, 57). Moreover, the lateral distribution of the proteins in the plane of the membrane may depend on the non-homogeneous distribution of lipids. On one hand, the properties of the bilayer surface (e.g. surface charge) affect the binding of proteins from the surrounding solvent (57). On the other hand, both lipids and the membrane-embedded proteins are able to diffuse in the plane of the membrane. This may result in either lipids diffusing to the vicinity of proteins they prefer or proteins diffusing to favourable lipid environments, or both. Either way, the idea is that proteins may this way end up in microdomains (*lipid rafts*) (18), that are enriched in certain lipid species that the protein prefers to mingle with (or vice versa). These microdomains are known to perform several key physiological functions (57). Finally, the surrounding lipids may affect the actual function of membrane proteins, an example of which has been seen in the ability of lipids to affect the opening probability of mechanosensitive channels (54).

The lipid environment can affect the embedded proteins in a general manner, through structural and material properties, as well as through more specific interactions related to the structure of individual lipids (57). The general membrane properties that have been suggested to be relevant for the embedded proteins include e.g. the hydrophobic thickness, elastic properties, phase behaviour, surface charge and the specific structure of the head group region (55). Moreover, crystallographic studies suggest that several membrane proteins include lipids as an integral part of their structure (56). Some of these lipids are shown to be specific for a given

protein, to bind to specific sites and to be essential for the structural integrity and proper function of the membrane proteins (56).

The one membrane protein discussed in this work, the cytochrome bc1 complex (cyt bc1), is a multisubunit complex embedded in a pivotal membrane for bioenergetics, either the inner mitochondrial membrane or a corresponding membrane in chloroplasts or bacteria. Cyt bc1 is part of the electron transport chain and is thus often called complex III of the chain. Essentially, the cyt bc1 complex couples electron transfer (from ubiquinol to cytochrome c) to pumping protons across the membrane. During the catalytic reaction, also called the Q-cycle, the transfers of electrons and protons between redox centers contribute to the creation of a proton gradient across the membrane. However, as this work focuses on the interactions of lipids with the protein complex, the fine details of the protein's reaction mechanism will not be elaborated here.

The presence of the surrounding phospholipids has been shown to be essential for the catalytic activity and native structure of the cyt bc1 complex (60). As with several other membrane proteins, especially CL has turned out to be of key importance for the cyt bc1 complex (61, 62).

2.2.2 Antimicrobial peptides attack membranes

Antimicrobial peptides represent the second type of membrane proteins considered in this work (in additon to membrane-embedded proteins), see Fig. 2.4. They are considered in this work due to the growing concerns about antibiotic resistance, as pathogens develop resistance against more and more conventional antibiotics. Consequently mew medical agents are constantly being searched for and antimicrobial peptides are one class of promising new therapeutics (63). As these relatively small peptides are found throughout the animal and plant kingdoms, they may have even been vital for the evolution of complex multicellular organisms (64). Importantly, antimicrobial peptides have remained effective against pathogens despite their ancient origins (64).

Antimicrobial peptides target microbial membranes, killing bacteria by membrane poration, lysis, or acting inside the cell. Larger peptides may puncture the membrane

by forming pores in it. However, smaller peptides, which are composed of less than 20 amino acids like the ones considered here, are too short to span a membrane. These short peptides have been suggested to gather on a membrane surface in carpet-like formations, each peptide lying parallel to the surface (65). This in turn may lead to membrane destabilization and lysis, however, the specific details of the lysis mechanism remain unclear.

The induction of non-lamellar lipid phases by the peptides has been proposed as a potential mode of action (66). The peptides would induce localized lipid phase change by altering packing, distribution of lipids or neutralization of negative lipid charges (66). Additionally, a mechanism based on molecular shape has been proposed, in which the disruption of the membrane would be explained by a wedge-like insertion of the peptides into the bilayer interface, resulting in alterations in lipid packing (67).

To work as efficient antibiotics, the peptides obviously have to act selectively against the membranes of pathogens, leaving the cells of the host untouched. It is often claimed that the selectivity would simply arise from different surface charge, as bacterial membranes contain more anionic lipids than mammalian membranes do. Only the different charge is not, however, a sufficient explanation. For example, SMAP-28 (sheep myeloid antimicrobial peptide-28), is haemolytic towards human erythrocytes but not towards closely related sheep erythrocytes (68).

As clearly the surface charge is not a sufficient explanation, other lipid properties have to be taken into account. Properties worth considering include for example head group structure and lipid tail structure, namely differences in length, degree of saturation and branching of the tails. In addition, the membranes are not homogeneous but the distribution of lipids within the membrane may vary, both within a leaflet and asymmetrically between the two leaflets. As a result the physical properties, such as thickness, fluidity, bending modulus and phase of membranes from different organisms differ significantly.

One hypothesis aiming to explain selectivity is based on matching the intrinsic curvature of the peptide (referring to the tendency of the peptide to be in a bended conformation) and that of the membrane. The location of residues that orient and

anchor the peptide would also play a role. Indeed, it has been shown in a previous simulation study that four antimicrobial peptides (aurein, citropin, maculatin and caerin) lost their helical content when bound to a planar DMPC bilayer (69). It should be noted, however, that this effect was least evident in the case of aurein, which remained helical in two of the three cases. Interestingly, the peptides adopted a fully helical conformation when bound to a toroidal pore within a POPC bilayer, a region of high local positive curvature.

2.3 Mitochondria

Mitochondria are tiny organelles found inside eukaryotic cells. Often called the powerhouses of the cell, mitochondria provide eukaryotic organisms with a way of converting the energy forms available in food into a more convenient form for the cell to utilize. This form is known as ATP (adenosine triphosphate), a nucleotide with two extra phosphate groups. The transition of ATP to a form with one less phosphate group (ADP, adenosine diphosphate) releases energy that may be used in cellular processes. As the daily functions of complex eukaryotic organisms require monstrous amounts of ATP, the importance of mitochondria can hardly be overestimated. In addition to energy production, mitochondria also have an important role in e.g. calcium metabolism of cells.

Mitochondria are flexible structures comprising two membranes: a porous outer membrane and a protein-rich, highly folded inner membrane. The folds of the inner membrane, called *cristae* (from a Latin word crest), are able to substantially increase the total area of the inner membrane. Due to the required electrochemical gradient for manufacturing ATP, the inner membrane needs to be highly impermeable to small molecules and ions. Furthermore, it is one of the most protein-rich membranes with a protein to lipid mass ratio of about 75:25 (70). CL is synthesized at the inner membrane and indeed nearly all of mitochondrial CL is located in there. Sterols are found only in small quantities.

As it acts as a site for the electron transport chain and ATP synthesis, the inner membrane can be considered as the heart of mitochondrial function. A schematic picture of the rough idea of manufacturing ATP at the inner membrane is sketched

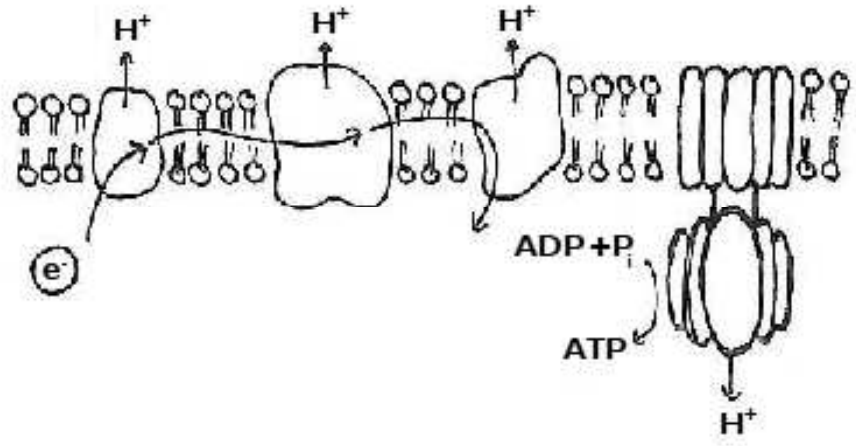

Figure 2.5: A schematic illustration of the respiratory chain and the creation of the proton gradient by proton-pumping proteins across the inner mitochondrial membrane. The ATP synthase on the right side of the picture uses the energy stored in the gradient to phosphorylate ADP to form ATP (3) (an artist's view).

in Fig. 2.5. As electrons travel down the chain (from left to right in the picture), the energy released during their passage from one carrier molecule to another drives the proton pumps embedded in the inner membrane. As discussed earlier, one of these proton pumps is also studied in this work. Translocation of protons across the membrane stores energy by establishing an electrochemical proton gradient. A large protein complex, called the ATP synthase (on the right in the picture), employs the gradient to catalyze the phosphorylation of ADP to form ATP, thus completing the process of oxidative phosphorylation (5). This mechanism of coupling the translocation of protons to the production of ATP is called the chemiosmotic energy coupling (71).

3. METHODS

So as to produce useful descriptions of the dauntingly complex biological systems, or of any real system for that matter, scientists have to make a simplified version, a *model* out of it. A model is basically any description of a part of reality, which is not the real version itself. The trick is to catch the essentials (for example by looks only): toy cars look roughly the same as real cars and fashion models look roughly like real women. Matters could be taken further still, e.g. by just considering one wheel of the car, describing its motion by a mathematical model and using a computer to calculate its *trajectory*, meaning where it goes and how quickly. Similarly, in this work we do not study whole organisms in their environment, not even whole organs, not even whole cells. Instead, we take a tiny organelle like a mitochondrion, think about what features are essential in its structure and function, focus on them, make further radical simplifications and end up with a model system of a tiny patch of a lipid bilayer, whose lipid concentrations generally reflect those of an actual mitochondrial membrane. Shortly said, we think that the lipid bilayer structure is an essential and interesting feature of mitochondria, focus on that and strip everything else away, including for example various kinds of proteins, all lipids except for the most important ones, all sugars and all nucleic acids. Also the time and length scales that can be considered using this model are limited. It should indeed be stressed that a particular model only describes what it was constructed to describe, for example the model in hand cannot describe e.g. the large scale metabolic pathways or smaller scale phenomena like proton tunneling. It can, however, yield useful information about the average physical properties and dynamics of the mitochondrial membranes, ideally complementing and explaining experimental data.

3.1 Quantum mechanical underpinnings of molecular mechanics

The classical molecular mechanics method used in this work has its roots in quantum mechanics (72). In the quantum mechanical approach (72), molecular structures and energies are derived from the underlying electronic and nuclear structures by solving the Schrödinger wave equation.

In practice, the quantum mechanical methods used are based on the so-called Born-Oppenheimer approximation. The nuclei are estimated to remain fixed on the timescale of electronic vibrations. Consequently, the motions of electrons and nuclei can be considered separately.

There are practically two approaches utilized to achieve a description for the system, empirical (ab initio) and semi-empirical quantum mechanics. In ab initio, the molecular orbitals (wave functions) are calculated as a linear combination of chosen atomic orbitals, minimizing the electronic energy of the molecule. The semi-empirical method replaces a part of the laborious calculations by a set of predetermined parameters that define the forms and energies of atomic orbitals, thus reducing the computational load (72).

3.2 Molecular dynamics simulations

As the quantum mechanical methods are computationally very heavy and in this work we study systems containing tens of thousands of atoms, more simple methods are needed. We consequently treat the system classically, with the approach known as molecular mechanics, also called the force field or potential energy method (72).

The modeling approach employed in this work, called *molecular dynamics* (MD), is based on this classical approach. It is (at least in principle) a simple but still a highly useful method to obtain information about molecular systems. In a nutshell, molecules are described classically as particles attached by springs, whose movements are computed using Newton's equations of motion (72). These computations, also called *simulations*, render a trajectory, i.e. the time evolution of the particles' coordinates and velocities.

Despite the simple idea of MD simulations, complications arise when they are employed in practice and the limitations of the method should always be taken into account when interpreting the results. Firstly, the classical approach does not allow the explicit description of phenomena (e.g. chemical reactions) that are quantum-mechanical in nature. It must also be stressed that only properties of a large enough number of molecules and/or over long enough time scales may be considered. The maximum time and length scales of the simulations are in turn limited by the time step length and available computer power. If the characteristic time or length scale of a given phenomenon exceeds that of the simulation, it falls outside the scope of the study. Finally, perhaps the most important and complicated question is how to realistically describe the interactions between the particles. Numerous different descriptions are available, none of which can be considered universally superior to others (72).

In this work, a molecular dynamics simulation engine called GROMACS was employed (73, 74). The following sections thus follow closely the GROMACS manual (74), where an interested reader is referred for further details.

3.2.1 Force field defines the interactions between particles

The potential energy function, from which the forces acting on the particles are derived, is called a *force field*. After defining both the functional form of the force field and the set of parameters associated with different interactions, the force on a given particle i can be calculated from the potential function $V(r_1, r_2, ..., r_N)$ in terms of

$$F_i = -\frac{\mathrm{d}V}{\mathrm{d}r_i}. \tag{3.1}$$

Originally, the parameters associated with the force field are determined using quantum mechanical calculations (discussed very briefly above) and experimental data such as crystal structures and vibrational spectroscopy (72). There are several different functional forms and associated parameter sets used in simulating biomolecular systems. Examples of the widely used ones include GROMOS, AMBER, CHARMM and OPLS (72). There is no force field which could be generally

argued to be somehow better than the others in every aspect, consequently the choice has to be made according to the system in question and practical conditions (72).

Let us now write down one choice for the functional form of the force field used in this work. Notably, the discussion here is restricted only to the definitions used in the GROMACS software package (73, 74), which represents one of all possible choices.

As a first step of tackling the laborious task, the interactions are divided into bonded and non-bonded ones, referring to those with chemical bonds and those without. These will be discussed in more detail below. Generally speaking, the potential energy function is assumed to be separable into basic physical potentials. Typically biomolecular force fields contain terms for van der Waals and electrostatic interactions, and terms arising from bond length, angle and torsion variations. In other words, the total potential function is written as a sum of these individual potentials, which in turn will be listed in the following sections. Ideally, the potentials should be universal in a sense that they would be transferable between systems and consequently potentials of smaller blocks could be applied to construct a potential for larger molecules. In practice, however, the matter is more complicated.

Bonded interactions

Bonded interactions define stretching of covalent bonds, vibration of bond angles, proper dihedral angles (angles between adjacent planes) and improper dihedral angles (used to force planar groups stay planar and prevent transition to a mirror image). The potentials for bond-stretching, angle-bending and proper- and improper dihedrals, in respective order, are written as follows:

$$V_b(r_{ij}) = \frac{1}{2}k^b_{ij}(r_{ij} - b_{ij})^2, \tag{3.2}$$

$$V_a(\theta_{ijk}) = \frac{1}{2}k^\theta_{ijk}(\theta_{ijk} - \theta^0_{ijk})^2, \tag{3.3}$$

$$V_d(\phi_{ijkl}) = k_\phi(1 + \cos n\phi - \phi_0) \tag{3.4}$$

$$V_d(\phi_{ijkl}) = V_0 + \frac{1}{2}(V_1(1+\cos\phi)) + V_2(1-\cos 2\phi) + V_3(1+\cos 3\phi), \tag{3.5}$$

$$V_{id}(\xi_{ijkl}) = k_\xi(\xi_{ijkl} - \xi_0)^2. \tag{3.6}$$

Here r_{ij} denotes the distance between atoms i and j, θ_{ijk} is the bond angle between the three atoms i, j and k, and b_{ij} and θ^0_{ijk} are reference values related to these. k^b_{ij}, k^θ_{ijk}, k_ϕ, k_ξ are force constants. There are two options listed for the treatment of proper dihedral interaction, a periodic function (3.4) or Ryckaert-Bellemans function (3.5) used in OPLS (75). In these ϕ_{ijkl} describes the rotation of bond $i-j$ around $j-k$ with respect to $k-l$, i.e. it is the angle between planes ijk and jkl. ϕ_0 is a reference value and the constants V_i are OPLS parameters. In the last equation, which describes the improper dihedral potential, ξ_{ijkl} is again the angle between the planes ijk and jkl and ξ_0 is the reference value.

So as to decrease the computational load, a constraint algorithm was employed to keep the bond lengths constant, thus ignoring the high-frequency bond vibrations and consequently allowing a larger time step. Due to the small amplitude of the bond vibrations described with a harmonic potential (3.2), they may be ignored without losing any crucial information. In this work the bonds were reset to their fixed lengths after every unconstrained update by using a linear constraints solver called LINCS (76).

Non-bonded interactions

The non-bonded interactions include electrostatic interactions between charged particles and van der Waals interactions between dipoles. The electrostatic interactions are described by the Coulombic potential and van der Waals interactions by the Lennard-Jones potential as follows:

$$V_{\mathrm{C}}(r_{ij}) = \frac{q_i q_j}{4\pi\varepsilon_0 r_{ij}}, \tag{3.7}$$

$$V_{\mathrm{LJ}}(r_{ij}) = \frac{C_{ij}^{(12)}}{r_{ij}^{12}} - \frac{C_{ij}^{(6)}}{r_{ij}^{6}}, \tag{3.8}$$

where q_i and q_j are the charges of atoms i and j, r_{ij} is their distance and $C_{ij}^{(12)}$ and $C_{ij}^{(6)}$ are parameters dependent on the pair of atom types.

Because of the slow decay rate of the electrostatic interactions, their treatment in simulations proves to be a rather challenging issue. The most simple approach would be to choose a cutoff distance and only consider charged pairs within that distance. This previously widely used scheme is, however, very sensitive to the details of the implementation and may induce artifacts to the simulation system (77), so alternative methods should be used instead. Another method, which overcomes the crude problems of the simple cutoff, is the *reaction field* method (78). It also involves a cutoff for the consideration of charged pairs but beyond this distance a correction is applied by assuming a uniform dielectric constant.

The third widely used method considers the total electrostatic energy of the system. As a result of the periodic boundary conditions, the studied system and its images form an infinite 3D lattice. Ewald or Particle Mesh Ewald (PME) (79) methods calculate the infinite sum over all charges and periodic boxes. When the point charges are represented as Gaussian charge densities, the convergent sum can be computed in reciprocal space and subsequently transformed back to real space (72). In practice, the calculations using Ewald methods also involve cutoffs: a distance cutoff for the real space summation and a number cutoff for the vectors in the reciprocal space summation. Of the available methods, PME is considered to be the most reliable (77), although the reaction field approach has been successful in many studies and scales better in some computing environments (80).

3.2.2 Movement is determined by solving Newton's equations of motion

Once the the force acting on each particle has been derived from the force field, the resulting movement of the particles can be solved by using Newton's equations of

motion

$$\frac{\mathrm{d}^2\vec{r_i}}{\mathrm{d}t^2} = \frac{\vec{F_i}}{m_i}, \quad i = 1, ..., N. \tag{3.9}$$

Here $\vec{r_i}$ and m_i stand for the position and mass of particle i, respectively, $\vec{F_i}$ is the total force exerted on the particle i, and N is the number of particles in the system. The equations of motion are integrated numerically over discrete time steps Δt to obtain a trajectory, that is, the time evolution of the positions and velocities of the particles at each time step. The integrator used in this work is the so-called leap-frog algorithm (81):

$$v\left(t + \frac{\Delta t}{2}\right) = v\left(t - \frac{\Delta t}{2}\right) + \frac{F(t)}{m}\Delta t, \tag{3.10}$$

$$r(t + \Delta t) = r(t) + v\left(t + \frac{\Delta t}{2}\right)\Delta t. \tag{3.11}$$

Here Δt stands for the length of the timestep, r for position at time t and v for velocity.

The maximum value for the time step is limited both by the stability of the used integrator and the time scale of the processes that are considered (72).

3.2.3 Temperature and pressure are usually kept constant

The velocities of the particles in an MD simulation can be connected to the temperature of the system via the equipartition theorem. To measure the pressure, there are multiple (equivalent) ways, the most common one of which is based on the virial equation for pressure, see (82) for more details.

During the simulations conducted in this work, the number of particles (N), temperature (T) and pressure (p) were kept constant. In other words an NpT ensemble was used. Keeping the particle number constant is obviously trivial, however, the treatment of temperature and pressure requires the use of special algorithms. These are called *thermostat* and *barostat*, respectively.

In the beginning parts of simulations reported in this work, a method called Berendsen temperature coupling (83, 84) was used for equilibrating the systems. Its idea is to mimic the weak coupling of the system to an external heat bath. This is accomplished by modifying the equations of motion, which effectively corresponds to

scaling of the velocity of each particle by a time-dependent factor at each time step. Consequently, the thermostat drives the system temperature towards a reference value T_0 at a rate determined by the time constant τ:

$$\frac{\mathrm{d}T}{\mathrm{d}t} = \frac{T_0 - T}{\tau}. \tag{3.12}$$

The so-called Nóse-Hoover thermostat couples the system to an external heat bath by including an extra degree of freedom to the system. It is consequently called an extended ensemble scheme. In practice, a frictional term is added to the equations of motions:

$$\frac{\mathrm{d}^2\vec{r_i}}{\mathrm{d}t^2} = \frac{\vec{F_i}}{m_i} - \xi\frac{\mathrm{d}\vec{r_i}}{\mathrm{d}t}, \tag{3.13}$$

where the heat bath parameter ξ follows the equation

$$\frac{\mathrm{d}\xi}{\mathrm{d}t} = \frac{T - T_0}{Q}. \tag{3.14}$$

The strength of the coupling is determined by the parameter Q.

As the Berendsen scheme suppresses the fluctuations of the kinetic energy and is thus physically unrealistic, another algorithm, such as the Nóse-Hoover, should be employed after the equilibration time. It should be noted, however, that the difference between the results yielded by the different thermostats described here are usually negligible. For a newer method see (85).

Analogous to temperature coupling, there are two methods available in GROMACS for pressure coupling. The straightforward Berendsen method (83) functions basically in the same way as the Berendsen temperature coupling, effectively rescaling the box dimensions at each time step, leading to an exponential relaxation of the pressure towards the reference value. This is a useful method mainly during the equilibration of the system. A more sophisticated Parrinello-Rahman approach (86, 87) should be used after the equilibration time has been passed. It is an extended ensemble approach with similar (but more complex) types of added terms in the equations of motions as in the case of the Nóse-Hoover thermostat. For more details about this approach see (86).

The Berendsen method is again useful during the equilibration time. However, if

the thermodynamic properties (or the fluctuations of pressure or volume for some other reason) of the system are of interest, one should switch to a more sophisticated method, such as the Parrinello-Rahman approach, after the equilibration of the system.

3.3 Analysis methods

3.3.1 Area and thickness reflect membrane packing

One simple property that can be easily calculated from a lipid bilayer simulation is the average area occupied by one lipid molecule. It is often used to estimate system equilibration and in the evaluation of simulation results as comparison to experimental data. Obviously, changes in the area occupied by the lipids are also reflected to the thickness of the membrane. Moreover, changes in the thickness and area per lipid imply changes in acyl chain ordering and condensation.

In one-component bilayers, the area per lipid is calculated simply by dividing the surface area of the membrane by the number of lipids in one leaflet. In case of several different lipid species being present, matters are somewhat more complicated. Bilayer thickness is usually estimated as an average distance between the head groups of opposite leaflets. In this work the thickness is calculated either in this way or as a distance between the points where the electron density profiles of bilayer atoms merge with the profiles of water.

Membrane structure is measured experimentally by X-ray and neutron diffraction (88) to produce electron and mass density profiles, respectively. Due to the large contribution of the head groups, the distance between the main peaks in the density profiles can be used to estimate the distance between the head groups and thus bilayer thickness (88, 89). By estimating the volume of a single lipid, a value for the area per lipid can also be calculated (88, 89). Experimental values for the area per lipid may be also extracted from e.g. Langmuir monolayer experiments, given that the amount of material is known (1).

3.3.2 Radial distribution function characterizes local structure

The radial distribution or pair correlation function is defined as the ratio of the number densities of certain particles at a distance r to the average global density of the same particles. In case the particles do not interact and thus their locations do not correlate with each other or their surroundings, the pair correlation function yields a value of $g(r) = 1$ for all $r \geq 0$. If the density of the given particles at a distance r exceeds their global density, then $g(r) \geq 1$, and correspondingly $g(r) \leq 1$ for a lower than average concentration.

In GROMACS the calculation of the $g(r)$ is implemented for particle types A and B as follows:

$$g_{AB}(r) = \frac{\langle \rho_B(r) \rangle}{\langle \rho_B \rangle_{\text{local}}} = \frac{1}{\langle \rho_B \rangle_{\text{local}} N_A} \sum_{i \in A}^{N_A} \sum_{j \in B}^{N_B} \frac{\delta(r_{ij} - r)}{4\pi r^2}, \tag{3.15}$$

where $\langle \rho_B(r) \rangle$ denotes the density of type B particles at a distance r measured from type A particles and $\langle \rho_B \rangle_{\text{local}}$ is the average density of type B particles inside a maximum radius around particles A (74). The outcome for soft-matter systems is intermediate to those of solid and liquid matter, the correlations between particle positions dying away slower than in a fluid but still lacking the long-range order of a solid. Experimental measurements such as neutron, X-ray, and light scattering yield information about the $g(r)$ (82).

The radial distribution function can further be utilized to calculate so-called coordination numbers, i.e. the number of certain type of particles within a certain distance of a central particle. This may be useful when examining e.g. ions near a membrane-water interface. In this case, the development of coordination numbers is a crucial indicator of system equilibration. The coordination number of a given ion with respect to e.g. oxygen can be calculated by counting the number of oxygen atoms inside its first hydration shell, in other words by evaluating the integral

$$N = \int_0^{r_{\min}} 4\pi \rho g(r) r^2 \mathrm{d}r. \tag{3.16}$$

Here ρ is the average number density of the given oxygens and $r_{\min}$ is the radius of the first hydration shell. The latter is defined as the distance of the first minimum in the radial distribution function of the given cation and water oxygens.

3.3.3 Order parameters describe orientational order of lipids

The lipid bilayer in a fluid state is characterized by a lack of positional order in the plane of the membrane, however, there is a significant degree of orientational order with respect to the bilayer normal. Often special attention is played to the orientational ordering of the lipid acyl chains and hence several related measures called order parameters have been used to quantify it. One of these, the deuterium order parameter S_{CD}, was used in this work. Conveniently, the simulation results can be verified by comparing to experimental ones measured with NMR (90).

Order parameters are represented by a tensor

$$S_{ij} = \frac{1}{2}\langle 3\cos\theta_i \cos\theta_j - \delta_{ij}\rangle, \tag{3.17}$$

where θ_i is the angle between the ith molecular axis and the bilayer normal (91). The deuterium order parameter is written differently depending on if there is a single or double bond between the chain carbons. For single bonds it is written as

$$-S_{\mathrm{CD}} = \frac{2}{3}S_{xx} + \frac{1}{3}S_{yy}. \tag{3.18}$$

For the methylene group C_n the z-direction is taken parallel to a vector $C_{n-1} - C_{n+1}$ and the yz-plane is defined as $C_{n-1} - C_n - C_{n+1}$ (91). If the methylene group under study is adjacent to a double bond, S_{CD} is calculated using

$$-S_{\mathrm{CD}} = \frac{1}{4}S_{zz} + \frac{3}{4}S_{yy} - \frac{\sqrt{3}}{2}S_{yz}. \tag{3.19}$$

Here the z direction is parallel to the adjacent double bond. This experessions can be derived from the definition of the order parameter (not shown here). In all-atom simulations, where hydrogens are included in the setup, S_{CD} may be calculated directly. Otherwise, in e.g. united-atom simulations, the hydrogen atoms are assumed

to be in their equilibrium positions.

3.3.4 Rotation is one mode of lipid movement

In addition to examining the ordering of lipid molecules, NMR is also used to obtain information about their dynamics, which can further be compared to simulations (92). The rotational motions of the simulated molecules or parts of them can be analyzed by examining the angular reorientation of selected molecular vectors. For a unit molecular vector $\hat{\mu}$ this is done by looking at the correlation between the vector at time t ($\hat{\mu}(t)$) and at some defined starting point ($\hat{\mu}(0)$), yielding an autocorrelation function:

$$C_2(t) \equiv \langle P_2(\hat{\mu}(0)) \cdot \hat{\mu}(t))\rangle = \left\langle \frac{3}{2}(\hat{\mu}(0)) \cdot \hat{\mu}(t))^2 - \frac{1}{2} \right\rangle . \tag{3.20}$$

This particular one is called the second rank reorientational correlation function (93), where $P_2(x)$ is the second order Legendre polynomial and the brackets denote averaging over all initial times in a long trajectory. Characteristic decay times related to the correlation functions can be compared to the relaxation times from NMR measurements.

3.3.5 Electrostatic potential arises from the charge distribution

Due to the great amounts of ions and charged macromolecules, electrostatic interactions play a crucial role in biological systems. In case of membranes, the uneven distribution of charged molecules and nonrandom orientation of electric dipoles of lipid head groups, carbonyl groups and water result in unbalanced charge distribution and hence potential differences.

Membrane potential, meaning the voltage difference across the whole bilayer, can be directly measured with electrodes. On the other hand, changes in the dipole potential of bilayers can be estimated from the conductances of hydrophobic ions (94).

From simulations the potential profiles can be calculated by using the charge density. It is computed by dividing the box into slices and counting the number of

charges in each slice. In case of a symmetric bilayer, the profile can be subsequently averaged over the two leaflets. The electrostatic potential is finally calculated by integrating this charge density profile ρ twice from the water phase towards the bilayer center as follows:

$$\Phi(z) - \Phi(0) = \frac{-1}{\varepsilon_0} \int_0^z \int_0^{z'} \rho(z'')\mathrm{d}z''\mathrm{d}z', \tag{3.21}$$

where $z = 0$ corresponds to the water phase and ε_0 is the permittivity of vacuum.

3.3.6 Lipids move in the plane of the membrane by diffusion

In addition to rotating in their places, lipids also move around in the plane of the membrane. The situation could be described as a two-dimensional fluid, the movement of a single lipid having a nature of a two-dimensional random walk. To quantify how quickly a single molecule moves around, its mean-squared displacement (MSD) $\langle |r(t)|^2 \rangle$ can be used to calculate the lateral tracer diffusion coefficient D_T:

$$D_\mathrm{T} = \lim_{t \to \infty} \frac{1}{2dt} \langle |r(t)|^2 \rangle. \tag{3.22}$$

The equation is called the Einstein relation, where $d = 2$ is the dimensionality of the surface and the brackets denote averaging over all initial times as well as over all chosen molecules in the system. As the monolayers may move with respect to each other during the simulation (12), the monolayer center of mass movement has to be taken into account when calculating the coefficients.

Comparing the obtained values to experiments is often difficult due to limited time scales and system sizes in simulations (95). Experimental techniques for measuring diffusion include tracking by video microscopy (96), NMR using pulsed magnetic field gradients (97), fluorescence correlation spectroscopy (98) and fluorescence recovery after photobleaching (99).

3.4 Overview of the systems studied in this work

In this work, molecular dynamics simulation method was employed to study the properties of two key components of biological membranes, cholesterol and car-

diolipin. Several model membrane systems containing different lipids and other components were constructed and simulated for tens to hundreds of nanoseconds each.

In *Paper I* five different systems were studied, each containing a membrane of 128 DPPC molecules and 32 modified cholesterol molecules (sterol concentration 20 mol%). The cholesterol molecules were modified by removing certain methyl groups and converting a double bond into a single bond. All bilayers were hydrated with 3500 water molecules and simulated for 50 ns in a temperature of 323 K.

In *Paper II* we studied six different membrane systems mimicking the mitochondrial membranes with three of them corresponding to the inner membrane and three to the outer one. The membranes were composed of PC, PE and CL, the concentrations mirroring those of the natural inner and outer mitochondrial membranes. The systems also contained 8500 water molecules, Na^+ counterions to neutralize the charge of cardiolipin head groups and 0.1 M concentration of NaCl and $CaCl_2$. After equilibration all systems were simulated for 100 ns in a temperature of 310 K.

In *Paper III* four configurations of the cytochrome bc1 membrane protein complex were studied. Each configuration reflected a different state of protein activity. The membranes in which the complexes were embedded were similar to those in *Paper II*, the concentrations of PC, PE and CL corresponding to those of an inner mitochondrial membrane. In addition to the lipids, protein and its ligands, the systems contained water and Na^+ counterions. All four systems were simulated for 200 ns in 310 K temperature.

In *Paper IV* several simulations with varying lipid and peptide amounts were carried out. First three systems, each containing one aurein peptide in a box of water, were simulated for 100 ns. All the other simulations consisted of PG-CL (25 mol% CL) bilayers of varying size (102/408 lipids), varying number of peptides (0–40 peptides), Na^+ and Cl^- counterions and water. Several simulations of different lengths (80–160 ns) and temperatures (298–338 K) were performed.

4. CHOLESTEROL'S METHYL GROUPS –MOLECULAR FOSSILS?

Promotion of orientational order in the lipid tails (11, 12) can be considered as the key feature underlying the biologically significant effects that cholesterol has on membranes. Cholesterol has been shown to make bilayers more condensed (100), increase their mechanical strength (16), reduce passive permeation through them (17) and decrease the diffusion rate of lipids in fluid-like membranes (99). Moreover, it is associated with domain formation and maintaining the liquid-ordered phase (101).

To some degree, practically all sterol molecules found in biological membranes promote order in the lipid acyl chains. There is, however, something special about cholesterol, as very small changes in its structure are able to considerably alter its biological function. For example desmosterol, which differs from cholesterol only by one double bond, cannot step into its shoes. Desmosterol is not able to form rafts in membranes as cholesterol does (102) and indeed the inability of the body to convert desmosterol into cholesterol causes a serious condition (19, 20). Moreover, the concentration of cholesterol varies significantly between different types of membranes, e.g. the mitochondrial membrane has practically none while the ocular lense membrane may contain as much as 80 mol% (7, 8).

Another clue implying high structural specificity and importance of cholesterol is the costly process of its synthesis, where excess methyl groups are removed from lanosterol (8, 21). Similarly, it has been suggested that cholesterol originally evolved from lanosterol driven by optimization of cholesterol's effects on certain physical properties of membranes, again essentially by removing excess methyl groups (22, 24, 25), see also Fig. 4.1. Curiously enough, there still remains some methyl groups in the ring structure, giving cholesterol a two-sided nature: a smooth α-face with

no methyl groups and a rough β-face with two methyl groups. A question arises, as to whether these remaining methyl groups are really necessary for the function of cholesterol or could they considered as molecular fossils (24). When in addition both experimental and computational studies show decreased interactions between sterol molecules and acyl chains when methyl groups are present, a physicist cannot help but try removing the last ones also.

This story is built around the idea that the biological purpose of cholesterol is to optimize membrane properties by increasing order in the lipid tail region and seeing the evolution of the molecule as fine-tuning for this task. A tempting question arises as to whether we would be able to guess the next step in evolution and further enhance the ordering capability of cholesterol.

The idea was first tested in a previous study (103), where contrary to expectations the removal of both of the two remaining methyl groups proved to have an adverse effect on the ordering effect. To further test the idea and elucidate the underlying mechanism of how cholesterol induces order in membranes, this work, based on *Paper I*, examines the two methyl groups attached to the ring one by one. Additionally, the role of the one methyl group attached to cholesterol's short tail is considered. First, the various modifications made to cholesterol structure are explained and subsequently their most important effects on a DPPC (dipalmitoylphosphatidylcholine, one of the most studied model membrane lipids) membrane are examined. The results highlight the importance of one methyl group in particular and also clarify the role of others in relation to sterol ordering capabilities.

4.1 The structural modifications made to cholesterol

The ring system is asymmetric about the ring plane, having a rough side (β-face) with two methyl groups C18 and C19 pointing out of the plane (see Fig. 4.1), and a smooth α-face with no substituents.

The structures and their abbreviations (Ste1–Ste3) are shown in Fig. 4.1 and summarized in Table 4.1. In the first three systems, one of the methyl groups (C18, C19, C21) was removed. For comparison, in Dchol (103) both methyl groups C18 and C19 on the rough β-side of cholesterol were removed. In this chapter the focus

will be on Ste1,2 and 3 and an interested reader is referred to *Paper I* and the article (103) for further details on Dchol and other modifications not listed here.

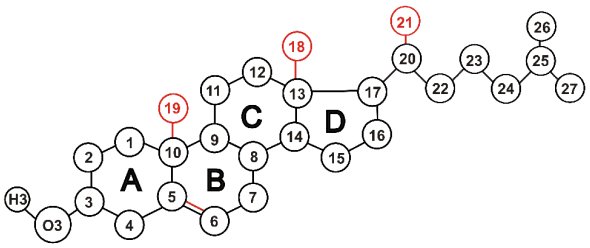

Figure 4.1: Cholesterol structure with the modified locations indicated in red.

Table 4.1: Abbreviations used for the modified sterols.

System	Methyl group removed
Ste1	C19
Ste2	C18
Ste3	C21
Dchol	C18 and C19

To the author's knowledge, the abovementioned modified sterols do not have identical natural counterparts. Interestingly, no common (natural) sterol found in the literature lacks the methyl group C18. Even while there are some sterols without C19, their lipid bilayer ordering capabilities are unknown and thus render little help for this work. It should be noted, however, that there are no fundamental obstacles to synthesizing the kind of sterols described here. There has indeed been encouraging progress on synthesizing natural sterols (104), steroids (105) and synthetic sterols (106, 107).

4.2 Effects on general bilayer structure

First we examine the effects of the modified sterols on the general structural features of the model bilayers. Since the aim was simply to compare the effect of different sterols on the bilayer, the absolute values of the area per lipid are rather irrelevant and there is no reason to complicate the matter by considering the areas of the sterols and other lipids separately. Consequently, the area per lipid was calculated by only

considering the DPPC lipids, thus omitting the sterols. The DPPC membranes containing Chol, Ste1 or Ste3 have essentially the same lipid area within error bars. In the system containing Ste2 the area is somewhat larger, however still smaller than in the complete absence of sterols. Hence every modified sterol presented here is concluded to have a condensing effect on the membrane as compared to the pure DPPC bilayer. The thickness of the membrane followed the same pattern.

Differences in the trans-bilayer structure and particularly in the vertical location of the different sterols can be seen in the electron density profiles in Fig. 4.2. This kind of profiles are interesting since cholesterol is known to affect the packing inside membranes (108). When all bilayer atoms and water are considered (panel a), the systems containing Chol, Ste1 (not shown for clarity) and Ste3 look practically identical. The narrow profile with lower peaks in the head group region for Ste2 implies a thinner, less ordered bilayer.

The density profiles for the sterol tail atoms can be seen in the center of panel b in Fig. 4.2. The profile for Ste2 is lower and broader as compared to Chol and Ste3. That of Ste3 is otherwise in line with Chol-containing system, except for the very center of the bilayer, where it seems the tails have stretched out and interdigitate more than Chol molecules do. As seen from panel a, however, due to the relatively small number of sterol molecules this has only a small effect on the overall density in the bilayer center.

4.3 Effects on sterol tilt and lipid packing

Figure 4.3 and Table 4.2 summarize the observed effects of the sterols on ordering of the acyl chains. Results are only shown for the sn-1 chain of DPPC since the ones for sn-2 would only tell the same story again. In line with the area per lipid and other structural results, the ordering capabilities of Ste1, Ste3 and Chol seem close to identical (within error boundaries) and those of Ste2 are considerably weaker. Further in line with weaker ordering, the tilt angle of the ring system of Ste2 with respect to the z axis (bilayer normal) is markedly larger compared to Chol. The tilt angle has indeed been previously shown to correlate well with the ordering abilities of sterols (13). Noteworthy, however, Ste1 induces order as well as Chol, irrespective

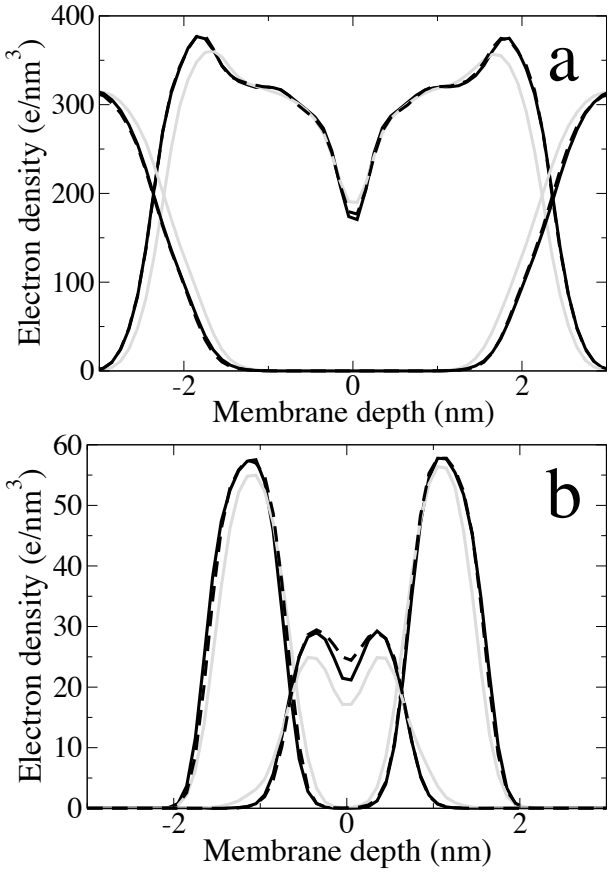

Figure 4.2: Electron density profiles for (a) bilayer atoms and water, (b) sterol ring and tail atoms for Chol (*black line*), Ste2 (*gray line*) and Ste3 (*dashed line*). Membrane depth at $z = 0$ corresponds to the membrane center. The profiles of the system containing Ste1 are not shown as they are practically identical to those of Chol.

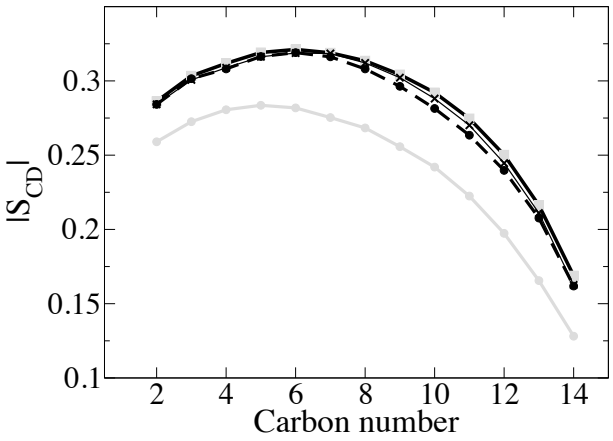

Figure 4.3: Deuterium order parameter profiles for the sn-1 chain of DPPC lipids in bilayers containing Chol (*thick black line, gray squares*), Ste1 (*thin black line, crosses*), Ste2 (*gray line, gray circles*) and Ste3 (*dashed line, black circles*). Small carbon numbers correspond to carbons close to the head group.

Table 4.2: Average values of deuterium order parameters and tilts of the sterol ring and tail. Tilts are given in units of degrees.

System	S_{CD} (sn-1)	Tilt (Ring)	Tilt (Tail)
Ste1	0.28 ± 0.01	22.1 ± 1.4	32 ± 1
Ste2	0.24 ± 0.02	26.0 ± 3.3	44 ± 3
Ste3	0.28 ± 0.01	20.7 ± 1.2	26 ± 1
Chol	0.28 ± 0.01	19.8 ± 0.2	28 ± 1

of its slightly larger tilt. This observation requires further elucidation as it seems to contradict previous results on the relationship of the sterol tilt and induced order.

The reason turns out to be enhanced packing of the lipid tail atoms near the sterol ring system. Removing the methyl group C19 from near the head group of the sterol presumably altered the hydrogen bonding between DPPC lipids and the sterol head group, changing the packing balance between the two sides of the ring system. In other words, without C19 being present the interactions of the OH head group, which is located on the β-face, could favor packing on the same side. This was indeed what was seen when calculating the number lipid tail atoms near the both faces of the sterols. Ste1 had more tail atoms near the β-face as compare to Chol and Ste3 which favored the α-face. The removal of C19 thus increased packing near the β-face and moreover ended up in Ste1 having a slightly larger total number of close-by tail atoms near the ring, effectively compensating the slightly larger tilt.

Removal of the C21 methyl group from the sterol's tail was expected to have at least some kind of effect on the sterol's ordering ability. This was due to previous simulation studies involving desmosterol, which showed the tail having a significant effect on the sterol's orientation and ordering capability (102). Instead, essentially the only effect resulting from the deletion of C21 is the slight decrease of the tail tilt, see Table 4.2. The changes in sterol ring system orientation and ordering of DPPC tails are within error boundaries from those of Chol. As the more vertical orientation of the sterol's tail increases the sterol concentration in the bilayer center and thus should induce spatial restrictions on the lipid tails, one could expect the ordering of end parts of the lipid tails increase. As seen from Fig. 4.3, no such effect can be seen, possibly due to the relatively short acyl chains (16 carbons) used in

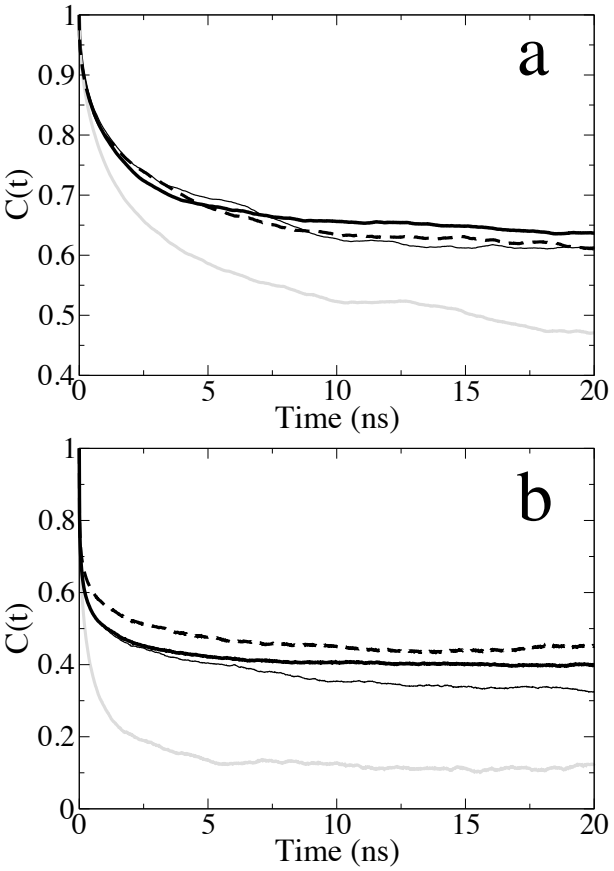

Figure 4.4: Rotation correlation functions for (a) sterol tilt vector C3-C17 and (b) sterol tail vector C17-C27. Different sterols are marked as follows: Chol (*thick black line*), Ste1 (*thin black line*), Ste2 (*gray line*) and Ste3 (*dashed line*).

this study.

Along with the static orientational aspects, the dynamics of the systems also change as a consequence of the modifications. The results for the speed of the lipid movement in the plane of the membrane (lateral diffusion), are qualitatively in line with the other results, i.e. the lipids move slower in the more ordered bilayers (data now shown). Another dynamic aspect studied was the rotational movement of the sterol ring system, sterol tail and lipid tails. The results for the lipid tails were in line with the order parameters, slower dynamics and larger plateau values indicating more ordered systems. For the sterol ring and tail, the rotational correlation functions are shown in Fig. 4.4. The results show that not only has Ste2 a considerably less vertical orientation in the bilayer, but it also has larger and faster fluctuations. Notice also the somewhat slower dynamics of the sterol tail of Ste3 in panel b, as may be expected based on its more vertical orientation.

4.4 Critical assessment and future perspectives

It should be noted that this study only focused on one (central) aspect of cholesterol function: its capability to induce order in lipid bilayers. The modifications made to the cholesterol structure were done with only this aspect in mind, and the results were analyzed accordingly. Consequently, we only comment on properties closely related to the ordering capabilities. Other important aspects of cholesterol function, such as its effect on proteins (see for example (109, 110)), might also be affected by the changes made here. Nevertheless, these speculations fall outside the scope of this study but afford an interesting subject for future research.

We considered the interactions of the sterols with only one model lipid (DPPC) and with only one fixed concentration of sterols. The simulations were rather short (50 ns), however, due to the use of previously simulated systems (over 100 ns) as initial structures with only rather small modifications, the systems may in this case have equilibrated during rather short times, as was concluded based on area per lipid and potential energy calculations.

Obviously, there is no experimental data to which we could compare our results of these exact modified sterols and neither could we find any suitable data concerning any similar sterols with the same methyl groups detached. Nevertheless, the cholesterol model used here has been compared to both experimental and simulation data (with good agreement), and the results of our analysis provide a logical picture, the general view provided by this study seems reliable. After this study, the work on cholesterol has been continued in the group, see for example (111, 112).

4.5 Conclusions

In summary, the methyl group C18 seems to be the most crucial one for maintaining proper sterol orientation and ordering of the lipid tails inside the bilayer. Every modification with the C18 deleted had considerably worse ordering capabilities as compared to Chol and indeed to the best of the author's knowledge there are no common biological sterols that lack C18. The changes resulting from removing C19 or C21 were not as drastic, the ordering of the lipid tails stayed essentially the same. The main consequences of removing these methyl groups were the altered packing

balance between the α- and β-faces in case of Ste1 and the more vertical orientation of Ste3. Notably, however, every modification involving the removal of two methyl groups simultaneously (discussed in more detail in *Paper I*) led to a less vertical orientation of the sterol and reduced ordering abilities.

In conclusion, we were unable to find any convincing evidence indicating that the methyl groups of Chol would be molecular fossils. As none of the modifications we made enhanced the ordering capabilities of Chol, we will simply have to behave and wait for some millions of years to see what actually happens.

5. THE INFLUENCE OF SALT ON CARDIOLIPIN-RICH BILAYERS

Due to the anionic nature and structural features (rigidity and the small head group, explained below) of CLs, we expect CL-rich membranes to be especially prone to the effects of ions. As both of the phosphate groups of CL are bound to the same glycerol, the structure of the head group region is rather rigid. In addition, the head group itself constitutes only of a small hydroxyl group. Consequently, as compared for example to a PC with a bulky choline head, the mobility of the CL head group region is rather limited and the shielding of its negative charges diminished, making it more susceptible to interactions with water and the ions dissolved in it (31). Thus it seems likely that the direct and indirect CL-ion interactions may be one of the keys to understanding how CL modulates the properties of mitochondrial and bacterial membranes.

To the author's knowledge, no previous simulation studies concerning CL-rich membranes under the influence of salt have been published. There are some atomic-scale simulation studies exploring the properties of CL-rich membranes without salt (113–115) and one coarse-grained simulation study examining the morphology of CL membranes (116). As the CL-ion interactions should be significant and indeed the effects of ions are expected to be stronger in CL-rich membranes as compared to CL-free membranes, we examine these effects here on atomic scale and see the mechanisms of how they occur. For this purpose, we employed MD simulations of six different model systems, as described in *Paper II*. The lipid compositions of the systems correspond to those of the natural mitochondrial membranes, the CL-rich inner membrane (IM) and the outer membrane (OM), which contains only a very small amount of CL. In addition to Na^+ counterions neutralizing the negative charges of CLs, two salts (NaCl, $CaCl_2$) relevant to mitochondrial physiology were added

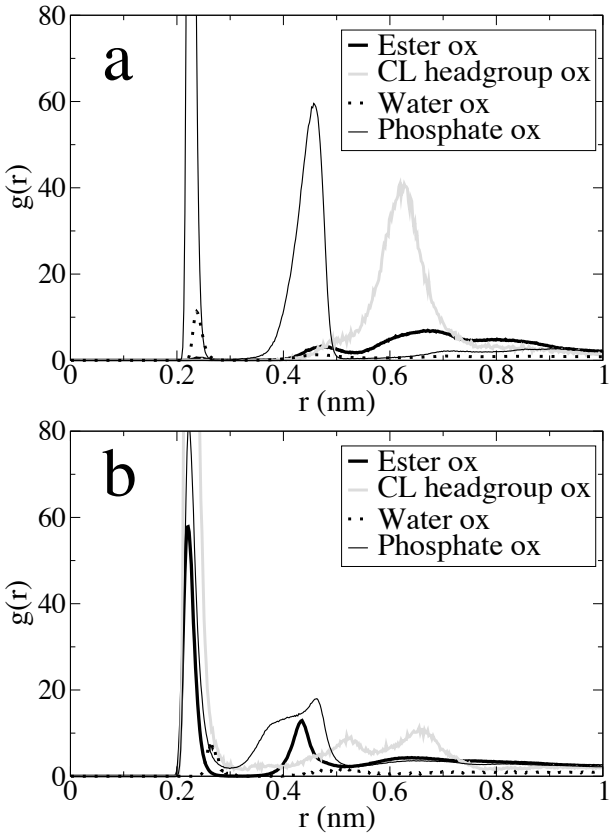

Figure 5.1: Radial distribution functions of ions with lipid and water oxygens in the inner mitochondrial membrane system. The data for Ca^{2+} ions is shown in (a) and that for Na^{+} ions in (b).

into the systems. For general discussion of the significance of ions for biological and model lipid membranes, see the Background chapter.

5.1 The binding of ions to the membrane surface

The binding of ions to the bilayer interface was quantified by radial distribution functions (rdf) of the ions with selected principal oxygens. The data obtained from the CL-rich IM system is shown in Fig. 5.1. The first hydration shell radius was defined as the distance to the first minimum of the ion-water oxygen rdf. As seen from the peaks inside the first shell, Ca^{2+} binds practically solely to phosphate oxygens. For Na^{+} the situation is more mixed, as binding also to the ester and CL head group oxygens is observed. The matter was further quantified by calculating the coordination numbers of ions with respect to the different oxygens. This was done by integrating the corresponding rdfs until the first-shell radius, i.e. calculating the number of given oxygens inside the first hydration shell. For Ca^{2+} ions, a first-

shell coordination with roughly 3–3.5 water oxygens and 3.5–3.7 phosphate oxygens was found. The numbers for Na^+ ions were lower, 2.8 and 1.8, respectively, as the ions also bound to other oxygens. The Na^+ ions coordinated with 1.1–1.4 ester oxygens and 0.2 CL head group oxygens, while the corresponding numbers for Ca^{2+} ions were negligible. The observation of both phosphate and ester oxygens being the primary binding sites for Na^+ is in agreement with a recent simulation study of CL bilayers with Na^+ counter ions, using a different force field (115).

5.2 Electrostatic potential

Of the rather small changes observed in the electrostatic potential, the one induced by Ca^{2+} on the IM seems the most interesting. In this case the potential is smaller in the bilayer center as compared to the salt-free system, and higher just outside the bilayer (at 3–4 nm). Notably, upon adding Ca^{2+} to the OM system with little CL, the potential difference between the center of bilayer and bulk water stays roughly the same (decrease of 1 %). In the CL-rich IM system, however, the potential difference decreases by 13 % when Ca^{2+} is added. Obviously, the accumulation of ions to the bilayer interface affects the electrostatic potential profile of the system. This effect is partly compensated by the reorientation of the lipid head group dipoles, notably less so in the CL-rich cases due to the small CL head group and restrictions imposed on head groups of other lipids.

The binding of ions to anionic membranes has been shown to either decrease the surface area of the membrane or to leave it unaffected (39, 117, 118). Furthermore interesting for the present study, a small condensing effect of CLs added into a mixed PC-PE-membrane has been observed (114). We could see significant effects neither on the area per lipid nor on the conformational order of the lipid tails, even when the salt concentrations used here (around 0.1 M) were larger than the physiological values (free cytoplasmic Ca^{2+} concentration is about 0.1 μM and can be up to around 10 times larger inside mitochondria) (5, 119–123). Thus we conclude that the effects of salt on these properties are likely marginal in actual mitochondrial membranes.

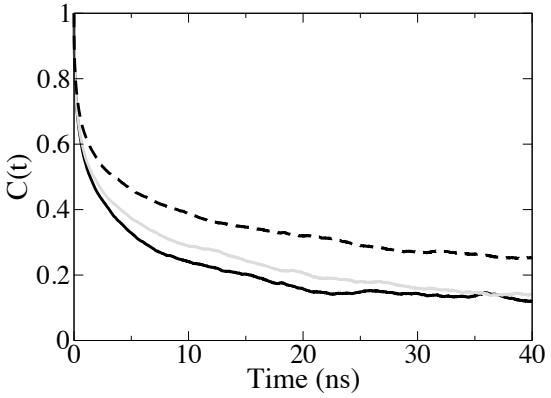

Figure 5.2: Rotational correlation functions of PE headgroups in the inner membrane systems. The pure system is marked with a black line, the one containing Na^+ ions with gray, and the with $CaCl_2$ with a dashed line.

5.3 Lipid dynamics

The effect of CL making the membrane more prone to salt effects is clearly seen when looking at the dynamics of PC and PE head groups. This was done by examining the reorientation of the PN-vectors (from phosphorus to nitrogen) of their head groups, for an example see Fig. 5.2. As seen from the slower decay of $C_2(t)$, the addition of salt restricts the dynamics, more so with $CaCl_2$. Interestingly, the restricting effect of salt is greater in the CL-rich systems. In other words, the dynamics of the head groups already restricted by the presence of CLs are furher restricted by salt addition and this effect is stronger than in the systems with less CLs. The stronger effect in the presence of CL is explained by the shielding of CL charges and the fact that CL restricts the head group dynamics to begin with.

Another way in which adding salt restricts the dynamics of the bilayer is complex formation. As single ions usually bound to more than one lipid, small local cluster were formed, as illustrated in Fig. 5.3. On average, Ca^{2+} formed slightly larger clusters than Na^+ (the life times of the clusters were not calculated by they were of the order of nanoseconds or tens of nanoseconds). Obviously, the complex formation restricts the movement of the lipids in the plane of the membrane. Consequently, a decrease of around 10–30 % in the lateral diffusion coefficient is seen in all systems upon adding salt. Naturally, the effect of Ca^{2+} was stronger. However, it should

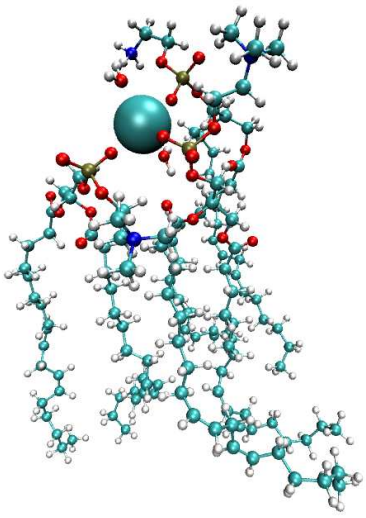

Figure 5.3: Complexes formed by ions interacting with oxygen atoms of lipid and water molecules. Calcium ion is surrounded by 2 water molecules, 2 PCs, and 1 PE. Oxygens are marked red.

be noted that this can be considered only as a local effect, as the physiological concentrations of Ca^{2+} ions are considerably smaller (121). In previous experimental and computational studies, both weak and significant changes in the lateral diffusion coefficient of the lipids have been observed (35, 41, 124).

5.4 Critical assessment and future perspectives

There are only two preceding atomic-scale simulation studies concentrating on the influence of CL on membrane properties: one which introduces the model used here (114) and one study concerning properties of CL/PC mixtures (116). When the CL model was constructed (114), comparison to experimental data was limited due to the small number of suitable research papers available. However, the experimental data that was available showed good agreement (114) and the results of the CL-PC mixture are also generally in line with another simulation study (116). Comparing the results of the present study that examines the effects of salt on a ternary mixture of CL, PC, and PE, is generally difficult since most studies concentrate on systems with one or two components only. However, some previous simulations studies have

yielded similar trends in the presence of salt as observed here. Examples include the decrease of PE and PC head group tilts (50, 125) and similar changes in the electrostatic potential (35, 40, 41). The alteration of the lateral diffusion coefficient as a result of lipid-ion complex formation has been observed both in experimental and computational studies (35, 124), however, here this phenomenon can only be considered at nanoscopic time and length scales. Additionally, the results for binding of Na^+ obtained here are in agreement with those from a recent simulation study of CL bilayers, where a different force field was used (115).

Another issue requiring attention in our model is the charge of CL, which depends on pH and environmental factors, such as the concentration of CLs. Due to the difficulties in determining the charge, the matter is debated and both single and double anionic charges have been suggested (126–128). We have used a double anionic CL in all studies presented in this thesis.

In this study, the lipid composition of the membrane was symmetrical among the two leaflets and the ions were allowed to move freely in the system, i.e. the salt concentration was the same on both sides of the membrane. When considering the real inner mitochondrial membrane, the situation is quite different, as lipids are asymmetrically distributed among the leaflets and ions are not allowed to diffuse freely to both sides of the membrane. These features would likely have a significant effect on e.g. the electrostatic potential and lateral pressure profile across the bilayer (possibly relevant for membrane-embedded proteins) and would hence be interesting to include in future studies.

5.5 Conclusions

The effects of salt are most clearly seen in the dynamic properties of the bilayer, whereas the structural properties, such as area per lipid and conformational order of the acyl chain, are only weakly affected. There were rather weak but possibly significant changes in the electrostatic potential, more so in the CL-rich systems. In the same spirit, the changes in the head group dynamics were also more strongly affected when significant amounts of CLs were present. Thus we conclude that CL indeed does seem to make some aspects of the bilayer more prone to salt effects.

6. THE INTERACTIONS OF CARDIOLIPIN WITH A MEMBRANE-EMBEDDED PROTEIN

Next we broaden our view of cardiolipin to include the interplay of cardiolipin with membrane-associated proteins. While approximately 20–30 % of all genes encode for membrane proteins, only 2 % of the known high-resolution structures are associated with them (58, 59). This is mainly due to the difficulties in crystal production required for structure analysis (129). Furthermore, even with the existing structures it may be questionable as to how much the stressful process of delipidation and crystal formation affect the native protein structure. Also worth noting is the fact that crystal structures only provide a static, frozen picture of a protein, omitting all dynamical phenomena. Consequently, considerable amounts of added value can be expected from molecular dynamics simulation approach, with which we are able to study membrane proteins in their natural environment, embedded in membranes.

Lipids, including both cholesterol and cardiolipin, have been shown to affect the structure and function of various membrane proteins (54, 110). In addition to the influence of the generic membrane properties, such as the hydrophobic thickness and phase behaviour (54, 55), lipids in some cases act through specific interactions and may be essential for the protein's functioning (56). The crystal structures of the cytochrome bc1 complex, one of the respiratory complexes coupling electron transport to proton pumping, have been observed to contain several tightly bound lipids, such as CLs (cardiolipin), PCs (phosphatidylcholine), PEs (phosphatidylethanolamine), and PIs (phosphatidylinositol) (130–135), indicating an integral role for these lipids in the protein's structure and function. Indeed, the enzymatic activity of the protein has been shown to be dependent on the presence of lipids, especially that of CL (60–62, 136, 137). On top of the peculiar structural features and phase behaviour of cardiolipin discussed earlier in this work, CLs are also able to carry out intramem-

brane proton transfer with their acidic head groups (30), making them even more intriguing concerning the proton-pumping respiratory complexes.

In the work described in *Paper III*, we embedded the cyt bc1 complex in its natural lipid environment, see Fig. 6.1. As the surrounding CLs and other lipids, ions, and water molecules were let to diffuse freely, we observed tight incorporation of the lipids into the protein structure. The lipids both cover the surface of the protein and also move inside it. Particularly interesting are the CL molecules, which bind near the reactive sites of the protein, and even form possible proton-uptake pathways with water molecules. The fact that these CLs, when left to diffuse freely, bind to the same spots as observed in crystal structures of different species (130–135, 138, 139), highlights their conserved and crucial role in the structure and function of this protein complex.

6.1 The entering of one cardiolipin inside the protein complex

When simulating a membrane protein in its native lipid environment, close interactions between the lipids and the protein surface can be expected to develop. What surprised the author, however, was the one CL molecule diffusing inside the protein complex, between the two monomers, see Fig. 6.2. As it happens, however, a similar location for a CL molecule has been observed also in the crystal structure of the yeast cyt bc1 complex (139). This location is also shown in the last snapshot of Fig. 6.2. Due to differences between the structures of the bacterial (used in the simulations) and the yeast cyt bc1, the location obtained by superimposing the structures is only approximate. In addition to the one CL we focus on here, other lipid species also entered between the monomers, see Fig. 6.5.

Notably, the CL molecule moved inside the protein in all four simulation setups, traveling a distance of around 20–25 Å from its initial spot, ending up close to the active sites of the protein (as discussed in more detail later). Most of the movement occurred during the first 20–40 ns.

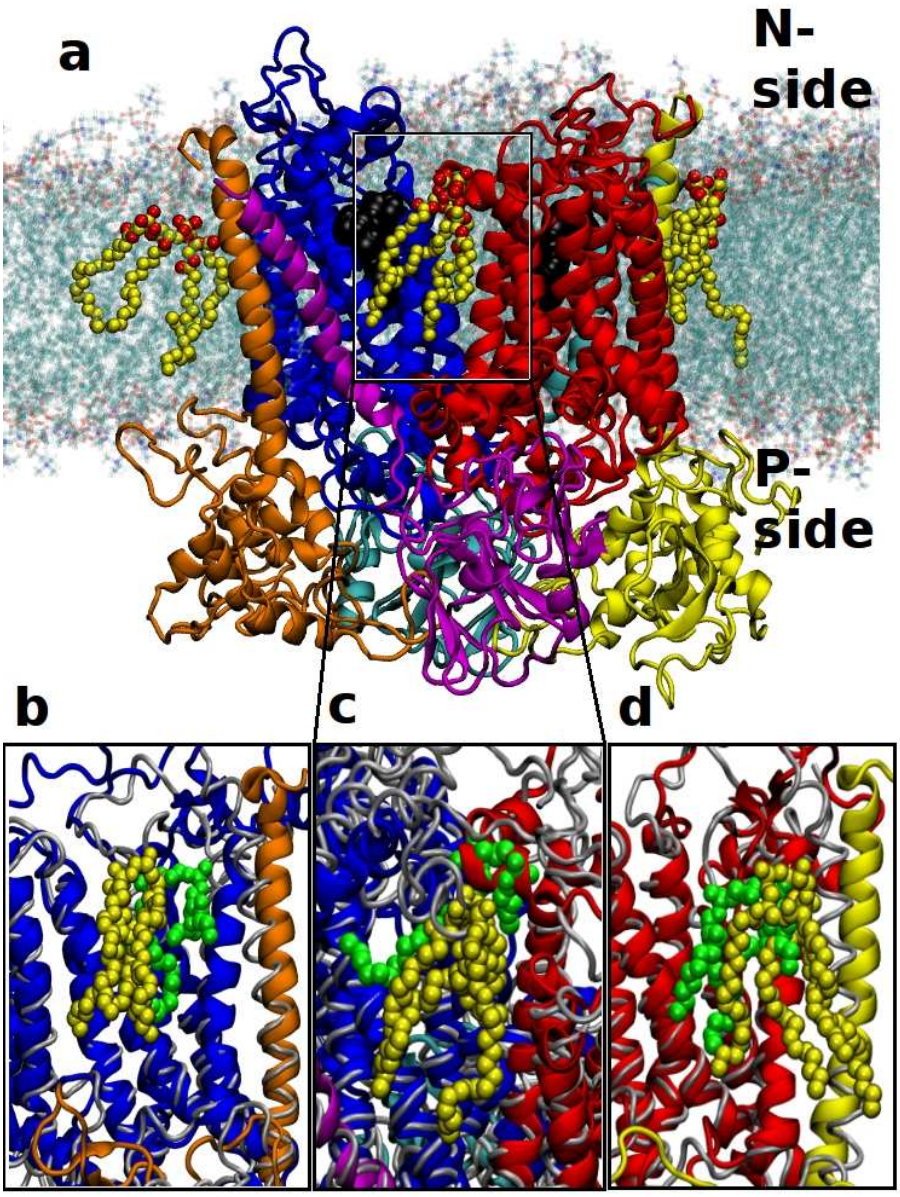

Figure 6.1: Cardiolipin diffuses spontaneously to similar binding sites as observed in X-ray crystal structures. A) The membrane protein studied in this work, the cyt bc1 complex, embedded in a membrane. The three cardiolipins highlighted with yellow (with red oxygens) beads are the main focus of this work. Other lipids are shown only in the background for clarity. N- and P- sides of the membrane refer to the sides from where the protons are taken from (negative side, N) and the side to where they are pumped to (positive side, P). The protein comprises two monomers: A-side (red, yellow, and magenta) and B-side (blue, orange, and cyan). These are further divided into the following subunits: cyt b (red and blue), cyt c1 (yellow and orange), and iron sulfur protein (cyan and magenta) The active sites referred to in the text are in the immediate vicinity of the b_H hemes (black beads). In panels B-D are shown close-up snapshots of the cardiolipin locations versus the locations observed in the crystal structure by Solmaz et al. (cite Solmaz, pdb: 3CX5). The yellow cardiolipin is the one observed in our MD simulations and the green one is from the crystal structure. The positions were obtained by superimposing the protein structures from MD simulations (colored ribbons) with the crystal structure (gray tubes). The different panels are examples of final snapshots of cardiolipin locations

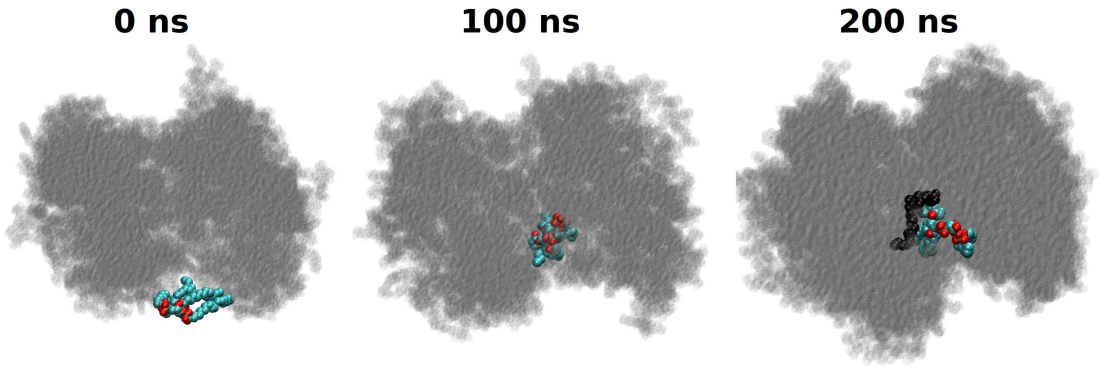

Figure 6.2: One CL molecule (cyan carbond, red oxygens) entering into the protein complex. The protein is shown in transparent grey, as viewed from the N-side. The black CPK-model in the last snapshot represents the approximate location of a CL molecule found in yeast cyt bc1 crystal structure (139). The lipid membrane is omitted for clarity.

A close-up view of the one CL binding inside the protein is shown in Fig. 6.3. As seen from panels b–e, the exact binding residues vary somewhat between the end configurations of different simulations. The closest location to the b_H hemes is reached in the simulations corresponding to panels c and e. Furthermore, as seen from the locations of two secondary structure elements shown as blue and brown cartoon models, the exact binding spot of CL has an effect on the tertiary structure of the protein. Indeed, the CL effectively links the two chains (blue and brown helices) together in the simulations shown in panels c and e. However, once the CL binds to TRP214 and detaches from ARG22 (panel e), the local conformation of the protein changes, quantified by the change between the ARG22 and TRP214 from around 1 nm to 3 nm. In addition, changes in the secondary structure of the protein as a result of CL binding were eagerly searched for. However no major changes, such as helix unwinding, were found, and it would in any case be difficult to analyze these since we do not have control simulations without CL to compare to.

6.2 Binding locations of cardiolipins near the active sites of the protein

In addition to the one CL in the central location, two other CLs bound near the active sites. They are located approximately symmetrically on the sides of the protein (one on the surface of each monomer), see Fig. 6.1. Similar locations to all of these three CLs have been observed in crystal structures from different species

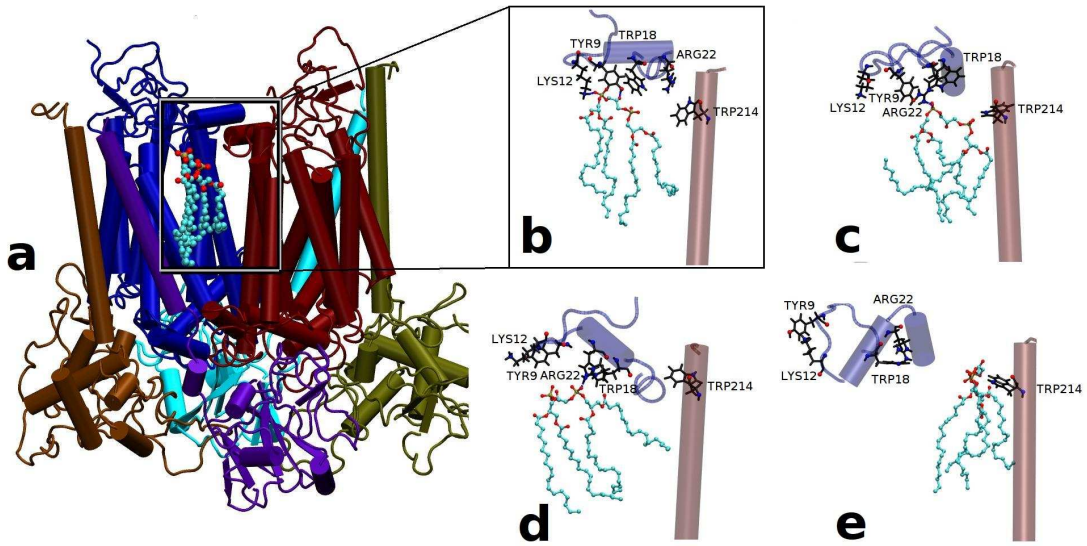

Figure 6.3: Cardiolipin binding inside the protein, as seen with the whole protein showing (a) and close-ups at the end of each simulation (b–e). In b–e panels parts of the protein secondary structure are shown with cartoon models (light red and blue are from different monomers) and the residues which CL binds to are highligted with black color. The carbons of CL are colored cyan, oxygens red, and phosphates brown.

(130–135, 138, 139). It should be noted that comparing the exact binding locations is difficult due to considerable differences in the protein complex structures originating from different species. Nevertheless, a rather good qualitative picture (Fig. 6.1) of the situation is achieved by superimposing selected chains of the simulated structure with that from a crystal structure.

It should be stressed that in our simulations all these CLs moved spontaneously into these locations, as they were let to diffuse freely. As the exact binding residues differ somewhat between the simulation setups, the most informative means to quantify the locations of CLs is based on their distance to the b_H heme groups (measured between then centers of mass of the CL head group phosphorus atoms and the b_H heme group). The CLs indeed bind very close to the b_H heme groups. In the end of the simulations, the two surface-bound CLs are found at distances ranging between 19 and 26 Å (in two cases out of eight the distance was somewhat larger). The centrally located CL was usually closer to one of the heme groups, typically at distances ranging from 18 to 24 Å in the ends of the simulations. The closest distances are well in line with the corresponding ones measured from crystal structures, which are in the range of 19.7–20.0 Å (PDB: 3CX5 (139)) for the central CL and 19.4–19.5 Å

(PDB: 3CX5 (139) PDB: 1KB9 (138)).

6.3 Possible role for cardiolipin in proton-uptake

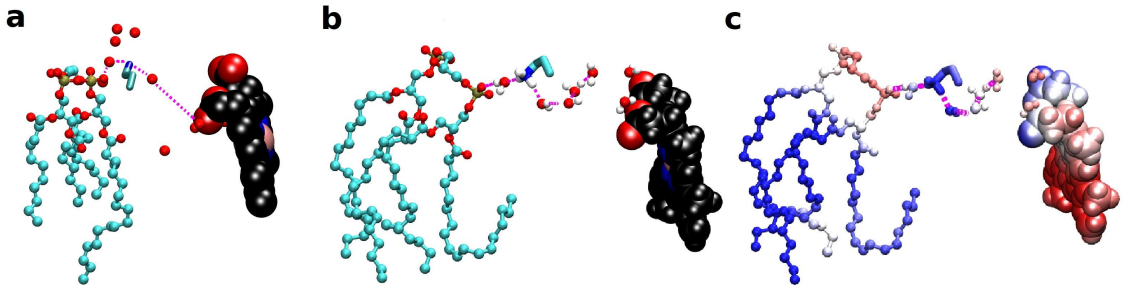

Figure 6.4: Possible proton-uptake pathway formed by CL, lysine, and water, shown in yeast cyt bc1 complex crystal structure (a) (PDB:1KB9 (138)), in our simulations (b), and in our simulations with the colors indicating electrostatic potential values (c, red color indicates negative potential, blue positive, and white neutral). The carbons CL and lysine are colored cyan and those of the b_H black, oxygens red, hydrogens white, nitrogens blue, and phosphates brown. The hydrogen bonds comprising the pathway are marked with magenta lines. Protein residues excluding the one lysine are omitted for clarity.

As the bulk solvent cannot reach the active sites of the protein, some kind of a pathway for the protons to be delivered to the sites is needed (138, 140). Such a connection involving a CL molecule has been suggested based on the yeast cyt bc1 crystal structure (138, 140). The CL bound close to the active site is supposed to pass a proton via a hydrogen-bonded chain of water molecules and a lysine side chain. As a proton moves along this 'wire', it would first hop from the CL head group via water to a nearby lysine and subsequently via water to the reduction reaction of ubiquinone at the active site, see Fig. 6.4a.

Interestingly, we see same kinds of arrangements in our simulations, see Fig. 6.4b. The Figure compares the situations in the crystal structure and the simulations, in both of which one CL, one lysine side chain and several water molecules form a hydrogen-bonded network. The proton would travel from the CL head group through water and lysine to the active site of the protein, marked in the picture with the b_H heme. Similar arrangements were observed in different simulations and part of the time the CL molecule was bound straight to the lysine without intermediate water molecules.

Panel c describes the electrostatic potential in this situation, calculated using

the contribution of all atoms in the system and averaged over the last 1 ns of one of the simulations (such a short period was chosen because the movement of the components in the system quickly averages out the discernable potential differences). The picture qualitatively supports the idea of the anionic CL head group attracting a proton and passing it on to the active site through the conduction pathway. It must be noted, however, that this picture is very qualitative in nature, the potential is displayed on a random molecular surface and the significance of the potential differences, i.e. their magnitude in relation to an ability to attract a proton in a heavily screened environment was not yet thoroughly examined.

The anionic head group of CL has indeed been suggested to deliver protons to the respiratory complexes, i.e. to act as a sink and source of protons in the relevant mitochondrial and bacterial membranes (126). CLs are also known to be able to carry out intramembrane proton transfer (30). In addition CL has been found to have conserved binding sites near the active sites of the cyt bc1 complex in different species. Now the role of CL in the proton uptake is also supported by MD simulation data, as we observed the CLs to freely diffuse to these spots in four independent simulations and form plausible uptake pathways with lysines and water.

6.4 General lipid interactions with the protein

As seen from Fig. 6.5, the packing of the lipids near the protein changes radically during the simulations. In the initial setup there is a hole in the membrane (upper panel on the left in Fig. 6.5) where the protein is embedded (the protein is shown separately on the lower left-side panel). In the end of the simulations, as shown on the right-hand panels, the lipid atoms have closely surrounded the protein and notably also moved inside it. Moreover, lipid atoms can be seen near the higher potential heme groups (b_H, shown in black), marking the places of the protein's reaction centers.

The packing of lipids close to the protein (quantified by counting the number of lipid atoms within a hydrogen bonding distance 0.325 nm of any protein atom) first increases rapidly and subsequently keeps slowly increasing throughout the simulations. We observed no preference for a particular lipid species to be near the protein.

This lack of preference might, however, be due to the slow diffusion of the bulky CL molecules as compared to the limited simulation time.

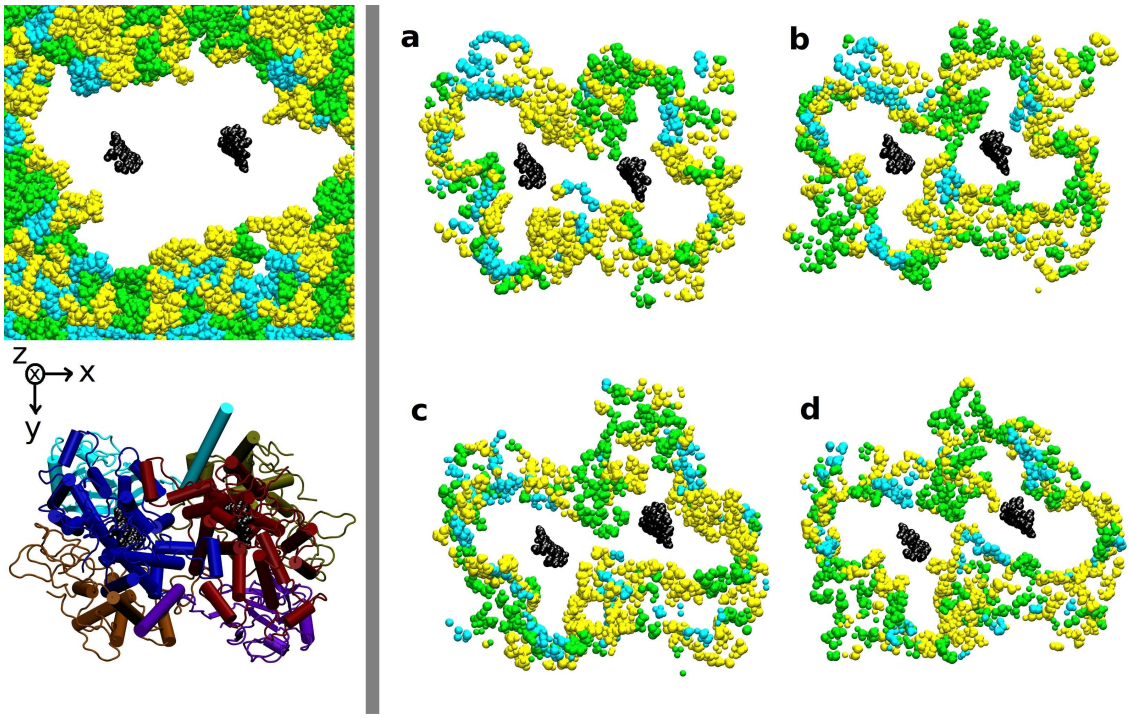

Figure 6.5: A top view (from the N-side of the membrane) to the lipid atoms surrounding the protein complex during the simulations, at the start (on the left, the protein is shown on the bottom), and in the end of every simulation (a–d). The b_H hemes are shown in black and the protein is not shown for clarity. Only CL (cyan), PC (yellow), and PE (green) atoms within 3.25 Å of any protein residue are shown.

So as to get a more detailed picture of the lipid-protein contacs, we analyzed the hydrogen bonding between the lipids and protein residues. A hydrogen bond is defined by geometric criteria, using a cut-off distance of 3.25 Å between the donor and acceptor and a cut-off angle (acceptor-donor-hydrogen) of 30 degrees. The occupancy of a hydrogen bond is determined as a percentage of trajectory frames when the bond exists. Only the hydrogen bonds with occupancies over 1 % are considered.

Because of the hydroxyl groups of CLs and ammonium groups of PEs, they can participate in hydrogen bonding also as donors, unlike PCs which act only as acceptors. When considering the whole simulation time, PCs and PEs form a greater number of but shorter-lived hydrogen bonds as compared to the bulkier and more negatively charged CLs. The life times are quantified by the occupancies of the bonds (the average occupancies of CL/PC/PE bonds are 20/9/14 %). When

considering the average number of hydrogen bonds at a given time step, CL and PE form slightly more hydrogen bonds than their molar concentrations would suggest (as can be expected based on the ability of CL and PE to act also as donors). During the last 10 ns of the simulations, CLs form on average seven hydrogen bonds with protein residues at each time step, as PCs form 23 and PEs 24. Thus, CL-protein hydrogen bonding accounts for 13 % of all hydrogen bonds at a given time step, while PCs account for 42 %, and PEs for 45 % of the bonds (the molar concentrations of CL/PC/PE in the membrane are 12/48/40 %, respectively).

The negatively charged CL molecules bind preferentially to positively charged lysine residues (on average 26 % of hydrogen bonds). This strong preference is evident in all simulations excluding one where tryptophan residues have a slightly stronger preference (26 % of hydrogen bonds). The second favored binding partners are the tryptophan residues forming 18 % of all hydrogen bonds on average. A slight preference for lysine residues is seen also for PC and PE. However, it is not as clear as in the case of CL. Other favored hydrogen bonding partners are tryptophan, asparagine, and tyrosine for PCs, and arginine, serine, and aspartic acid for PEs.

6.5 Tight cardiolipin binding to the protein's surface

A special attention is given to the long-lived hydrogen bonds that the lipids form with protein residues, as we wish to see how many lipids bind strongly to the protein's surface. Here 'long-lived' is defined as a bond with an occupancy of 30 % or more. This value is based on the diffusion behaviour of CLs that was examined in a previous simulation study (*Paper II*): the occupancy of 30 % corresponds to 60 ns (out of a 200 ns trajectory), which is roughly the time it takes for a CL molecule to move across its own area in the membrane plane. While the time would be longer if the diffusion were considered in the immediate vicinity of the protein (141), we expect this value to adequately describe the average lipid diffusion process.

Five tightly bound CLs are found on the protein surface, including the two that are near the active sites, as discussed earlier. In line with experimental results (142), the majority of these (4 out of 5) are on the N side of the membrane and only one on the P side. One of the CLs is particularly strongly bound, it stayed in the same

binding location for a major part of all of the 200 ns simulations. This location of CL also induces minor conformational changes (helix reorientation) in two of the simulations. The long-lived binding of PC and PE are analyzed similarly as that of CL (using the same 30 % cut-off occupancy). Due to the great number of these bonds, the selection is further refined to include only hydrogen bonds that were found in at least three out of the four simulations. Interestingly, half of the tightly bound lipids are on the P side rather than on the N side, as was the case with the tightly bound CLs.

A specific CL-protein binding pattern, designated as XXY, where one molecule would bind to two positively charged residues (XX) and one polar residue Y, was suggested by Palsdottir et al. (142). Accordingly, there is one bound CL molecule in every simulation that follows this pattern (CL binds to two positive lysine residues and a polar asparagine residue). The occupancies vary a lot between simulations, ranging from 6 to 75 % for individual hydrogen bonds. Simultaneous binding to all these residues was observed to happen only momentarily in three simulations. This binding pattern did not occur with the other CL molecules in any of the simulations, which implies that this suggested arrangement is not a generally favored one with the membrane-embedded cyt bc1 complex. Altogether, it is fair to say that we did not find a universal binding pattern for CL.

6.6 Critical assessment and future perspectives

Perhaps the most obvious criticism would be that we do not have control simulations without CL. Instead, every simulation has the same membrane composition. Consequently, it is difficult or even impossible to assign effects such as changes in the protein structure directly to the presence of CL. The effect of the general lipid environment could be discussed but even this is problematic since we are again only comparing simulations with the lipid environment to a crystal structure, and have no simulations e.g. in vacuum or water.

Also, one has to keep in mind the limited length of the simulations (200 ns) when considering the diffusion of the bulky CL molecules. As mentioned earlier, it takes roughly 60 ns for a CL molecule to move across its own area and the movement may

be considerably slower near the protein's surface. Thus one has to be careful when making conclusions e.g. about whether there is a preference for a particular lipid species to be near the protein.

The main finding of this study was the free diffusion of three CL molecules to locations near the active sites of the protein, as has been previously predicted in crystal structures. It should be noted that comparing the exact binding locations is difficult due to considerable differences in the protein complex structures originating from different species. The situation was clarified by measuring the distance of the selected CLs to the active sites and also by superimposing selected chains of the simulated structure with that from a crystal structure (Fig. 6.1).

The uncertainty about the charge state of CL remains, see Chapter 5 for a short discussion.

The most interesting future prospect would (will) be the closer examination of the possible proton-uptake pathways involving cardiolipin. As proton tunneling can not be modeled with the classical approach used in this study, the description here should be accompanied with quantum mechanical calculations.

6.7 Conclusions

Experimental studies of the cyt bc1 crystal structures have revealed conserved binding sites for CL in different species. Moreover, the anionic head group of CL is able to to carry out intramembrane proton transfer (30) and has indeed been suggested to deliver protons to the respiratory complexes (138, 140), i.e. to act as a sink and source of protons in the relevant mitochondrial and bacterial membranes (126). In our MD simulation study, we observe five tightly bound CLs on the surface of the cyt bc1 membrane protein, the majority of which are on the N side of the membrane. Particularly interesting, however, are the three CLs that are observed to diffuse freely into similar locations, as observed in the crystal structures, near the active sites of the protein. One of these occupies a central location between the two monomers of the protein. We conclude that our simulation studies support the proposed integral role of CL in the structure and function of the cyt bc1 complex.

7. THE EFFECT OF ANTIMICROBIAL PEPTIDES ON A CARDIOLIPIN-RICH MEMBRANE

The second example of cardiolipin-protein interactions considered in this work is the interplay of tiny antimicrobial peptides with a cardiolipin-rich membrane. Due to the increasing problems caused by microbes resistant to conventional antibiotics, the search for new antimicrobial agents, such as antimicrobial peptides, is an urgent quest. In the work presented in *Paper IV*, we wished to study two matters regarding the smallest antimicrobial peptide aurein 1.2: the details of its disruption mechanism and the reason for its selectivity against anionic membranes typical for bacterial and cancer cells.

Aurein 1.2 is a tiny peptide with only 13 amino acids, see Fig. 7.1. Consequently, it is too short to span a membrane and has been suggested to act via carpet mechanism (143–145). The findings of several studies are generally in line with the carpet mechanism (see e.g. (146–148)), nevertheless the atomic-scale details of the mechanism remain unknown and it would thus be exciting to see the mechanism happening in MD simulations. It should also be noted that the time scale at which the lysis is expected to occur is not certain, leaving the possibility that our simulations could be too short for the lysis to occur. Previously, MD simulations have already provided substantial added value for studies concerning antimicrobial peptides and related membrane disruption by other mechanisms, see e.g. (149–151).

As a result of the cationic nature of aurein, it is supposed to selectively attack anionic membranes (152, 153). The membrane interactions of aurein have indeed been studied with a range of zwitterionic and anionic bilayers (143, 144), and evidence to support for this claim have been found (145, 146, 152). However, there are also contrary examples, such as aurein disturbing a neutral DMPC membrane more

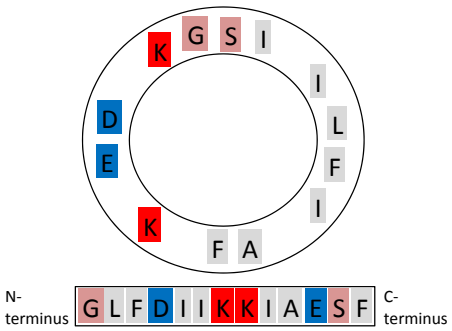

Figure 7.1: Linear sequence and helical wheel (Edmundson projection) representations of aurein. Positive residues are shown in red, negative in blue, polar in light red and hydrophobic in grey. The C-terminus is amidated.

than a partly anionic DMPC/DMPG mixture, and lack of lysis in systems containing DMPC/DMPG/cholesterol, DMPE/DMPC, and *E. coli* extract (contains CL) (145).

CL has indeed been previously suggested to provide protection against antimicrobial peptides (31). This might be due to the unique double lipid structure of CL, which has been suggested to induce greater cohesion in the interfacial region of membranes, leading to greater structural integrity of the bilayer (31).

Despite the suggestions about the protective role of CL, we chose a mixture of CL and PG to achieve an extremely anionic membrane. This was supposed to be an ideal target as possible for aurein and let us see the destruction mechanism on atomic-scale in MD simulations. Instead we saw a significant disruption without membrane lysis, which led us to speculate about the mechanisms of how CL would protect the microbial membranes.

7.1 Helical content of the peptides

We simulated aureins both in water and in association with a membrane. In the first simulations, an ideal helix was used as a starting structure and in the latter ones mainly nonhelical starting conformations picked from the water-simulations were used. When immersed in water, aurein lost and recovered its helical structure multiple times, consistent with the random coil conformation observed in experiments (152). Further in line with experiments (152, 154), the helicity of aurein, that is,

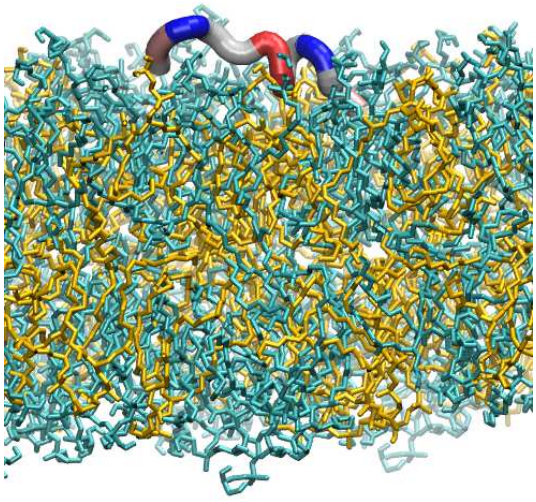

Figure 7.2: A snapshot of one aurein molecule on the bilayer surface. Positive protein residues are shown in red, negative in blue, polar in light red and hydrophobic in grey.

the percent of its residues in helical conformation, increases upon binding to bilayer surface. The helical content of aurein produced by our simulations was, however, only partly in line with experimental data. In our simulations, the helical content with low peptide concentrations (peptide:lipid ratio of 1:100 or 2:100) was roughly around 20–30 %. Experimentally, the helicity has been observed to be around 34–54 % for related peptides (at peptide:lipid ratio of 1:100) interacting with a CL/PG membrane (155). The peptides used in (155), namely aurein 2.2, aurein 2.3 and aurein 2.3-COOH, are slightly longer than aurein 1.2 used in this study and the CL concentration was 50 % of the membrane lipids as opposed to the 25 % used here. The study also observed the helical content to increase with increasing peptide:lipid ratio, up close to 100 % in high peptide concentration. Our simulations fail to produce a similar trend (see the discussion about Fig. 7.4), possibly due to time scale or force field issues.

Aurein in its α-helical conformation has well-defined hydrophilic and hydrophobic regions, as seen from Fig. 7.1. This implies a possible binding mode on the bilayer surface, an example of which is shown in Fig. 7.2. The picture shows a simulation snapshot of one partly helical aurein bound to the surface of the PG-CL membrane. As the overall helicity of aureins in our simulations remained rather low, however, this was by no means the only binding mode observed. In contrast, most of the

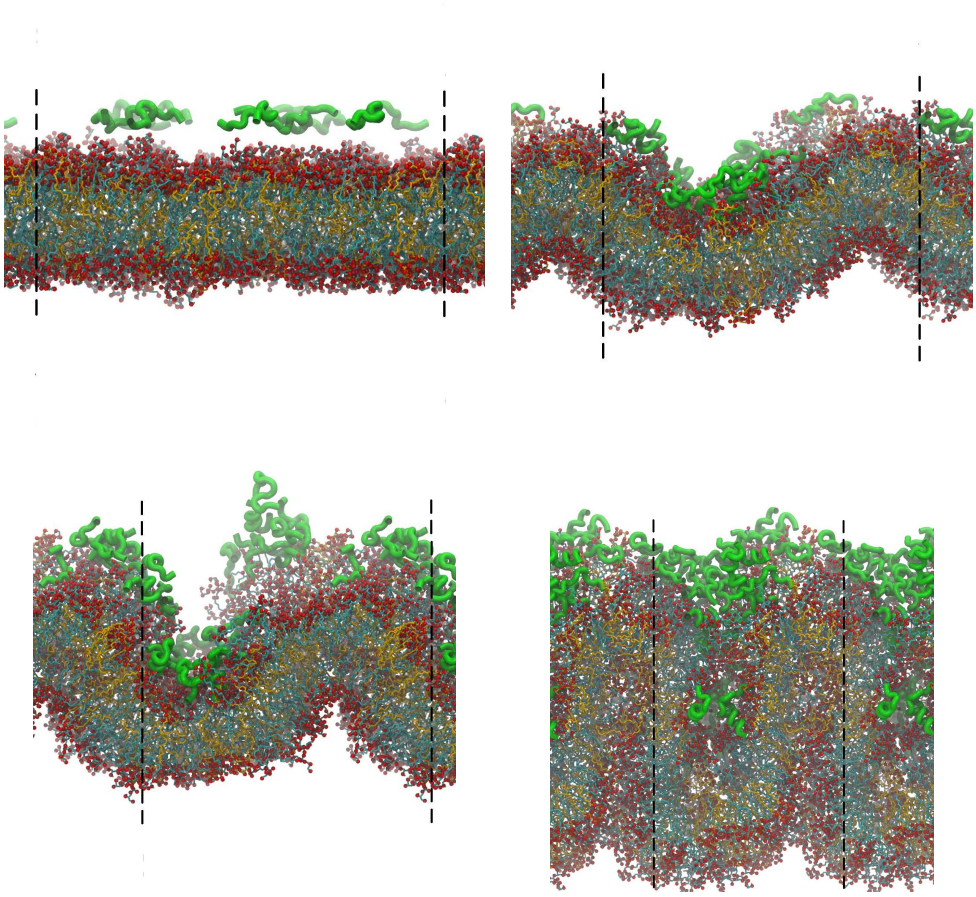

Figure 7.3: The effect of increasing peptide concentration on the bilayer. Snaphots of at 0, 50, 100 and 160 ns, in normal reading order. Dashed lines mark the borders of the periodic box. Peptides are colored green, CL orange, PG cyan, and lipid oxygens red. Water and ions are not shown for clarity.

peptides do not have their hydrophobic and hydrophilic residues as well aligned.

It takes around 10–20 ns for the peptides to move to the bilayer surface and bind there. Once bound, the peptides stick to the bilayer interface, neither moving back to the water nor to the interior of the bilayer. This surface interaction is also supported by experiments (145–148, 152). Notably, the peptides did not show any clear binding preference between CL and PG.

7.2 Membrane curvature

The main purpose of this work was to see mechanism by which aurein lyses the membrane. Instead, when the amount of peptides attacking the membrane were stepwise increased (up to a ratio of 1 peptide to 10 lipids), the membrane adapted

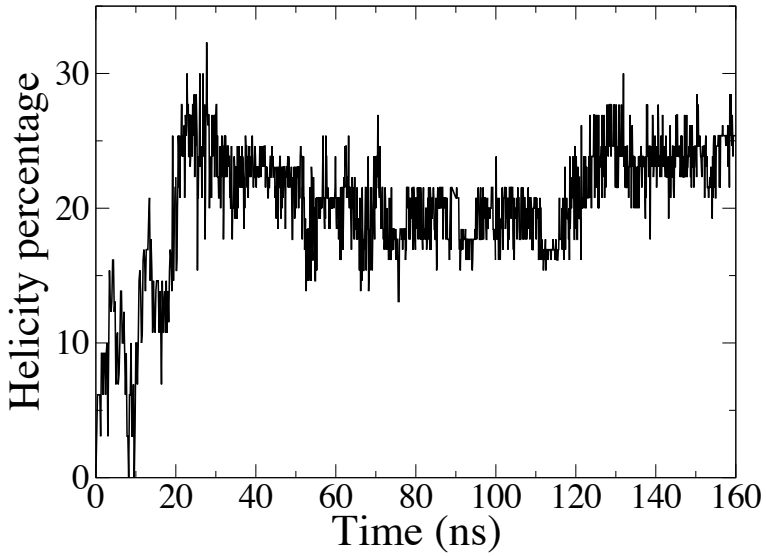

Figure 7.4: Helicity percentage as a function of time of the first 10 aureins added into the system at 0 ns. Aureins bind to the membrane surface during the first 10–20 nanoseconds and the bilayer curvature increases dramatically during the rest of the simulation.

to the situation by increasing its curvature, see Fig. 7.3. Notably also, as the reverse effect was tested, i.e. decreasing the peptide amount on an already curved bilayer, the bilayer flattened again, indicating that the membrane can actually recover from the peptide attack.

Despite high curvature, the membrane was able to retain its bilayer structure. The change in membrane thickness was surprisingly small and no clear leakage of water molecules through the membrane was observed. In addition, the helicity of aureins did not increase even when they were bound to the bilayer for 140–150 ns, see Fig. 7.4. When more peptides were added, helicity first increases but then decreases to a lower level. Towards the end of the simulation, after 120 ns, the helicity increases again to roughly 24 percent. By comparison, the average helicity of the last 10 peptides added over the same time period was only 10 percent. From these results it cannot be concluded that aurein would be more helical with increasing curvature for this type of membrane. It should be noted, however that the fact that our model does not produce more helicity may also the due to the limitations of the modeling procedure itself, such as the limited time scale or a force field which does not produce the helical content correctly.

In summary, aureins were not able to destroy the bilayer structure of the highly anionic PG-CL membrane. Instead, they induced very high membrane curvature.

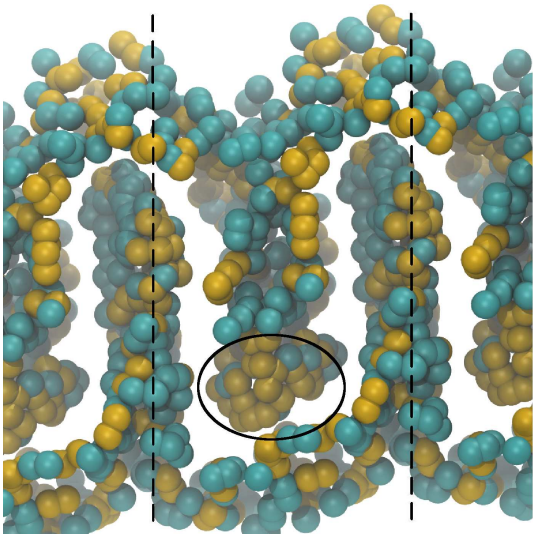

Figure 7.5: A snapshot of the phosphorus atoms at 160 ns. CL atoms are shown in orange and PG atoms in cyan. Note the distribution of CL atoms between areas of different curvature, especially in the circled region of high negative curvature. The difference in membrane integrity between the upper leaflet where the peptides are bound and the lower one without peptides is also clearly visible. Dashed lines mark the borders of the periodic box.

This might naturally be a matter of insufficient peptide concentration, time scale, or box-size effects. On the other hand, also the properties of cardiolipin seem to explain the situation, as explained below.

Due to its unique geometry and anionic charge, CLs are known to form inverted hexagonal structures when neutralized by divalent cations, such as Ca^{2+} and Mg^{2+} (28). Moreover, it has been shown that cardiolipin microdomains gather to regions of high intrinsic negative curvature (32). Fig. 7.5 shows the phosphorus atoms of lipids in the end of the simulation. As can indeed be seen from the distribution, the concentration of cardiolipin molecules in the region of highest negative curvature is nearly 40 percent, significantly larger than the overall concentration of 25 percent. Charge alone, however, is an insufficiently explanation for the induced curvature, as the peptides are monovalent and there are only 40 of them. Before the addition of aureins the bilayer was a stable bilayer, its negative charge neutralized by Na^+ counterions. Furthermore, the charge of the added peptides was compensated by an equivalent addition of Cl^- ions.

Let us presume that aurein acts by imposing positive curvature strain on a membrane and requires an α-helical conformation to function properly. This would be

in line with our results, as it would explain why the presence of negative curvature-inducing lipids, such as CL, inhibits its action. This kind of behaviour has been previously suggested for the antimicrobial peptide magainin (156). Moreover, aureins remained largely unhelical, meaning that aureins could not adopt their ideal amphipathic conformation for attacking the membrane. Interestingly, there were nearly no aureins present in the regions of highest positive curvature, likely due to the smaller lipid surface charge density attracting aureins less than the negatively curved regions.

7.3 Critical assessment and future perspectives

There are two main concerns regarding this study: the helical content of aurein and the credibility of the argument that it is precisely the presence of CL that prevents lysis, and not other issues such as limited time scale, insufficient peptide concentration, or box-size effects. Surely, we also did not do control simulations with CL-free membranes.

The observation that aurein loses and recovers its helical structure multiple times in the simulations of single aurein peptides in water is consistent with the random coil conformation observed in experiments (152). Also the increase of helicity upon binding to a bilayer surface is qualitatively in line with experiments (152, 154), but the actual helical content produced is only partly in line with experiments. Especially at high peptide concentrations, experiments on related (longer) peptides bound to a similar membrane (CL content was double compared this study) showed considerably higher helical content (155). This might be due to the limited time scale or the force field not producing the helical content correctly.

The uncertainty about the charge state of CL remains, see Chapter 5 for a short discussion.

The most obvious future continuation of this study would be to examine the effect of aurein on membranes without CL. This might provide further support for the proposed protective role of CL and more information about the disruption mechanism, which still remains unclear. The use of a more coarse-grained description should be considered to increase the time and length scales of the simulations.

7.4 Conclusions

It has been suggested that the physical characteristics of pure cardiolipin bilayers can largely be explained by the relative rigidity and limited mobility of the head group, leading to greater cohesion in the interfacial region and increased structural integrity of the bilayer (31). Moreover, adding CL into a PC-PE mixture has been shown to condense the bilayer (114). These properties might provide explanations as to why the membrane retained its bilayer-like structure even under considerable disruption. Indeed, CL-containing membranes have been shown to be more resistant to the effects of some antimicrobial peptides than are membranes containing other negatively charged lipids (31). Some organisms are also known to increase the CL content of their membranes in case of resource depletion and halophilic stress (31). Consequently, instead of finding a weapon for humans to use against bacteria, we may have come across a potential mechanism bacteria could use to protect themselves against new antibiotic peptides.

8. CONCLUDING REMARKS

Molecular dynamics simulations can give considerable added value to experiments. They may yield atomic-scale explanations for complex nano-scale phenomena and predictions for cases that have not yet been or cannot be considered through experiments. In this thesis, MD simulations were employed to explore the properties of two lipids in particular, cholesterol and cardiolipin.

Since the synthesis of sterols is a tedious task indeed, the molecular dynamics approach provided us with an easier way of trying out different modified structures and seeing whether the methyl groups could be considered as molecular fossils. The method could be also used to guide experiments, in case some mutations seemed promising they could be further examined experimentally. As it turned out, the methyl groups are important structural elements of cholesterol and we could not find convincing evidence to justify calling them molecular fossils.

Concerning cardiolipin, we came across several interesting features of its function in membranes. Cardiolipin amplified some of the effects that the presence of salt had on our model membrane, particularly affecting the dynamics of the other lipids' head groups. In the study concerning the role of cardiolipin in the structure and function of a membrane protein, cardiolipin turned out to have an integral role in the complex. With the simulation approach, we were able to provide a dynamic view of the whole protein complex in a membrane environment, circumventing the sometimes detrimental effects of experimental procedures such as crystallization. Indeed, we saw cardiolipins to freely diffuse to binding sites which may be important for the proton-uptake of the complex. Finally, our results indicated that cardiolipin may provide a potential protection mechanism against antimicrobial peptides.

Several further research ideas arise from these results. Firstly, further examining the possible proton-uptake pathways involving cardiolipin would be highly interesting. As proton tunneling is a phenomenon involving quantum mechanics,

a hybrid quantum mechanical and molecular dynamics approach should and likely will be used. The study of the antimicrobial peptide aurein should be continued, as its disruption mechanism still remains fairly uncertain. Next step from this study would obviously be the examining of large aurein quantities with cardiolipin-free membranes, both anionic and neutral.

REFERENCES

1. O. G. Mouritsen. *Life -as a matter of fat.* Springer, Berlin, 1 edition, 2005.

2. W. W. Christie, editor. *High-performance liquid chromatography and Lipids: A Practical Guide.* Pergamon Press, Oxford, 1987.

3. B. Alberts, D. Bray, K. Hopkin, A. Johnson, J. Lewis, M. Raff, K. Roberts, and P. Walter. *Essential Cell Biology.* Garland, New York, 2. edition, 2004.

4. R. A. L. Jones. *Soft condensed matter.* Oxford University Press, New York, 2006.

5. D. Bray B. Alberts, J. Lewis, M. Raff, K. Roberts, and J. D. Watson. *Molecular Biology of the Cell.* Garland, New York, 3. edition, 1994.

6. D. E. Vance and H van der Bosch. Cholesterol in the year 2000. *Biochim. Biophys. Acta*, 1529:1–373, 2000.

7. L. K. Li, L. So, and A. Spector. Membrane cholesterol and phospholipid in consecutive concentric sections of human lenses. *J. Lipid Res.*, 26:600–609, 1985.

8. L. Finegold. *Cholesterol in Membrane Models.* CRC Press, Boca Raton, 1993.

9. E. Oldfield and D. Chapman. Effects of cholesterol and cholesterol derivatives on hydrocarbon chain mobility in lipids. *Biochem. Biophys. Res. Commun.*, 43:610–616, 1971.

10. R. A. Haberkorn, R. G. Griffin, M. D. Meadows, and E. Oldfield. Deuterium nuclear magnetic resonance investigation of the dipalmitoyl lecithin-cholesterol-water system. *J. Am. Chem. Soc.*, 99:7353–7355, 1977.

11. S. W. Chiu, E. Jakobsson, R. J. Mashl, and H. L. Scott. Cholesterol induced modifications in lipid bilayers: A simulation study. *Biophys. J.*, 83:1842–1853, 2002.

12. C. Hofsass, E. Lindahl, and O. Edholm. Molecular dynamics simulation of phospholipid bilayers with cholesterol. *Biophys. J.*, 84:2192–2206, 2003.

13. J. Aittoniemi, T. Róg, P. S. Niemela, M. Pasenkiewicz-Gierula, M. Karttunen, and I. Vattulainen. Tilt: major factor in sterols' ordering capability in membranes. *J. Phys. Chem. B Lett.*, 110:25562–25564, 2006.

14. E. Falck, M. Patra, M. Karttunen, M. T. Hyvonen, and I. Vattulainen. Lessons of slicing membranes: Interplay of packing, free area, and lateral diffusion in phospholipid/cholesterol bilayers. *Biophys. J.*, 87:1076–1091, 2004.

15. H. I. Petrache, D. Harries, and V. A. Parsegian. Alteration of membrane rigidity by cholesterol and its metabolic precursors. *Macromol. Symp.*, 219:39–50, 2005.

16. M. Y. El-Sayed, T. A. Guion, and M. D. Fayer. Effect of cholesterol on viscoelastic properties of dipalmitoylphosphatidylcholine multibilayers as measured by a laser-induced ultrasonic probe. *Biochemistry*, 25:4825–4832, 1986.

17. R. Bittman, S. Clejan, S. Lund-Katz, and M. C. Phillips. Influence of cholesterol on bilayers of ester and ether linked phospholipids: permeability and ^{13}C-nuclear magnetic resonance measurements. *Biochim. Biophys. Acta*, 772:117–126, 1984.

18. K. Simons and E. Ikonen. Functional rafts in cell membranes. *Nature*, 387:569–572, 1997.

19. H. R. Waterham, J. Koster, G. J. Romeijn, R. C. Hennekam, P. Vreken, H. C. Andersson, D. R. FitzPatrick, R. I. Kelley, and R. J. Wanders. Mutations in the 3beta-hydroxysterol delta24-reductase gene cause desmosterolosis, an autosomal recessive disorder of cholesterol biosynthesis. *Am.J.Hum.Genet.*, 69:685–694, 2001.

20. D. R. FitzPatrick, J. W. Keeling, M. J. Evans, A. E.Kan, M. E. Poreous, K. Mills, R. M. Winter, and P. T. Clayton. Clinical phenotype of desmosterolosis. *Am.J.Med. Genet.*, 75:145–152, 1998.

21. K. Bloch. The biological synthesis of cholesterol. *Science*, 150:19–28, 1965.

22. K. Bloch. Speculations on the evolution of sterol structure and function. *CRC Crit. Rev. Biochem.*, 7:1–5, 1979.

23. K. Bloch. Sterol structure and membrane function. *CRC Crit. Rev. Biochem.*, 14:47–92, 1983.

24. L. Miao, M. Nielsen, J. Thewalt, J. H. Ipsen, M. Bloom, M. J. Zuckermann, and O. G. Mouritsen. From lanosterol to cholesterol: Structural evolution and differential effects on lipid bilayers. *Biophys. J.*, 82:1429–1444, 2002.

25. M. Bloom and O. G. Mouritsen. *The evolution of membranes, In Handbook of Biological Physics, R. Lipowsky and E. Sackmann, editors.* Elsevier Science, Amsterdam, 1:65-95 edition, 1995.

26. T. Róg and M. Pasenkiewicz-Gierula. Cholesterol effects on the phosphatidylcholine bilayer nonpolar region: A molecular simulation study. *Biophys. J.*, 81:2190–2202, 2001.

27. T. Róg and M. Pasenkiewicz-Gierula. Non-polar interaction between cholesterol and phospholipids: A molecular dynamics simulation study. *Biophys. Chem.*, 107:151–164, 2004.

28. F. L. Hoch. Cardiolipins and biomembrane function. *Biochim. Biophys. Acta*, 1113:71–133, 1992.

29. H. Deguchi, J. A. Fernández, T. M. Hackeng, C. L. Bankadagger, and J. H. Griffin. Cardiolipin is a normal component of human plasma lipoproteins. *Proc. Natl. Acad. Sci. U.S.A.*, 97:1743–1748, 2000.

30. D. Rua M. Schlame and M. L. Greenberg. The biosynthesis and functional role of cardiolipin. *Prog. Lipid Res.*, 39:257–288, 2000.

31. R. N. A. H. Lewis, D. Zweytick, G. Pabst, K. Lohner, and R. N. McElhaney. Calorimetric, x-ray diffraction, and spectroscopic studies of the thermotropic phase behavior and organization of tetramyristoyl cardiolipin membranes. *Biophys. J.*, 92:3166–3177, 2007.

32. L. D. Renner and D. B. Weibel. Cardiolipin microdomains localize to negatively curved regions of escherichia coli membranes. *PNAS*, 108:6264–6269, 2011.

33. M. Zhang, E. Mileykovskaya, and W. Dowhan. Gluing the respiratory chain together. *J. Biol. Chem.*, 277:43553–43556, 2002.

34. T. H. Haines and N. A. Dencher. Cardiolipin: A proton trap for oxidative phosphorylation. *FEBS Lett.*, 26508:1–5, 2002.

35. R. A. Böckmann, A. Hac, T. Heimburg, and H. Grubmüller. Effect of sodium chloride on a lipid bilayer. *Biophys. J.*, 85:1647–1655, 2003.

36. P. Nelson. *Biological physics*. W. H. Freeman and Company, New York, 1. edition, 2004.

37. G. Cevc. Membrane electrostatics. *Biochim Biophys Acta*, 1031:311–382, 1990.

38. G. Pabst, A. Hodzic, J. Strancar, S. Danner, M. Rappolt, and P. Laggner. Rigidification of neutral lipid bilayers in the presence of salts. *Biophys. J.*, Published ahead of print, 2007.

39. P. Mukhopadhyay, L. Monticelli, and D. P. Tieleman. Molecular dynamics simulation of a palmitoyl-oleoyl phosphatidylserine bilayer with Na^+ counterions and NaCl. *Biophys. J.*, 86:1601 – 1609, 2004.

40. S. A. Pandit, David Bostick dagger, and Max L. Berkowitz. Molecular dynamics simulation of a dipalmitoylphosphatidylcholine bilayer with NaCl. *Biophys. J.*, 84:3743–3750, 2003.

41. M. S. Miettinen, A. A. Gurtovenko, I. Vattulainen, and M. Karttunen. Ion dynamics in cationic lipid bilayer systems in saline solutions. *J. Phys. Chem. B*, 113:9226–9234, 2009.

42. A. A. Gurtovenko and I. Vattulainen. Effect of NaCl and KCl on phosphatidylcholine and phosphatidylethanolamine lipid membranes: Insight from atomic-scale simulations for understanding salt-induced effects in the plasma membrane. *J. Chem. Phys.*, 112:1953–1962, 2008.

43. H. I. Petrache, S. Tristram-Nagle, D. Harries, N. Kucerka, J. F. Nagle, and V. A. Parsegian. Swelling of phospholipids by monovalent salt. *J. Lipid Res.*, 47:302–309, 2006.

44. J. R. Rydall and P. M. Macdonald. Investigation of anion binding to neutral lipid membranes using ^2H NMR. *Biochemistry*, 31:1092–1099, 1992.

45. M. F. Brown and J. Seelig. Ion-induced changes in head group conformation of lecithin bilayers. *Nature*, 269:721–723, 1977.

46. P. M. Macdonald and J. Seelig. Anion binding to neutral and positively charged lipid membranes. *Biochemistry*, 27:6769–75, 1988.

47. M. Roux and M. Bloom. Ca^{2+}, Mg^{2+}, Li^+, Na^+, and K^+ distributions in the headgroup region of binary membranes of phosphatidylcholine and phosphatidylserine as seen by deuterium NMR. *Biochemistry*, 29:7077–7089, 1990.

48. M. E. Loosley-Millman, R. P. Rand, and V. A. Parsegian. Effects of monovalent ion binding and screening on measured electrostatic forces between charged phospholipid bilayers. *Biophys J*, 40:221–232, 1982.

49. R. J. Clarke and C. Lüpfert. Influence of anions and cations on the dipole potential of phosphatidylcholine vesicles: A basis for the Hofmeister effect. *Biophys J*, 76:2614–2624, 1999.

50. J. N. Sachs, H. Nanda, H. I. Petrache, and T. B. Woolf. Changes in phosphatidylcholine headgroup tilt and water order induced by monovalent salts: Molecular dynamics simulations. *Biophys. J.*, 86:3772–3782, 2004.

51. J. N. Sachs and T. B. Woolf. Understanding the Hofmeister effect in interactions between chaotropic anions and lipid bilayers: Molecular dynamics simulations. *J. Am. Chem. Soc.*, 125:8742–8743, 2003.

52. H. Akutsu and T. Nagamori. Conformational analysis of the polar head group in phosphatidylcholine bilayers: a structural change induced by cations. *Biochemistry*, 30:4510–4516, 1991.

53. J. Seelig, P. M. Macdonald, and P. G. Scherer. Phospholipid headgroups as sensors of electric charge in membranes. *Biochemistry*, 26:7535–7541, 1987.

54. R. Phillips, T. Ursell, Paul Wiggins, and P. Sens. Emerging roles for lipids in shaping membrane-protein function. *Nature*, 459:379–385, 2009.

55. A. G. Lee. How lipids affect the activities of integral membrane proteins. *Biochim. Biophys. Acta*, 1666:62–87, 2004.

56. C. Hunte and S. Richers. Lipids and membrane protein structures. *Curr. Opin. Struct. Biol.*, 18:406–411, 2008.

57. T. J. McIntosh and S. Simon. Roles of bilayer material properties in function and distribution of membrane proteins. *Annu. Rev. Biophys. Biomol. Struct.*, 35:177–98, 2006.

58. R. Arias-Cartin, S. Grimaldi, P. Arnoux, B. Guigliarelli, and A. Magalon. Cardiolipin binding in bacterial respiratory complexes: Structural and functional implications. *Biochim. Biophys. Acta*, in press, 2012.

59. P. Raman, V. Cherezov, and M. Caffrey. The membrane protein data bank. *Cell Mol. Life Sci.*, 63:36–51, 2006.

60. H. Schagger, T. Hagen, B. Roth, U. Brandt, T. A. Link, and G. von Jagow. Phospholipid specificity of bovine heart bc1 complex. *Eur. J. Biochem.*, 190:123–130, 1990.

61. M. Fry and D. E. Green. Cardiolipin requirement for electron transfer in complex i and iii of the mitochondrial respiratory chain. *J. Biol. Chem.*, 256:1874–80, 1981.

62. B. GomezJr. and N. C. Robinson. Phospholipase digestion of bound cardiolipin reversibly inactivates bovine cytochrome bc1. *Biochemistry*, 38:9031–9038, 1999.

63. A. Giuliani, G. Pirri, and S. F. Nicoletto. Antimicrobial peptides: An overview of a promising class of therapeutics. *Cent. Eur. J. Biol.*, 2:1–33, 2007.

64. M. Zasloff. Antimicrobial peptides of multicellular organisms. *Nature*, 415:389–395, 2002.

65. Y. Pouny, D. Rapaport, A. Mor, P. Nicolas, and Y. Shai. Interaction of antimicrobial dermaseptin and its fluorescently labeled analogues with phospholipid membranes. *Biochemistry*, 31:12416–12423, 1992.

66. E. F. Haney, S. Nathoo, H. J. Vogel, and E. J. Prenner. Induction of non-lamellar lipid phases by antimicrobial peptides: A potential link to mode of action. *Chemistry and Physics of Lipids*, 163:82–93, 2010.

67. B. Bechinger. Rationalizing the membrane interactions of cationic amphipathic antimicrobial peptides by their molecular shape. *Curr. Opin. Colloid Interface Sci.*, 14:349–355, 2009.

68. R. M. Dawson and C. Q. Liu. Cathelicidin peptide smap-29: Comprehensive review of its properties and potential as a novel class of antibiotics. *Drug Dev. Res.*, 70:481–498, 2009.

69. R. Chen and A. E. Mark. The effect of membrane curvature on the conformation of antimicrobial peptides: implications for binding and the mechanism of action. *Eur. Biophys. J.*, 40:545–553, 2011.

70. D. Ardail, J. Privat, M. Egret-Charlier, C. Levrat, F. Lerme, and P. Louisot. Mitochondrial contact sites. Lipid composition and dynamics. *J. Biol. Chem.*, 265:18797–18802, 1990.

71. P. Mitchell. Coupling of phosphorylation to electron and hydrogen transfer by a chemio-osmotic type of mechanism. *Nature*, 191:144, 148.

72. T. Schlick. *Molecular modeling and simulation*. Springer, New York, 1. edition, 2002.

73. H. J. C. Berendsen, D. van der Spoel, and R. van Drunen. Gromacs: A message-passing parallel molecular dynamics implementation. *Comp. Phys. Comm.*, 91:43–56, 1995.

74. E. Lindahl, B. Hess, and D. van der Spoel. Gromacs 3.0: A package for molecular simulation and trajectory analysis. *J. Mol. Mod.*, 7:306–317, 2001.

75. W. L. Jorgensen and J. Tirado-Rives. The OPLS potential functions for proteins. energy minimizations for crystals of cyclic peptides and crambin. *J. Am. Chem. Soc.*, 110:1657–1666, 1988.

76. B. Hess, H. Bekker, H. J. C. Berendsen, and J. G. E. M. Fraaije. Lincs: A linear constraint solver for molecular simulations. *J. Comp. Chem.*, 18:1463–1472, 1997.

77. M. Patra, M. Karttunen, M. T. Hyvönen, , E. Falck, P. Lindqvist, and I. Vattulainen. Molecular dynamics simulations of lipid bilayers: Major artifacts due to truncating electrostatic interactions. *Biophys. J.*, 84:3636–3645, 2003.

78. L. Onsager. Electric moments of molecules in liquids. *J. Am. Chem. Soc.*, 58:1486–1493, 1936.

79. U. Essman, L. Perera, M. L. Berkowitz, H. L. T. Darden, and L. G. Pedersen. A smooth particle-mesh Ewald method. *J. Chem. Phys.*, 103:8577–8592, 1995.

80. M. Patra, M. T. Hyvonen, E. Falck, M. Sabouri-Ghomi, I. Vattulainen, and M. Karttunen. Long-range interactions and parallel scalability in molecular simulations. *Computer Physics Communications*, pages 14–22, 2007.

81. R. W. Hockney, S. P. Goel, and J. W. Eastwood. Quiet high-resolution computer models of a plasma. *J. of Comp. Phys.*, 14:148–158, 1974.

82. D. Frenkel and B. Smit. *Understanding molecular simulation.* Academic Press, San Diego, 1996.

83. H. J. C. Berendsen, J. P. M. Postma, A. DiNola, and J. R. Haak. Molecular dynamics with coupling to an external bath. *J. Chem. Phys.*, 81:3684–3690, 1984.

84. M. P. Allen and D. J. Tildesley. *Computer simulation of liquids.* Oxford University Press, New York, 1987.

85. G. Bussi, T. Zykova-Timan, and M. Parrinello. Isothermal-isobaric molecular dynamics using stochastic velocity rescaling. *The Journal of Chemical Physics*, 130(7):074101, 2009.

86. M. Parrinello and A. Rahman. Polymorphic transitions in single crystals: A new molecular dynamics method. *J. Appl. Phys.*, 52:7182–7190, 1981.

87. S. Nóse and M. L. Klein. Constant pressure molecular dynamics for molecular systems. *Mol. Phys.*, 50:1055–1076, 1983.

88. J. F. Nagle and S. Tristram-Nagle. Structure of lipid bilayers. *Biochim. Biophys. Acta*, 1469:159–195, 2000.

89. S. Tristram-Nagle and J. F. Nagle. Lipid bilayers: Thermodynamics, structure, fluctuations, and interactions. *Chem. Phys. Lipids*, 127:3–14, 2004.

90. H. I. Petrache, S. W. Dodd, and M. F. Brown. Area per lipid and acyl length distributions in fluid phosphatidylcholines determined by ^{2}H NMR spectroscopy. *Biophys. J.*, 79:3172–3192, 2000.

91. D. P. Tieleman, S. J. Marrink, and H. J. C. Berendsen. A computer perspective of membranes: Molecular dynamics studies of lipid bilayer systems. *Biochim. Biophys. Acta*, 1331:235–270, 1997.

92. E. Lindahl and O. Edholm. Molecular dynamics simulation of NMR relaxation rates and slow dynamics in lipid bilayers. *J. Chem. Phys.*, 115:4938–4950, 2001.

93. K. Merz and B. Roux, editors. *Biological membranes*. Birkhauser, Boston, 1996.

94. H. Brockman. Dipole potential of lipid membranes. *Chem. Phys. Lipids*, 73:57, 1994.

95. J. Wohlert and O. Edholm. Dynamics in atomistic simulations of phospholipid membranes: Nuclear magnetic resonance relaxation rates and lateral diffusion. *J. Chem. Phys.*, 125:204703, 2006.

96. T. Fujiwara, K. Ritchie, H. Murakoshi, K. Jacobson, and A. Kusumi. Phospholipids undergo hop diffusion in compartmentalized cell membrane. *J. Cell Biol.*, 157:1071–1081, 2002.

97. G. Oradd and G. Lindblom. Lateral diffusion studied by pulsed field gradient nmr on oriented lipid membranes. *Magn. Reson. Chem.*, 42:123–131, 2004.

98. P. Schwille, J. Korlach, and W. W. Webb. Fluorescence correlation spectroscopy with single-molecule sensitivity on cell and model membranes. *Cytometry*, 36:176–182, 1999.

99. P. F. F Almeida, W. L. C Vaz, and T. E. Thompson. Lateral diffusion in the liquid phases of dimyristoylphosphatidylcholine/cholesterol lipid bilayers: A free volume analysis. *Biochemistry*, 31:6739–6747, 1992.

100. H. I. Petrache, K. Tu, and J. F. Nagle. Analysis of simulated NMR order parameters for lipid bilayer structure determination. *Biophys. J.*, 76:2479–2487, 1999.

101. M. Bloom, E. Evans, and O. G. Mouritsen. Physical properties of the fluid lipid-bilayer component of cell membranes. *Q. Rev. Biophys.*, 24:293–397, 1991.

102. S. Vainio, M. Jansen, M. Koivusalo, T. Róg, M. Karttunen, I. Vattulainen, and E. Ikonen. Desmosterol cannot replace cholesterol in lipid rafts. *J. Biol. Chem.*, 281:1121–1135, 2006.

103. T. Róg, M. Pasenkiewicz-Gierula, I. Vattulainen, and M. Karttunen. What happens if cholesterol is made smoother: Importance of methyl substituents in cholesterol ring structure on phosphatidylcholine-sterol interaction. *Biophys. J.*, 92:3346–3357, 2007.

104. C. Yang, J. G. McDonald, A. Patel, Y. Zhang, M. Umetani, F. Xu, E. J. Westover, D. F. Covey, D. J. Mangelsdorf, J. C. Cohen, and H. H. Gobbs. Sterol intermediates from cholesterol biosynthetic pathway as liver X receptor ligands. *J. Biol. Chem.*, 281:27816–27826, 2006.

105. Z. Y. Cai and D. F. Covey. A facil total synthesis of *ent*-17β-estradiol and structurally related analogues. *Steroids*, 72:351–359, 2007.

106. S. D. Rychnovsky and D. E. Mickus. Synthesis of *ent*-cholesterol, the unnatural enantiomer. *J. Org. Chem.*, 57:2732–2736, 1992.

107. E. J. Westover and D. F. Covey. The enantiomer of cholesterol. *J. Membr. Biol.*, 202:61–72, 2004.

108. T. J. McIntosh. The effect of cholesterol on the structure of phosphatidylcholine bilayers. *Biochim. Biophys. Acta*, 513:43–58, 1978.

109. D. Lingwood, B. Binnington, T. Róg, I. Vattulainen, M. Grzybek, U. Coskun, C. A. Lingwood, and K. Simons. Cholesterol modulates glycolipid conformation and receptor activity. *Nature Chemical Biology*, 7:260–262, 2011.

110. R. M. Epand. Cholesterol and the interaction of proteins with membrane domains. *Progress in Lipid Research*, 45(4):279 – 294, 2006.

111. H.-J. Kaiser, A. Orlowski, T. Róg, T. K. M. Nyholm, W. Chai, T. Feizi, D. Lingwood, I. Vattulainen, and K. Simons. Lateral sorting in model membranes by cholesterol-mediated hydrophobic matching. *Proceedings of the National Academy of Sciences*, 2011.

112. H. Martinez-Seara, T. Róg, M. Karttunen, I. Vattulainen, and R. Reigada. Cholesterol induces specific spatial and orientational order in cholesterol/phospholipid membranes. *PLoS ONE*, 5(6):e11162, 06 2010.

113. M. Dahlberg. Polymorphic phase behavior of cardiolipin derivatives studied by coarse-grained molecular dynamics. *J. Phys. Chem. B*, 111:7194–7200, 2007.

114. T. Róg, H. Martinez-Seara, R. Reigada, N. Munck, M. Oresic, M. Karttunen, and I. Vattulainen. Role of cardiolipins in lipid bilayer structure - properties of water membrane interface. *J. Phys. Chem. B*, 113:3413–3422, 2009.

115. D. Aguayo, F. D. González-Nilo, and C. Chipot. Insight into the properties of cardiolipin containing bilayers from molecular dynamics simulations, using a hybrid all-atom/united-atom force field. *Journal of Chemical Theory and Computation*, 8:1765–1773, 2012.

116. M. Dahlberg and A. Maliniak. Molecular dynamics simulations of cardiolipin bilayers. *J. Phys. Chem. B*, 112:11655–11663, 2008.

117. S. A. Pandit and M. L. Berkowitz. Molecular dynamics simulation of dipalmitoylphosphatidylserine bilayer with Na^+ counterions. *Biophys. J.*, 82:1818–1827, 2002.

118. U. R. Pedersen, C. Leidy, P. Westh, and G. H. Peters. The effect of calcium on the properties of charged phospholipid bilayers. *Biochim Biophys Acta*, 1758:573–582, 2006.

119. P. Donoso, J. G. Mill, S. C. O'Neill, and D. A. Eisner. Fluorescence measurements of cytoplasmic and mitochondrial sodium concentration in rat ventricular myocytes. *J. Physiol.*, 448:493–509, 1992.

120. S. Baron, A. Caplanusi, M. van de Ven, M. Radu, S. Despa, I. Lambrichts, M. Ameloot, P. Steels, and I. Smets. Role of mitochondrial Na^+ concentration, measured by corona red, in the protection of metabolically inhibited MDCK cells. *J. Am. Soc. Nephrol.*, 16:3490–3497, 2005.

121. S. Chalmers and D. Nicholls. The relationship between free and total calcium concentrations in the matrix of liver and brain mitochondria. *J. Biol. Chem.*, 278:19062–19070, 2002.

122. P. Bernardi. Mitochondrial transport of cations: channels, exhangers and permeability transition. *Physiol. Rev.*, 79:1127–1155, 1999.

123. H. Miyata, H. S. Silverman, S. J. Sollot, E. G. Lakatta, M. D. Stern, and R. G. Hansford. Measurement of mitochondrial free Ca^{2+} concentration in living single rat cardiac myocytes. *Am. J. Physiol. Heart Circ. Physiol.*, 261:1123–1134, 1991.

124. A. A. Gurtovenko. Asymmetry of lipid bilayers induced by monovalent salt: Atomistic molecular-dynamics study. *J. Chem. Phys.*, 122:244902, 2005.

125. W. Zhao, T. Rog, A. Gurtovenko, I. Vattulainen, and M. Karttunen. Role of phosphatidylglycerols in the stability of bacterial membranes. *Biochimie*, 90:930–938, 2008.

126. T. H. Haines and N. A. Dencher. Cardiolipin: A proton trap for oxidative phosphorylation. *FEBS Lett.*, 26508:1–5, 2002.

127. S. Nichols-Smith and T. Kuhl. Electrostatic interactions between model mitochondrial membranes. *Colloids Surf. B-Biointerfaces*, 41:121–127, 2005.

128. M. Dahlberg, A. Marini, B. Mennucci, and A. Maliniak. Quantum chemical modeling of the cardiolipin headgroup. *J. Phys. Chem. A*, 114:4375–4387, 2010.

129. M. Caffrey. Membrane protein crystallization. *J. Struct. Biol.*, 142:108–132, 2003.

130. Z. Zhang, L. S. Huang, V. M. Shulmeister, Y. I. Chi, K. K. Kim, L. W. Hung, A. R. Crofts, E. A. Berry, and S. H. Kim. Electron transfer by domain movement in cytochrome bc1. *Nature*, 392:677–684, 1998.

131. H. Palsdottir, C. G. Lojero, B. L. Trumpower, and C. Hunte. Structure of the yeast cytochrome bc1 complex with a hydroxyquinone anion Qo site inhibitor bound. *J. Biol. Chem.*, 278:31303–31311, 2003.

132. L. S. Huang, D. Cobessi, E. Y. Tung, and E. A. Berry. Binding of the respiratory chain inhibitor antimycin to the mitochondrial bc1 complex: A new crystal structure reveals an altered intramolecular hydrogen-bonding pattern. *J. Mol. Biol.*, 351:573–597, 2005.

133. E. A. Berry, L. S. Huang, D. W. Lee, F. Daldal, K. Nagai, and N. Minagawa. Ascochlorin is a novel, specific inhibitor of the mitochondrial cytochrome bc1 complex. *Biochim. Biophys. Acta*, 1797:360–370, 2010.

134. E. A. Berry, Z. Zhang, H. D. Bellamy, and L. Huang. Crystallographic location of two Zn^{2+}-binding sites in the avian cytochrome bc(1) complex. *Biochim. Biophys. Acta*, 1459:440–448, 2000.

135. L. Esser, B. Quinn, Y. F. Li, M. Zhang, M. Elberry, L. Yu, C. A. Yu, and D. Xia. Crystallographic studies of quinol oxidation site inhibitors: A modified classification of inhibitors for the cytochrome bc(1) complex. *J. Mol. Biol.*, 341:281–302, 2004.

136. T. Wenz, R. Covian, P. Hellwig, F. MacMillan, B. Meunier, B. L. Trumpower, and C. Hunte. Mutational analysis of cytochrome b at the ubiquinol oxidation site of yeast complex iii. *J. Biol. Chem.*, 282:3977–3988, 2007.

137. T. Wenz, R. Hielscher, P. Hellwig, H. Schägger, S. Richers, and C. Hunte. Role of phospholipids in respiratory cytochrome bc1 complex catalysis and supercomplex formation. *Biochim. Biophys. Acta*, 1787:609–616, 2009.

138. C. Lange, J. H. Nett, B. L. Trumpower, and C. Hunte. Specific roles of protein-phospholipid interactions in the yeast cytochrome bc1 complex structure. *EMBO J.*, 20:6591–6600, 2001.

139. S. R. N. Solmaz and C. Hunte. Structure of complex iii with bound cytochrome c in reduced state and definition of a minimal core interface for electron transfer. *J. Biol. Chem.*, 283:17542–17549, 2008.

140. C. Hunte, H. Palsdottir, and B. L. Trumpower. Protonmotive pathways and mechanisms in the cytochrome bc1 complex. *FEBS Lett.*, 545:39–46, 2003.

141. P.S. Niemela, M.S. Miettinen, L. Monticelli, H. Hammaren, P. Bjelkmar, T. Murtola, E. Lindahl, and I. Vattulainen. Membrane proteins diffuse as dynamic complexes with lipids. *J. Am. Chem. Soc.*, 132:7574–7575, 2010.

142. H. Palsdottir and C. Hunte. Lipids in membrane protein structures. *Biochim. Biophys. Acta*, 1666:2–18, 2004.

143. M. P. Boland and F. Separovic. Membrane interactions of antimicrobial peptides from australian tree frogs. *Biochim. Biophys. Acta*, 1758:1178–1183, 2006.

144. D. I. Fernandez, J. D. Gehman, and F. Separovic. Membrane interactions of antimicrobial peptides from australian frogs. *Biochim. Biophys. Acta*, 1788:1630–1638, 2009.

145. T. Lee, C. Heng, M. J. Swann, J. D. Gehman, F. Separovic, and M. Aguilar. Real-time quantitative analysis of lipid disordering by aurein 1.2 during membrane adsorption, destabilisation and lysis. *Biochim. Biophys. Acta*, 1798:1977–1986, 2010.

146. A. Mechler, S. Praporski, K. Atmuri, M. Boland, F. Separovic, and L. L. Martin. Specific and selective peptide-membrane interactions revealed using quartz crystal microbalance. *Biophys. J.*, 93:3907–3916, 2007.

147. J. D. Gehman, F. Luc, K. Hall, T-H Lee, M. P. Boland, T. L. Pukala, J. H. Bowie, M-I Aguilar, and F. Separovic. Effect of antimicrobial peptides from australian tree frogs on anionic phospholipid membranes. *Biochemistry*, 47:8557–8565, 2008.

148. E. E. Ambroggio, F. Separovic, J. H. Bowie, G. D. Fidelio, and L. A. Bagatolli. Direct visualization of membrane leakage induced by the antibiotic peptides: Maculatin, citropin, and aurein. *Biophys. J.*, 89:1874–1881, 2005.

149. A. A. Gurtovenko, J. Anwar, and I. Vattulainen. Defect-mediated trafficking across cell membranes: Insights from in silico modeling. *Chemical Reviews*, 110:6077–6103, 2010.

150. H. Leontiadou, A. E. Mark, and S. J. Marrink. Antimicrobial peptides in action. *J. Am. Chem. Soc.*, 128:12156–61, 2006.

151. P. L. Rocca, P. C. Biggin, P. Tieleman, and M. S. P. Sansom. Simulation studies of the interaction of antimicrobial peptides and lipid bilayers. *Biochim. Biophys. Acta*, 1462:185–200, 1999.

152. G. W.J. Seto, S. Marwaha, D. M. Kobewka, R. N.A.H. Lewis, F. Separovic, and R. N. McElhaney. Interactions of the australian tree frog antimicrobial peptides aurein 1.2, citropin 1.1 and maculatin 1.1 with lipid model membranes: Differential scanning calorimetric and Fourier transform infrared spectroscopic studies. *Biochim. Biophys. Acta*, 1768:2787–2800, 2007.

153. S. R. Dennison, F. Harris, and D. A. Phoenix. The interactions of aurein 1.2 with cancer cell membranes. *Biophys. Chem.*, 127:78–83, 2007.

154. T. Rozek, K. L. Wegener, J. H. Bowie, I. N. Olver, J. A. Carver, J. C. Wallace, and M. J. Tyler. The antibiotic and anticancer active aurein peptides from the australian bell frogs litoria aurea and litoria raniformis. *Eur. Biophys. J.*, 267:5330–5341, 2000.

155. J. T. Cheng, J. D. Hale, M. Elliott, R. E. Hancock, and S. K. Straus. The importance of bacterial membrane composition in the structure and function of aurein 2.2 and selected variants. *Biochim. Biophys. Acta*, 1808:622–633, 2011.

156. K. Matsuzaki, K. Sugishita, N. Ishibe, M. Ueha, S. Nakata, K. Miyajima, and R. M. Epand. Relationship of membrane curvature to the formation of pores by magainin 2. *Biochemistry*, 37:11856–11863, 1998.

Paper I

S. Pöyry, T. Róg, M. Karttunen and I. Vattulainen. The significance of cholesterol methyl groups. J. Phys. Chem. B, **112** (10), 2922 -2929, (2008).

Significance of Cholesterol Methyl Groups

Sanja Pöyry,[†] Tomasz Róg,[‡,§] Mikko Karttunen,[||] and Ilpo Vattulainen*[,†,⊥,#]

Institute of Physics, Tampere University of Technology, Finland, Faculty of Electrical Engineering, Helsinki University of Technology, Finland, Department of Biophysics, Faculty of Biotechnology, Jagiellonian University, Kraków, Poland, Department of Applied Mathematics, The University of Western Ontario, London (ON), Canada, Laboratory of Physics and Helsinki Institute of Physics, Helsinki University of Technology, Finland, and MEMPHYS-Center for Biomembrane Physics, University of Southern Denmark

Received: October 16, 2007; In Final Form: January 7, 2008

Cholesterol is an indispensable molecule in mammalian cell membranes. To truly understand its role in the functions of membranes, it is essential to unravel cholesterol's structure−function relationship determined by underlying molecular interactions. For this purpose, we elaborate on this issue by considering the previously proposed idea that cholesterol's effects on a number of physical properties of membranes have been optimized during the evolution by removal of its excess methyl groups from the α-face of cholesterol, thus "smoothening" the structure. Consequently, the methyl groups still attached to cholesterol are one of the most intriguing structural features of the molecule. An obvious question arises: Why do these methyl groups still exist, and could cholesterol properties be further optimized by their removal? Because of the nature of the biosynthetic pathways of cholesterol, and the evidence of decreased interactions between sterols and lipid acyl chains when methyl groups are present, it seems plausible that removal of the methyl groups might indeed lead to stronger ordering and condensing effects of the cholesterol molecule. Atomic-scale molecular dynamics simulations of numerous modified sterols embedded in saturated lipid bilayers demonstrate, however, that the issue is more subtle. The analysis reveals a complex interplay between the lipid acyl chains and the structural details of cholesterol. Changes in cholesterol structure typically do not improve its performance in terms of promoting membrane order. This view is substantiated by a detailed analysis of the simulation data. In particular, it highlights the importance of the methyl group C18 for cholesterol properties. The C18 group resides between the third and fourth ring of cholesterol on its "rough" β-side, and the results provide compelling evidence that C18 is crucial for the proper orientation of the sterol. More generally, the data provide insight into the role of the methyl groups of cholesterol.

I. Introduction

Cholesterol is one of the key molecules affecting a variety of membrane properties in animal cells. Cholesterol modulates lipid bilayer properties by increasing the ordering of the phospholipid acyl chains,[1,2] thus condensing the bilayer.[3] It is also involved in modifying structural and dynamical membrane properties by increasing their mechanical strength,[4] reducing passive permeation,[5] and decreasing the diffusion rate of lipids in fluidlike membranes.[6] Also, as cholesterol is known to promote the formation of the liquid-ordered phase characterized by enhanced packing and ordering of lipids around cholesterol, it is often associated with domain formation and maintaining proper fluidity of the bilayer.[7] Cholesterol is not only a membrane component, but it is also an important metabolite and precursor for bile salts, some lipid soluble vitamins, and (steroid) hormones.[8] The significance of cholesterol for health is perhaps best understood by realizing that both excess cholesterol and lack of properly structured cholesterol can lead to serious conditions.[9]

As for its structure, cholesterol is a seemingly simple molecule. It comprises a planar, relatively rigid tetracyclic ring system with a 3β-hydroxyl (OH) group and an 8-carbon chain (iso-octyl tail) attached to C17; see Figure 1. The ring system is asymmetric about the ring plane, having a rough side (β-face) with two methyl groups C18 and C19 pointing out of the plane (see Figure 1) and a smooth α-face with no substituents.

Considering the rigidity of cholesterol, one is tempted to assume that its functions are not particularly specific but mainly originate from steric effects by which cholesterol orders molecules in its vicinity. To some extent, this idea holds true: essentially all sterol molecules share the generic property of promoting order in a membrane. However, the minor structural differences between different sterol molecules are exceptionally important and affect the functions of sterols in cellular membranes. For example, for reasons that are largely unknown, the concentrations of cholesterol and other sterols range substantially from one membrane type to another. While mitochondrial membranes are essentially cholesterol-free, plasma membranes contain typically about 30 mol % cholesterol, and in ocular lens membranes, the concentration of cholesterol can be as large as about 80 mol %.[10,11]

The interactions of cholesterol with other lipids and proteins seem to dictate the amount of cholesterol needed for functions

* To whom correspondence should be addressed. E-mail: Ilpo.Vattulainen@csc.fi.
† Tampere University of Technology.
‡ Faculty of Electrical Engineering, Helsinki University of Technology.
§ Jagiellonian University.
|| The University of Western Ontario.
⊥ Laboratory of Physics and Helsinki Institute of Physics, Helsinki University of Technology.
University of Southern Denmark.

10.1021/jp7100495 CCC: $40.75
Published on Web 02/16/2008

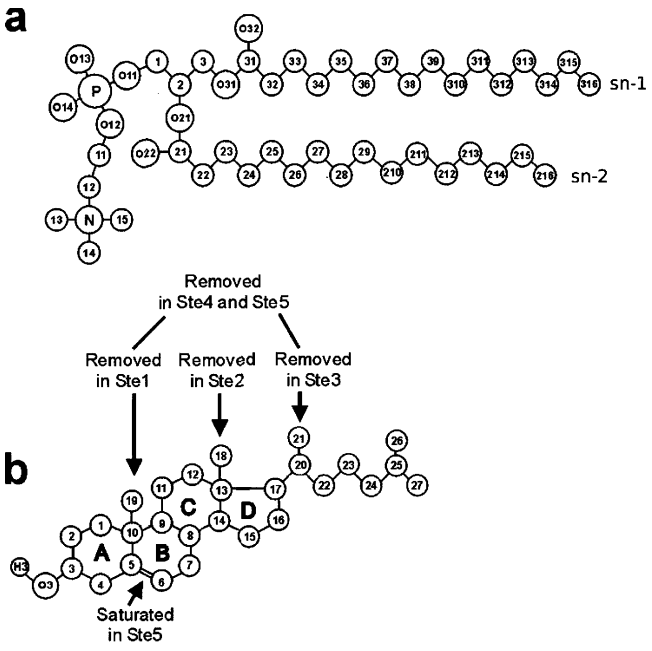

Figure 1. Structures of (a) DPPC and (b) cholesterol. For the modifications made to the cholesterol structure, see Table 1.

where cholesterol is involved. In this regard, one of the intriguing properties of cholesterol is its ability to promote the formation of the liquid-ordered phase, which is characterized by significant conformational order in the lipid hydrocarbon chain region, while the membrane is also fluid in terms of not expressing any translational long-range order. While sterols such as ergosterol also promote the formation of the liquid-ordered phase,[12] there are several other sterols such as lanosterol that do not have this property.[13] The importance of the liquid-ordered phase is related to its biological relevance, since there is evidence supporting the idea that lipid rafts are domains in the liquid-ordered phase.[14] Consequently, cholesterol is considered to be an irreplaceable ingredient of rafts,[15,16] since other sterols seem to not be capable of replacing cholesterol; for example, lanosterol is a poor raft former,[17] and desmosterol, which differs from cholesterol only by one double bond in the short hydrocarbon tail, cannot substitute for cholesterol either.[18] Obviously there is something unique in cholesterol and its structure−function relationship.

A question arises as to why cholesterol is the sterol needed in eukaryotic cells, and what is its origin. Of all the possible options, evolution has led to cholesterol, universally present in mammalian cell membranes, and to ergosterol, common in many yeasts and fungi. One hypothesis suggests that cholesterol's effects on certain physical properties of membranes were optimized during the evolution by removal of its excess methyl groups from the α-face, "smoothening" the structure.[13,19,20] Experimental and computational studies alike show decreased interactions between sterol molecules and lipid acyl chains when methyl groups are present. Indeed, near the smooth α-face, the ordering of acyl chains is higher[21] and the packing of chain atoms more tight[22] compared to the rough β-face. The smooth structure of cholesterol may also explain why its ordering effects on lipid hydrocarbon chains are most pronounced in saturated lipid bilayers.[23] In membranes comprised of unsaturated lipids, the effects of cholesterol are considerably weaker, and also the ordering induced by different sterols is then largely similar.[23] A question arises as to whether the evolution has reached its goal or is there a next step to come, a sterol which would have even more effective ordering and condensing capabilities. A tempting idea would be that further smoothening of the cholesterol structure by removal of the methyl groups from the β-face, also, might improve its function still. This has led to studies of a demethylated cholesterol (Dchol) from which two methyl groups (C18 and C19 in Figure 1) have been removed: [24] using atomistic simulations, Róg and co-workers compared the properties of membranes consisting of pure dipalmitoylphosphatidylcholine (DPPC) with those comprised of DPPC with either cholesterol (Chol) or demethylated cholesterol. Contrary to expectations, the ordering and condensing capability of Dchol turned out to be weaker than that of Chol.

TABLE 1: Abbreviations Used for the Modified Sterols

system	methyl group removed
Ste1	C19
Ste2	C18
Ste3	C21
Ste4	C19 and C21
Ste5	C19 and C21, no double bond in ring system
Dchol	C18 and C19

Our objective in the present study is to further elucidate the specific relations between cholesterol structure and function, particularly the role of the two methyl groups attached to the cholesterol ring and the one methyl group attached to its short tail. For this purpose, the methyl groups were first removed one by one and then two of them simultaneously. Also, the effect of the double bond in the ring system was examined. By comparing the data obtained from this and the previous study,[24] insight on the significance of these methyl groups is gained. The atom-scale simulations employed for this purpose allow us to elucidate these effects in a very detailed manner and clarify the significance of each functional unit one by one. The methyl group C18 attached to the β-side of cholesterol turns out to be of particular importance for cholesterol properties, since removing this group leads to a significant increase of the sterol tilt angle in a saturated lipid bilayer, thus reducing the sterol's ordering and condensing capabilities.

II. System Description and Simulation Details

Atomistic molecular dynamics simulations of five different systems were carried out, each system containing 128 DPPC molecules and 32 modified cholesterol molecules (sterol concentration of 20 mol %). The structures and their abbreviations (Ste1−Ste5) are shown in Figure 1 and summarized in Table 1. In the first three systems, one of the methyl groups (C18, C19, C21) was removed. Both C19 and C21 were removed from the sterols of the remaining two systems, and in the last one, the double bond from the ring system was also converted into a single bond. For comparison, in Dchol, the methyl groups C18 and C19 on the rough β-side of cholesterol were removed.[24] All bilayers were hydrated with 3500 water molecules. The initial structures of the bilayers were constructed from previously simulated systems (over 100 ns) composed of DPPC and cholesterol[24] by removing the methyl groups in question, and modifying the double bond in the sterol structure where appropriate. The energy of the initial structures was minimized prior to molecular dynamics simulations using the steepest-descent algorithm.[25] Like in ref 24, we used the standard united atom force field parameters for DPPC molecules,[26] where the partial charges were taken from the underlying model description.[27] For water, we employed the simple point charge (SPC) model.[28] For the sterol force field, we used the description of Holtje et al.[29] including a correction described elsewhere.[24]

The simulations were carried out using the GROMACS software package, version 3.1.4.[25] The total simulation time was

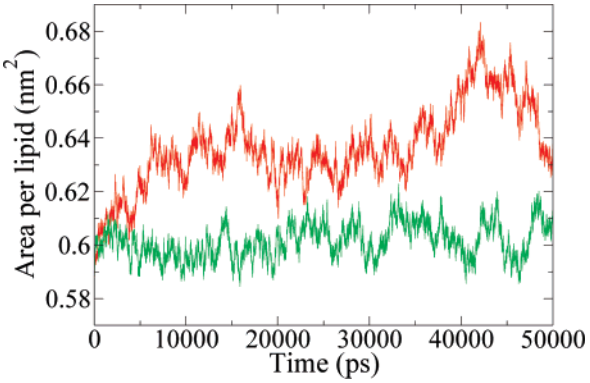

Figure 2. Average surface area per lipid versus time for Ste2 (red line) and Ste3 (green line).

TABLE 2: Average Area per Lipid and Membrane Thickness (The Area Is Given in Units of nm^2 and Membrane Thickness in Units of Nanometers)

system	area	thickness
Ste1	0.60 ± 0.01	4.7 ± 0.05
Ste2	0.64 ± 0.02	4.5 ± 0.20
Ste3	0.60 ± 0.01	4.7 ± 0.05
Ste4	0.62 ± 0.01	4.6 ± 0.05
Ste5	0.61 ± 0.01	4.6 ± 0.05
Chol	0.60 ± 0.04	4.7 ± 0.05
Dchol	0.62 ± 0.04	4.5 ± 0.05
DPPC	0.66 ± 0.04	4.0 ± 0.05

50 ns with a time step of 2 fs. The neighbor list was updated every 10 steps. Periodic boundary conditions were used in all directions. For calculating electrostatic energy, the particle-mesh Ewald (PME) method was used[30] with a real space cutoff distance of 1 nm. The PME method has recently been shown to perform very well in membrane simulations.[31,32] The LINCS algorithm[33] was used to preserve the bond length in the sterol hydroxyl group, and the SETTLE algorithm was used for water.[34] The weak coupling method[35] was utilized with a coupling constant of 0.6 ps until equilibrium was reached at 10 ns. From then on, the Nosé−Hoover thermostat[36,37] was employed, and the coupling constant was changed to 0.1 ps. Water and bilayer temperatures were controlled separately at a reference temperature of 323 K. For pressure we used the Berendsen semi-isotropic coupling[35] with a coupling constant of 1.0 ps and a reference pressure of 1.0 bar.

A. Results. *1. Area per Lipid.* Because of the condensing effect of Chol, the average area per lipid decreases when Chol is added to a bilayer.[3] The area occupied by one lipid was calculated by dividing the total area of the bilayer by the number of DPPC molecules in one leaflet, thus ignoring the sterols. For further discussion on how to define the area in different membrane systems, see ref 24. Here, we just note that the approach used in this work is reasonable, since the main purpose here is to compare the effects of different sterols on the bilayer, thus making the absolute value irrelevant.

The area per lipid together with potential energy was used for estimating system equilibration, which was observed to take place in about 10 ns. The average areas per lipid versus time are illustrated in Figure 2; for clarity, only Ste2 and Ste3 are shown. Ste2 was found to have significantly larger fluctuations than the other systems, leading to larger error bars in that case.

The average values for the average area per lipid for each system were computed using a time interval of 10−50 ns. As seen from the results presented in Table 2, the systems containing Chol, Ste1, or Ste3 in addition to DPPC have the same area per lipid within the error bars. For the other systems,

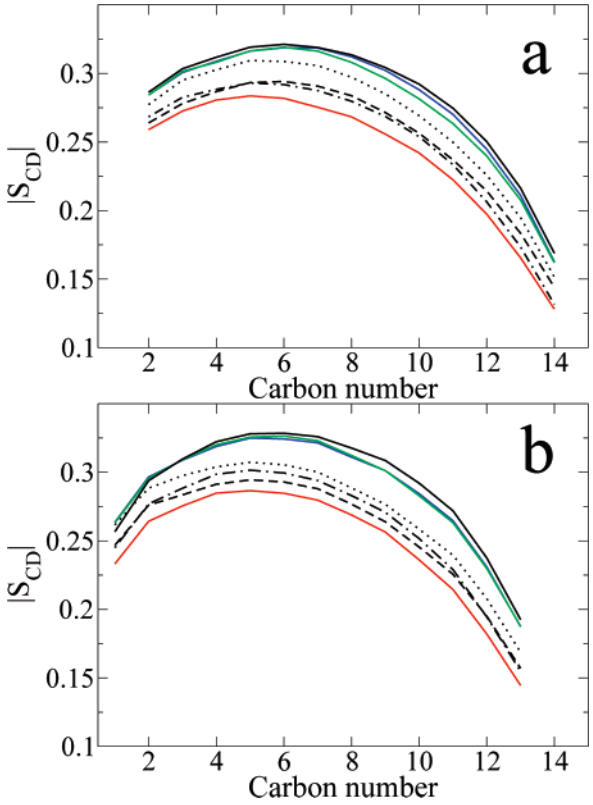

Figure 3. Deuterium order parameter profiles for (a) *sn*−1 chain and (b) *sn*−2 chain in Chol (black line), Ste1 (blue line), Ste2 (red line), Ste3 (green line), Ste4 (dashed line), Ste5 (dotted line), and Dchol (dash−dot line). Small carbon numbers correspond to carbons close to the head group.

the area is somewhat larger, indicating a thinner and a more disordered bilayer. However, as indicated by the fact that the pure DPPC system has the largest area of all, every modified sterol examined here has a condensing effect on the bilayer.

The area per lipid is closely associated with the bilayer thickness, which was calculated as a distance between the points where the electron density profiles of bilayer atoms merge with the profiles of water; see Table 2.

2. Ordering and Conformation of Acyl Chains. There are numerous closely related order parameters that can be used to describe the ordering of the acyl chains. The one used here, the deuterium order parameter, S_{CD}, is convenient because it can also be measured with NMR, and thus verified by comparing with experimental data.

The order parameter S_{CD} is computed for all carbons along the acyl chains and derived from

$$S_{CD} = \left\langle \frac{3}{2}\cos^2\theta - \frac{1}{2} \right\rangle \quad (1)$$

where θ is the angle between a given C−H vector and the bilayer normal. Because of the united atom model used here, S_{CD} was computed from the trajectories by reconstructing hydrogen positions in C−H bonds assuming ideal geometry.

Several NMR studies have provided evidence of the influence of cholesterol on lipid chain ordering; see, e.g., refs 38 and 39. In the same spirit, simulations have also shown evidence of increased chain order due to cholesterol.[1,2,18,23,24,40] The results in Figure 3 for cholesterol are in full agreement with the previous experimental and simulation studies.

What is more, the results in Figure 3 and Table 3 highlight the specificity of cholesterol's structure−function relationship.

TABLE 3: Average Values of Deuterium Order Parameters and Tilts of the Sterol Ring and Tail (Tilts Are Given in Units of Degrees)

system	S_{CD} (*sn*−1)	S_{CD} (*sn*−2)	tilt (ring)	tilt (tail)
Ste1	0.28 ± 0.01	0.29 ± 0.01	22.1 ± 1.4	32 ± 1
Ste2	0.24 ± 0.02	0.25 ± 0.02	26.0 ± 3.3	44 ± 3
Ste3	0.28 ± 0.01	0.29 ± 0.01	20.7 ± 1.2	26 ± 1
Ste4	0.25 ± 0.01	0.26 ± 0.01	24.3 ± 2.0	30 ± 2
Ste5	0.27 ± 0.01	0.27 ± 0.01	23.0 ± 1.4	29 ± 1
Chol	0.28 ± 0.01	0.29 ± 0.01	19.8 ± 0.2	28 ± 1
Dchol	0.25 ± 0.01	0.26 ± 0.01	25.3 ± 0.2	51 ± 2

We find that some of the very subtle modifications in the structure of cholesterol cause a rather major difference in the ordering of lipid acyl chains. The ordering capabilities of Chol, Ste1, and Ste3 are essentially similar, while there is yet a slight but finite difference in favor of cholesterol. A peculiar detail is that despite the fact that the methyl group removed from Ste1 is originally near the head group and that of Ste3 in the tail, the plots for these two are almost identical. All of the sterols with more than one methyl group removed are less efficient than Chol in terms of promoting the acyl chain order. The weakest one, however, is Ste2, which has C18 removed. The sterol Ste5, with its double bond in the sterol ring converted into a single bond, promotes order more than its single-bonded counterpart Ste4 but is still inferior to Chol. Nonetheless, all of the modified sterols increase the order of the fatty acyl chains compared to pure DPPC.

Previous simulation studies for desmosterol have shown that the short hydrocarbon tail can significantly affect the orientation of a sterol in a bilayer and consequently also its ordering properties.[18,23] As for the sterols studied in this work, Figure 4 depicts the ordering of the short sterol tail. The tails from which the methyl group C21 was removed, namely, Ste3, Ste4, and Ste5, exhibit more order in the middle part of the chain, with Ste3 having the most ordered tail. The differences are rather minor; however, the only exception is Ste1, with C19 removed from the sterol moiety.

When examining the conformation of the fatty acyl chains of DPPC, only torsion angles 4−6 were taken into account; see details in refs 21 and 24. The differences between the average numbers of *gauche* conformations in the chains are rather small between the systems; see Table 4. There are, however, fairly significant distinctions between the systems when the lifetimes of *trans* conformations are considered; see Figure 5 and Table 4 for a summary. For clarity, only the profiles for Chol, Ste1, Ste2, and Ste3 are shown; the profiles

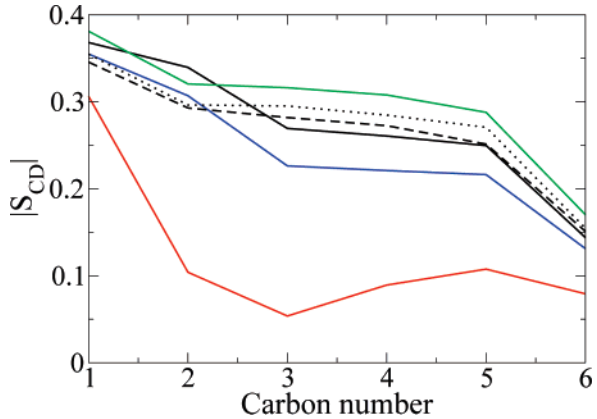

Figure 4. Deuterium order parameter for the sterol's tail in Chol (black line), Ste1 (blue line), Ste2 (red line), Ste3 (green line), Ste4 (dashed line), and Ste5 (dotted line). Small carbon numbers correspond to carbons close to the steroid moiety.

TABLE 4: Number of *gauche* Conformations per Chain and Lifetimes of *trans* Conformations

	number of *gauche*		lifetime of *trans*	
system	*sn*−2	*sn*−1	*sn*−2	*sn*−1
Ste1	2.3 ± 0.05	2.3 ± 0.05	121 ± 4	117 ± 4
Ste2	2.6 ± 0.05	2.6 ± 0.05	108 ± 4	105 ± 4
Ste3	2.3 ± 0.05	2.4 ± 0.05	119 ± 4	113 ± 4
Ste4	2.5 ± 0.05	2.5 ± 0.05	111 ± 4	108 ± 4
Ste5	2.4 ± 0.05	2.4 ± 0.05	113 ± 4	112 ± 4
Chol	2.3 ± 0.05	2.3 ± 0.05	120 ± 4	118 ± 4
Dchol	2.5 ± 0.05	2.5 ± 0.05	114 ± 4	111 ± 4

of other systems lie between Ste2 and Ste3. It is evident from the figures that Chol, Ste1, and Ste3 are approximately equally effective in stabilizing the *trans* conformation, while Ste2 and other systems are somewhat less effective.

3. Location and Orientation of Sterols. The location of different sterols is quantified by considering the electron density profiles calculated across the lipid bilayers. Experimental studies for density profiles have shown that Chol affects the packing inside the membrane;[41] thus, the electron density profile in a pure DPPC bilayer is distinctly different from a membrane with a large amount of Chol. With this in mind, we focus on the different sterol-containing systems.

The profiles for the whole bilayer, water, and sterol ring and tail are depicted in Figure 6. For clarity, only those cases with the greatest differences, namely, Ste2 and Ste3, are being compared to Chol. As indicated by the order parameter and the average area per lipid, the bilayer thickness differs between the systems. The profiles also imply deviations in the ring and tail orientations of the sterols; see below. The tail densities show that, in the bilayer center, Ste3 has the highest density and Ste2 has the lowest. Higher tail density in the bilayer center is indicative of enhanced interdigitation of the sterol tail part.

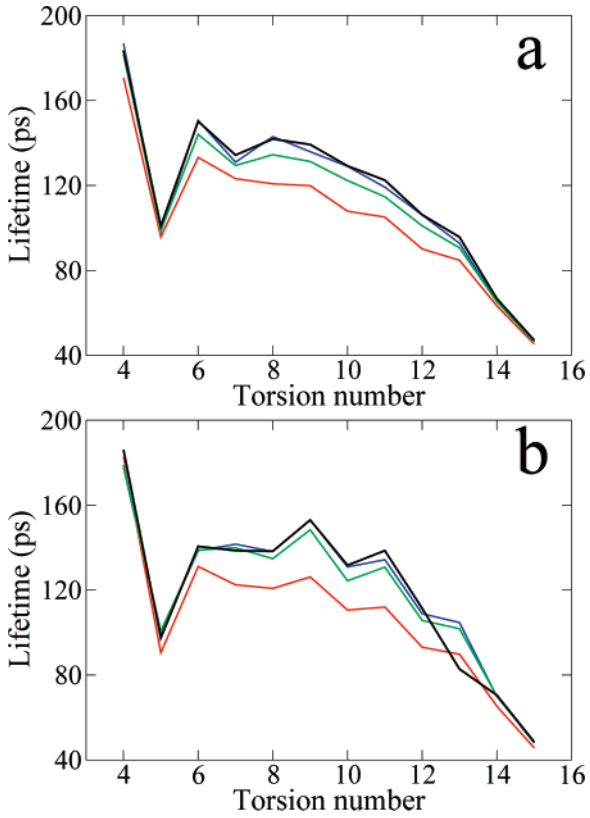

Figure 5. Lifetimes of the *trans* conformations along the (a) *sn*−1 and (b) *sn*−2 chains for Chol (black line), Ste1 (blue line), Ste2 (red line), and Ste3 (green line).

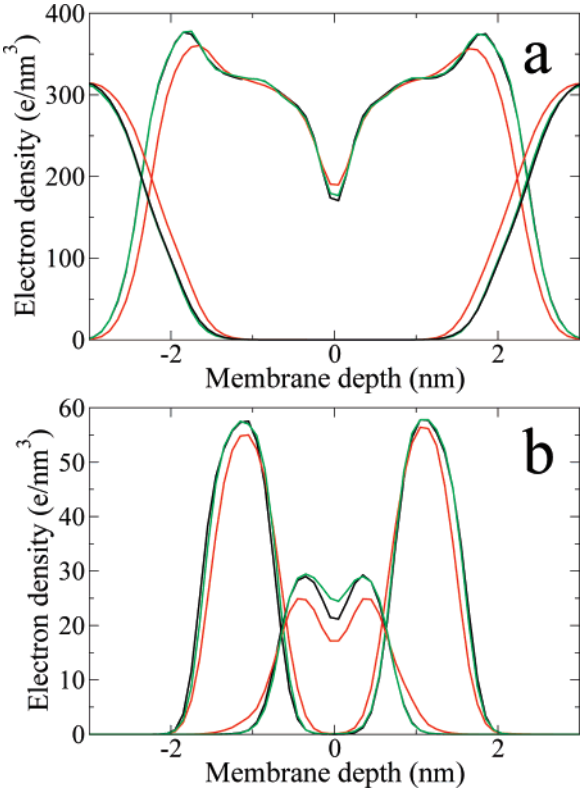

Figure 6. Electron density profiles for (a) bilayer atoms and water, (b) sterol ring and tail atoms for Chol (black line), Ste2 (red line), and Ste3 (green line). Membrane depth at $z = 0$ corresponds to the membrane center.

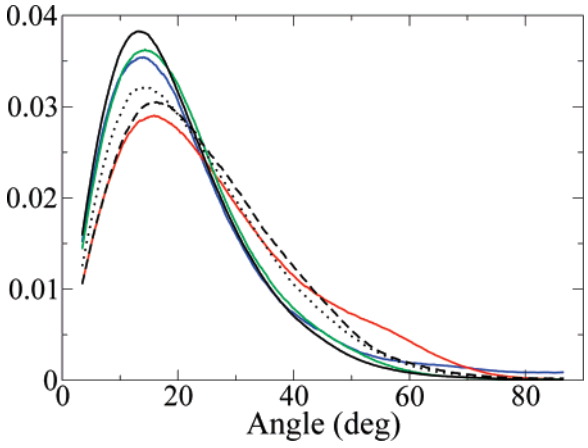

Figure 7. Tilt angle distribution of the sterol ring for Chol (black line), Ste1 (blue line), Ste2 (red line), Ste3 (green line), Ste4 (dashed line), and Ste5 (dotted line).

To further elucidate how the sterols reside in the bilayer, we computed tilt angle distributions for the sterol ring system and the sterol tail. Sterol tilt, the angle between the vector C3−C17 and the bilayer normal, correlates well with the sterol's ordering effects,[23] and it can be measured also experimentally through NMR.[42]

Figure 7 depicts the tilt distributions of the steroid part, and Table 3 summarizes the average tilt values. We first find that the tilt of cholesterol, 19.8°, agrees with the experimental value of 16−19° found for a system of cholesterol molecules in DPPC liposomes at 297 and 333 K,[42] as well as with previous simulations.[23] The tilts found for the other sterols are larger. The ones closest to Chol are given by Ste1 and Ste3, whose tilt distributions in Figure 7 demonstrate that the differences in these cases are very minor: the peaks of Ste1 and Ste3 are located almost identically with Chol at about 13°, and the difference with respect to cholesterol arises mainly from the long tail at large angles, showing how Ste1 and Ste3 fluctuate slightly more than Chol. The largest tilt of all the sterols considered is given by Ste2.

TABLE 5: Average Number of Neighbors of the Sterol Ring System (Results Are Given for the Total Number as Well as for the α- and β-Faces Separately)

system	total	α	β
Ste1	38.6 ± 0.5	18.9 ± 0.5	19.7 ± 0.5
Ste2	36.9 ± 0.5	20.7 ± 0.5	16.2 ± 0.5
Ste3	38.2 ± 0.5	21.3 ± 0.5	16.9 ± 0.5
Ste4	38.5 ± 0.5	18.5 ± 0.5	20.0 ± 0.5
Ste5	38.7 ± 0.5	19.0 ± 0.5	19.8 ± 0.5
Chol	37.8 ± 0.5	21.1 ± 0.5	16.6 ± 0.5
Dchol	38.2 ± 0.5	17.8 ± 0.5	20.4 ± 0.5

It seems that removal of the methyl group from the cholesterol tail, as done with Ste3, has only a slight effect on the orientation of the ring system. Instead, it is related to a decrease of the tail tilt. Deletion of the methyl group C19 in Ste1, in turn, leads to a slight increase in both ring and tail tilt. The most important of all structural features is C18, though. Without a doubt, the group C18 is crucial for the proper orientation of the sterol, since removing it results in a considerable increase in the ring and tail tilts alike. Also, the removal of the two methyl groups simultaneously increases the tilt.

4. Packing of Atoms Relative to Sterol Ring Atoms. To better understand why C18 is particularly important for sterol ordering properties, we elucidate the packing of atoms around the steroid entity, thus gauging indirectly the role of van der Waals interactions in the hydrophobic membrane region. Here, due to the structure of cholesterol, the ordering effects are different for lipids located on the α- and β-faces of the ring. Consequently, when the structure is being modified, changes are expected. The packing of atoms near the two faces of the cholesterol ring can be examined by calculating the number of neighbors using the method described in ref 43. For a given carbon atom, we define its neighbors as atoms belonging to a different molecule and located no further than 0.7 nm from the carbon atom in question. Further, to establish whether a carbon atom C is located on the α- or β-face, the angle between the C10−C19 bond and the C10−C vector was calculated. For atoms located on the β-face, the angle is less than or equal to 90°. For molecules without C19, we used the vectors C13−C18 and C13−C, and in the cases of Dchol, Ste4, and Ste5 that lack both C18 and C19, the position of C19 was determined using tetrahedral geometry. Identical results were found if the C19 group was reconstructed into any of the molecules using tetrahedral geometry.

Like cholesterol, Ste2 and Ste3 have more neighbors on the α-face; see Table 5. This was expected for Ste3 because no modifications to the ring structure were made. As seen from Table 5 (see also Figure 8), the average number of neighbors is essentially the same for Ste3 and Chol on both α- and β-sides, except for carbons 11−17 that have a higher number of neighbors in the case of Ste3. Ste2 follows the same pattern, albeit the numbers are lower.

The sterols with C19 removed, namely, sterols Ste1, Ste4, Ste5, and Dchol, clearly prefer the β-face. The differences are most pronounced for carbons 5−8 and 12−17; see Figure 8. As suggested in ref 24, this redistribution of material from the α- to the β-face might be facilitated by hydrogen bonding between the OH group of the sterols and the lipid carbonyl groups. In contrast to sterols Ste1 and Ste4, converting the C5−C6 double bond into a single bond in Ste5 led to a different

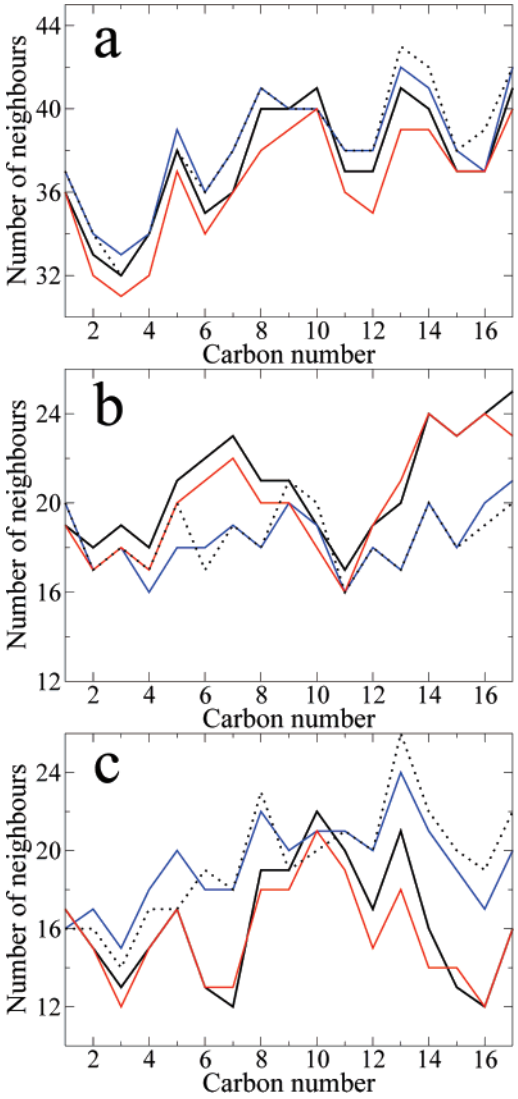

Figure 8. Number of neighbors close to the sterol ring atoms: (a) total number of neighbors; (b) number on the α-face; (c) the number on the β-face. Results are shown for Chol (black line), Ste1 (blue line), Ste2 (red line), and Ste5 (dotted line). Small carbon numbers correspond to atoms close to the sterol's hydroxyl group.

distribution of atoms between the α- and β-faces in the vicinity of the bond. Possibly because of the lack of C21 in the sterol tail, Ste4 and Ste5 have a somewhat larger number of neighbors accompanying carbons 12−17 on the β-face.

III. Discussion and Concluding Remarks

The initial spark that led to these studies of modified cholesterols resulted from considerations on the nature of the biosynthetic pathways of cholesterol. In the process of transforming lanosterol to cholesterol, methyl groups are removed from the α-face. This is assumed to reflect the evolutionary optimization of cholesterol structure to reach the most favorable properties. An alluring thought was, would it be possible to further enhance the effects that cholesterol has on membranes, for example, to increase its ordering capabilities? The first attempt, however, did not lead to the results desired, quite the contrary. Removing both C18 and C19 groups from the ring system led to a less favorable orientation of the sterol and to a decrease in its ordering effects.[24] In this study, we have concentrated on the effects of removing separately methyl groups from the ring (C18 and C19) and from the tail (C21) as well as simultaneously removing methyl groups C19 and C21. In the last case, we also examined the effect of the double bond in ring B on the sterol properties.

In all cases, the removal of methyl groups changes the sterol ring orientation by increasing the tilt of the sterol ring and tail. This increase is of the order of 1−6°. This finding is highly interesting, since it has been shown recently that there is a strong correlation between the tilt of a sterol and its effect on bilayer properties.[23] The tilt-related mechanism by which a sterol modifies the properties of lipid bilayers seems to be largely independent of the particular interactions between the sterol and acyl chains. Rather, its origin seems to be related to the increase of interactions between the chains imposed by cholesterol.[43] However, our results show that direct interactions can also modify sterol effects on a bilayer. Increase of packing of acyl chains around the sterol ring can increase sterol ordering ability. The case of Ste1, where the methyl group C19 was removed, is a good illustration of the interplay of these two effects: a small increase of ring tilt angle of 2° is compensated by direct ring−chain interactions manifested by better packing next to the sterol ring. As a result, this sterol is practically as effective as cholesterol as a promoter of membrane order. A similar effect was observed for Ste3 where the methyl group C21 was removed.

The increase in sterol tilt due to modifications in cholesterol structure is consistent with earlier atomistic simulations.[44,45] Smondyrev and Berkowitz[44] modeled DMPC bilayers in the fluid phase at a sterol concentration of 11 mol % and found that the area per lipid and S_{CD} order parameters were essentially identical (within error bars) for cholesterol, lanosterol, and ergosterol. However, for the sterol tilt with respect to the membrane normal, they found the tilt of cholesterol to be clearly smaller than that for the other sterols. Further studies at a sterol concentration of 50 mol % supported this view. More recently, Cournia et al.[45] have considered the same sterols in a fluid DPPC bilayer at a sterol concentration of 40 mol % and found ergosterol to be most efficient as a promoter of the liquid-ordered phase, followed by cholesterol (intermediate) and lanosterol (weakest ordering capability). These simulation studies support the view that even seemingly minor changes in cholesterol structure do influence its tilt and ordering capability.

In this respect, our studies showed that the methyl group C18 of cholesterol is the most essential one for maintaining proper sterol tilt. The lack of this group led to a 6° increase of the tilt angle and significantly decreased the sterol's ordering and condensing effects.

The key question arises, as to what is the atom-level mechanism responsible for sterol tilt modulation. The results provided in Table 5 and Figure 8 suggest that changing the balance between the packing of the α- and β-faces has a strong influence on the sterol tilt. A significantly lower number of neighbors on the α-face compared to the β-face indicates larger tilt. As discussed earlier,[24] this redistribution of packing is probably caused by hydrogen bonding between the DPPC head group and the hydroxyl group of the sterols, as the OH group is positioned on the β-face and can favor packing on the same side. The only sterol which does not follow this pattern is Ste2. However, this is rather expected, since the packing around this sterol is substantially worse than that for the other sterols.

Converting the double bond into a single bond in the sterol's ring system, i.e., conversion of Ste4 into Ste5, increases the acyl chain ordering and also slightly the number of neighbors close to the sterol's ring structure. This may sound peculiar, as one might have expected the double bond to make the ring

system more rigid and hence facilitate tighter packing inside the bilayer. On the other hand, 7-dehydrocholesterol, the most recent precursor of cholesterol along its Kandutsch−Russel biosynthetic pathway, differs from cholesterol only by one additional double bond in ring B. However, there is data suggesting that 7-dehydrocholesterol promotes membrane order less than cholesterol.[46,47] The clarification of the significance of the double bond's location in the ring structure would clearly require further efforts. For the present case, we only characterized the effect of the double bond in the ring B for the geometry of cholesterol. To this end, we computed the angle between the normals of the planes of rings A, B, C, and D. In Ste5, in which the double bond between carbons C5 and C6 has been removed (see Figure 1), the angle between the planes of rings A and B changed by about 11°. However, this change is difficult to interpret, since in Ste5 not only the double bond but also the methyl groups C19 and C21 have been deleted. For comparison, in Ste4 (which is identical to Ste5 except for the removal of the double bond), the same A−B angle changed by about 7° instead of 11. Clearly, the removal of the double bond has certain effects on sterol geometry and packing, but the effects are difficult to quantify given the many changes induced concurrently. Here, let us instead conclude that all changes in sterol geometry that were observed in this study were local; that is, they took place in the vicinity of the induced structural deformation. The largest effect occurred when the methyl group C18 was removed (Ste2). In that case, the angle between the planes of rings A and B changed by about 12° with respect to cholesterol.

To the best of our knowledge, no common sterol in nature lacks the methyl group C18. This fact seems to further support the importance of this group to sterols' function. There are some sterols without C19, such as 19-nor-sterols in marine invertebrates and sterols with an aromatic ring. However, to our knowledge, the detailed membrane-modulating properties of these sterols are unknown and thus comparison with cholesterol remains to be done.

Despite the lack of natural sterols identical to those considered in this work, there is reason to mention that there is no fundamental obstacle to synthesizing such sterols. While the task would be a hard one due to the stereospecific nature of the sterols, previous progress in synthesizing natural sterols,[48] steroids,[49] and synthetic sterols such as *ent*-cholesterol[50,51] is encouraging.

The results presented in this paper clearly demonstrate that the methyl groups C18, C19, and C21 are important structural elements of cholesterol and cannot be considered as evolutionary fossils. Their role seems to be somehow related to the maintenance of optimal tilt of the sterol ring system, thus promoting the nonspecific mechanism by which cholesterol increases order in saturated membranes. It should be noted, however, that in unsaturated membranes cholesterol and other sterols closely related to cholesterol have essentially similar ordering capabilities.[23] The significance of cholesterol's structural specificity thus becomes most evident only in membranes comprising at least partly saturated lipids.[23] It might be plausible that while the smooth α-face prefers being next to the saturated chains, a rough β-face would be needed to interact with the unsaturated ones. This suggestion is in line with cholesterol's preference to reside at the interface between domains rich in saturated and unsaturated chains found in simulations.[52] According to a hypothesis presented elsewhere,[52] a reduced interfacial line tension between these regions would be a consequence of cholesterol molecules orienting their α-face toward saturated chains and their β-face toward unsaturated chains.

Acknowledgment. This work was supported by the Academy of Finland, the Emil Aaltonen Foundation, and the Natural Sciences and Engineering Research Council of Canada (NSERC). Computational resources were provided by the Finnish IT Center for Science (CSC), the HorseShoe supercluster computing facility at the University of Southern Denmark, and the SharcNet computing facility (www.sharcnet.ca). T.R. has been supported by the Marie Curie Intra-European Fellowship "024612-Glychol".

References and Notes

(1) Chiu, S. W.; Jakobsson, E.; Mashl, R. J.; Scott, H. L. *Biophys. J.* **2002**, *83*, 1842−1853.
(2) Hofsäss, C.; Lindahl, E.; Edholm, O. *Biophys. J.* **2003**, *84*, 2192−2206.
(3) Petrache, H. I.; Tu, K.; Nagle, J. F. *Biophys. J.* **1999**, *76*, 2479−2487.
(4) El-Sayed, M. Y.; Guion, T. A.; Fayer, M. D. *Biochemistry* **1986**, *25*, 4825−4832.
(5) Bittman, R.; Clejan, S.; Lund-Katz, S.; Phillips, M. C. *Biochim. Biophys. Acta* **1984**, *772*, 117−126.
(6) Almeida, P. F. F.; Vaz, W. L. C.; Thompson, T. E. *Biochemistry* **1992**, *31*, 6739−6747.
(7) Bloom, M.; Evans, E.; Mouritsen, O. G. *Q. Rev. Biophys.* **1991**, *24*, 293−397.
(8) Alberts, B.; Bray, D.; Lewis, J.; Raff, M.; Roberts, K.; Watson, J. D. *Molecular Biology of the Cell*, 3rd ed.; Garland: New York, 1994.
(9) Kelley, R. I.; Herman, G. E. *Annual Rev. Genomics Hum. Genet.* **2001**, *2*, 299−341.
(10) Li, L. K.; So, L.; Spector, A. *J. Lipid Res.* **1985**, *26*, 600−609.
(11) Finegold, L. *Cholesterol in Membrane Models*; CRC Press: Boca Raton, FL, 1993.
(12) Hsueh, Y. W.; Gilbert, K.; Trandum, C.; Zuckermann, M.; Thewalt, J. *Biophys. J.* **2005**, *88*, 1799−1808.
(13) Miao, L.; Nielsen, M.; Thewalt, J.; Ipsen, J. H.; Bloom, M.; Zuckermann, M. J.; Mouritsen, O. G. *Biophys. J.* **2002**, *82*, 1429−1444.
(14) Mouritsen, O. G.; Zuckermann, M. J. *Lipids* **2004**, *39*, 1101−1113.
(15) Simons, K.; Ikonen, E. *Nature* **1997**, *387*, 569−572.
(16) Niemela, P.; Ollila, S.; Hyvonen, M. T.; Karttunen, M.; Vattulainen, I. *PLoS Comput. Biol.* **2007**, *3*, 304−312.
(17) Xu, X.; London, E. *Biochemistry* **2000**, *39*, 843−849.
(18) Vainio, S.; Jansen, M.; Koivusalo, M.; Róg, T.; Karttunen, M.; Vattulainen, I.; Ikonen, E. *J. Biol. Chem.* **2006**, *281*, 1121−1135.
(19) Bloom, M.; Mouritsen, O. G. In *Handbook of Biological Physics*; Lipowsky, R., Sackmann, E., Eds.; Elsevier: Amsterdam, The Netherlands, 1995; pp 65−95.
(20) Bloch, K. *Crit. Rev. Biochem.* **1979**, *7*, 1−5.
(21) Róg, T.; Pasenkiewicz-Gierula, M. *Biophys. J.* **2001**, *81*, 2190−2202.
(22) Róg, T.; Pasenkiewicz-Gierula, M. *Biophys. Chem.* **2004**, *107*, 151−164.
(23) Aittoniemi, J.; Róg, T.; Niemela, P. S.; Pasenkiewicz-Gierula, M.; Karttunen, M.; Vattulainen, I. *J. Phys. Chem. B* **2006**, *110*, 25562−25564.
(24) Róg, T.; Pasenkiewicz-Gierula, M.; Vattulainen, I.; Karttunen, M. *Biophys. J.* **2007**, *92*, 3346−3357.
(25) Lindahl, E.; Hess, B.; van der Spoel, D. *J. Mol. Model.* **2001**, *7*, 306−317.
(26) Berger, O.; Edholm, O.; Jahnig, F. *Biophys. J.* **1997**, *72*, 2002−2013.
(27) Tieleman, D. P.; Berendsen, H. J. C. *J. Chem. Phys.* **1996**, *105*, 4871−4880.
(28) Berendsen, H. J. C.; Postma, J. P. M.; van Gunsteren, W. F.; Hermans, J. In *Intermolecular Forces*; Pullman, B., Ed.; Reidl: Dordrecht, The Netherlands, 1981; pp 331−342.
(29) Holtje, M.; Foster, T.; Brandt, B.; Engels, T.; von Rybinski, W.; Holtje, H. D. *Biochim. Biophys. Acta* **2001**, *1511*, 156−167.
(30) Essman, U.; Perere, L.; Berkowitz, M. L.; Darden, H. L. T.; Pedersen, L. G. *J. Chem. Phys.* **1995**, *103*, 8577−8592.
(31) Patra, M.; Karttunen, M.; Hyvönen, M. T.; Falck, E.; Lindqvist, P.; Vattulainen, I. *Biophys. J.* **2003**, *84*, 3636−3645.
(32) Patra, M.; Karttunen, M.; Hyvönen, M. T.; Falck, E.; Vattulainen, I. *J. Phys. Chem. B* **2004**, *108*, 4485−4494.
(33) Hess, B.; Bekker, H.; Berendsen, H. J. C.; Fraaije, J. G. E. M. *J. Comput. Chem.* **1997**, *18*, 1463−1472.

(34) Miyamoto, S.; Kollman, P. A. *J. Comput. Chem.* **1992**, *13*, 952−962.
(35) Berendsen, H. J. C.; Postma, J. P. M.; DiNola, A.; Haak, J. R. *J. Chem. Phys.* **1984,** *81*, 3684−3690.
(36) Nosé, S. *Mol. Phys.* **1984**, *52*, 255−268.
(37) Hoover, W. G. *Phys. Rev. A* **1985**, *31*, 1695−1697.
(38) Oldfield, E.; Chapman, D. *Biochem. Biophys. Res. Commun.* **1971**, *43*, 610−616.
(39) Haberkorn, R. A.; Griffin, R. G.; Meadows, M. D.; Oldfield, E. *J. Am. Chem. Soc.* **1977**, *99*, 7353−7355.
(40) Falck, E.; Patra, M.; Karttunen, M.; Hyvonen, M. T.; Vattulainen, I. *Biophys. J.* **2004**, *87*, 1076−1091.
(41) McIntosh, T. J. *Biochim. Biophys. Acta* **1978**, *513*, 43−58.
(42) Murari, R.; Murari, M. P.; Baumann, W. J. *Biochemistry* **1986**, *25*, 1062−1067.
(43) Róg, T.; Pasenkiewicz-Gierula, M. *FEBS Lett.* **2001**, *502*, 68−71.
(44) Smondyrev, A. M.; Berkowitz, M. L. *Biophys. J.* **2001**, *80*, 1649−1658.
(45) Cournia, Z.; Ullmann, G. M.; Smith, J. C. *J. Phys. Chem. B* **2007**, *111*, 1786−1801.
(46) Berring, E. E.; Borrenpohl, K.; Fliesler, S. J.; Serfis, A. B. *Chem. Phys. Lipids* **2005**, *136*, 1−12.
(47) Petrache, H. I.; Harries, D.; Parsegian, V. A. *Macromol. Symp.* **2005**, *219*, 39−50.
(48) Yang, C.; McDonald, J. G.; Patel, A.; Zhang, Y.; Umetani, M.; Xu, F.; Westover, E. J.; Covey, D. F.; Mangelsdorf, D. J.; Cohen, J. C.; Gobbs, H. H. *J. Biol. Chem.* **2006**, *281*, 27816−27826.
(49) Cai, Z. Y.; Covey, D. F. *Steroids* **2007**, *72*, 351−359.
(50) Rychnovsky, S. D.; Mickus, D. E. *J. Org. Chem.* **1992**, *57*, 2732−2736.
(51) Westover, E. J.; Covey, D. F. *J. Membr. Biol.* **2004**, *202*, 61−72.
(52) Pandit, S. A.; Jakobsson, E.; Scott, H. L. *Biophys. J.* **2004**, *87*, 3312−3322.

Paper II

S. Pöyry, T. Róg, M. Karttunen and I. Vattulainen. Mitochondrial membranes with mono- and divalent salt: Changes induced by salt ions on structure and dynamics. J. Phys. Chem. B **113**, 15513-21 (2009).

Mitochondrial Membranes with Mono- and Divalent Salt: Changes Induced by Salt Ions on Structure and Dynamics

Sanja Pöyry,[†] Tomasz Róg,[†] Mikko Karttunen,[‡] and Ilpo Vattulainen*[,†,§,∥]

Department of Physics, Tampere University of Technology, Finland, Department of Applied Mathematics, The University of Western Ontario, London (ON), Canada, Department of Applied Physics, Helsinki University of Technology, Finland, and MEMPHYS-Center for Biomembrane Physics, University of Southern Denmark, Denmark

Received: June 24, 2009; Revised Manuscript Received: September 03, 2009

We employ atomistic simulations to consider how mono- (NaCl) and divalent ($CaCl_2$) salt affects properties of inner and outer membranes of mitochondria. We find that the influence of salt on structural properties is rather minute, only weakly affecting lipid packing, conformational ordering, and membrane electrostatic potential. The changes induced by salt are more prominent in dynamical properties related to ion binding and formation of ion-lipid complexes and lipid aggregates, as rotational diffusion of lipids is slowed down by ions, especially in the case of $CaCl_2$. In the same spirit, lateral diffusion of lipids is slowed down rather considerably for increasing concentration of $CaCl_2$. Both findings for dynamic properties can be traced to the binding of ions with lipid head groups and the related changes in interaction patterns in the headgroup region, where the binding of Na^+ and Ca^{2+} ions is clearly different. The role of cardiolipins in these phenomena turns out to be important.

I. Introduction

Cardiolipin (CL, see Figure 1) is one of the most intriguing members of the lipid family. It has a unique dimeric structure with two negatively charged phosphatidyl moieties attached to a glycerol group and a total of four acyl chains. The name cardiolipin refers to the mitochondria-rich heart tissue from which it was first isolated.[1] Considering its prevalence in mitochondria and various different eubacteria, it seems likely that cardiolipin occurred already in the rather early stages of evolution.[1] Cardiolipin usually resides in membranes that have coupled electron transport and phosphorylation, namely bacterial plasma membranes, chromatophores, chloroplasts and mitochondria.[2] It is also found in, for example, plasma lipoproteins.[3] In mitochondria, cardiolipin is primarily localized in the inner membrane (IM),[4] where it plays a crucial role in the energy production machinery. Cardiolipins are also found in the outer membrane (OM), though the concentration therein is more modest than in IM.[4]

Cardiolipins have two acidic sites that can be ionized implying that they are essentially always charged. The charge state of CLs is unresolved and both single and double charged cardiolipins have been proposed.[5] This uncertainty seems to arise from difficulties in determining its charge, since it depends on pH and on environmental factors such as the concentration of CLs.[5] Nonetheless, the small headgroup and the charged nature of cardiolipins highlight the view that ion−CL interactions are likely at the core of understanding the detailed mechanisms by which CLs modify or even control properties of mitochondrial membranes. Consequently, the main objective of the present study is to provide atomistic insight into the understanding of ion−CL interactions and the implications that emerge from them.

Because of their biological importance and unique properties, cardiolipins have been the object of many studies including conditions in salt-free systems as well as under the influence of different salts. Because of their large hydrocarbon volume and small headgroup, cardiolipins are able to form inverted hexagonal phases when neutralized by divalent cations[2] such as Ca^{2+} and Mg^{2+}. This is thought to be relevant in the formation of contact sites between IM and OM, which are enriched in cardiolipin.[1] In the IM, however, cardiolipins remain in the lamellar phase.

It has been suggested that the physical characteristics of pure cardiolipin bilayers can largely be explained by the relative rigidity and limited mobility of the headgroup by the binding of both of the phosphates to the same glycerol moiety.[6] This impairs the headgroup's capability of participating in the intra- and intermolecular interactions with other phosphate groups thereby diminishing the shielding of the two negative charges. Consequently, the charges of the phosphate groups become more susceptible to interactions with water and the ions dissolved in it. Together with the geometry of the CL molecule, this feature presumably induces greater cohesion in the interfacial region of CL membranes and leads to greater structural integrity of the bilayer. These properties may be the reason why some CL containing membranes are resistant against antimicrobial peptides and why some organisms increase their CL content under resource depletion and halophilic stress.[6]

A multitude of mitochondrial proteins have been shown to interact with cardiolipin, mostly in the protein-rich IM.[1] Cardiolipin appears to be a prerequisite for the proper function of several pivotal proteins such as some carriers and respiratory chain complexes. There is also evidence indicating that cardiolipin has a key role in the higher order organization of the components of the respiratory chain, literally gluing the chain

* To whom correspondence should be addressed. E-mail: Ilpo.Vattulainen@tut.fi.
[†] Tampere University of Technology.
[‡] The University of Western Ontario.
[§] Helsinki University of Technology.
[∥] University of Southern Denmark.

10.1021/jp905915m CCC: $40.75
Published on Web 11/03/2009

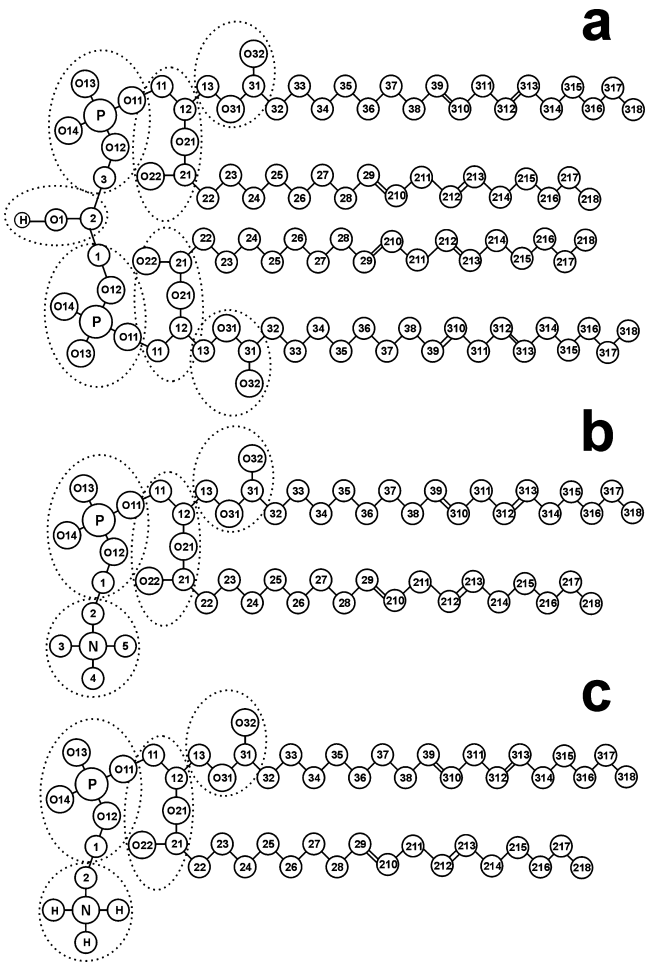

Figure 1. The structure and atom numbering of (a) cardiolipin, (b) PC, and (c) PE molecules used in this work.

together.[7] In addition, cardiolipin has been suggested to participate in the maintenance of the membrane potential via the barrier properties of the IM.[1] Furthermore, CL serves as a sink for protons employed in phosphorylation and for protons that are going to be transported across the IM.[8] The acidic head groups of CL are able to carry out intramembrane proton transfer, possibly contributing to the direct coupling between the respiratory chain and the ATP synthase.[1]

In addition to energy production, mitochondria participate in ion metabolism of cells. Their role as calcium collectors and buffers is of particular significance. The ionic content of the surrounding aqueous buffer obviously influences the electrostatics of membranes, thus changing their structural and dynamical features. Ions contribute to essential activities, such as membrane fusion, phase transitions and transport across the membrane,[9] and formation of surfactant aggregates in saline solutions.[10] While cations have been found to bind predominantly to the phosphate and the carboxylic groups, anions seem to prefer the amine groups.[11] Simulations of lipid membranes with Na^+ involved have demonstrated cations to reside mostly near the ester,[12,13] carboxylate[9,13,14] and phosphodiester groups.[15] The polarity (hydrophobicity) of the membrane surface governs the structural changes imposed on the bilayer upon ion binding.[11] In principle, for increasing polarity, fluidity tends to increase and packing becomes more loose. The effects depend also on ion type, size, valency and polarizability,[16] following the Hofmeister series.[17]

NaCl and $CaCl_2$ have been experimentally shown to increase the lipid conformational order within a lipid bilayer, subsequently decreasing the membrane elasticity and altering the main phase transition temperature.[18] The effect was observed mainly with high salt concentrations and was more noticeable in the presence of Ca^{2+}. Simulations have produced similar results, as NaCl appears to increase lipid conformational order,[9,12,19] thus shrinking area per lipid[9,19] and increasing bilayer thickness.[9] When interacting with a bilayer, Na^+ ions may enforce spatial restrictions on the carbonyl oxygens and water[12] and assemble lipids to form small complexes with limited mobility.[9] In addition to the intrabilayer modifications, the interactions between neighboring bilayers are also affected.[20]

The head groups, in proximity of which the ions reside, are naturally most affected by the presence of ions. Although the ion is stripped of its surrounding water molecules upon binding,[12] the hydration of the head groups remains rather stable.[19] Salts are, however, able to change the conformations and dynamics of the dipolar phosphatidylcholine (PC) head groups.[17,21−26] Ions have a marked but local influence on the headgroup tilt, although the global average tilt remains roughly unaffected.[21,27] Lipid dipole reorientation and altered polarization of the water molecules generally counterbalance the effects on the electrostatic potential.[9] However, changes in the electrostatic potential have been observed as a result of adding NaCl to a PC membrane. The peak of the potential in the interfacial region was increased and shifted toward the water phase. The overall potential difference across one leaflet was also increased.[9,19,28]

The above stresses the view that ion-lipid interactions can play a crucial role in membrane properties. One of the most obvious techniques to gauge related phenomena are atom-scale simulations that have been shown to provide a great deal of added value for membrane studies,[29−31,13] complementing experiments. However, regardless of the great amount of attention that cardiolipin has spurred over the last decades, computational studies focusing on CL have been few. Currently, to the authors' knowledge no simulation studies focusing on CL−salt ion interactions have been published, and even the cases with neutralizing counterions are few.[32,33] The morphology of membranes with CLs has been dealt with coarse-grained simulations,[34] and two atomic-scale studies have concentrated on the influence of CL on membrane properties.[32,33]

The objective of the present study is to elucidate the interplay between ions and mitochondrial membranes. Atomic-scale molecular dynamics simulations of six different model systems have been carried out. The model bilayer compositions correspond to natural mitochondrial membranes (IM, OM), and the effect of two different salts (NaCl, $CaCl_2$) relevant to mitochondrial physiology have been investigated.

II. Model Description and Simulation Details

We studied six different membrane systems mimicking mitochondrial membranes with and without salt. Three of them corresponded to the inner membrane and three to the outer one. All systems included Na^+ counterions. The reference systems for IM without salt were obtained from our previous study.[33] The membranes were composed of PC (phosphatidylcholine), PE (phosphatidylethanol), and CL (see Figure 1). Linoleic acid was used as the acyl chains of the lipids, two chains in PC and PE and four in each CL. With double bonds in positions 9 and 11, linoleic acid is a diunsaturated chain of 18 carbons in length. In the inner membrane model, the composition was 54 PC, 46 PE, and 14 CL molecules.

For the outer membrane, the IM structures were revised to obtain bilayers with 64 PC, 56 PE, and 4 CL molecules, respectively. The compositions for IM and OM mirror those of

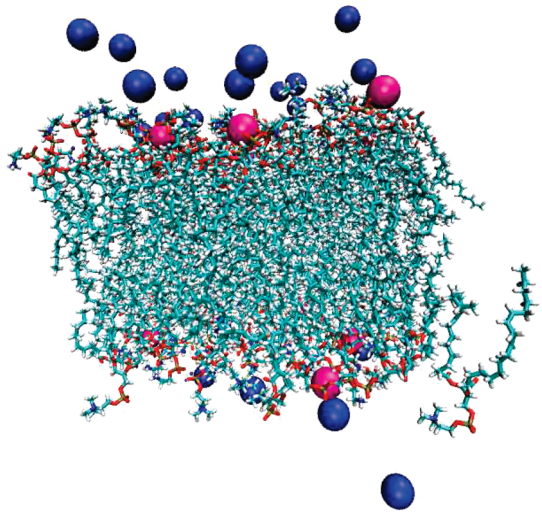

Figure 2. A snapshot of one of the simulated systems, the inner membrane with $CaCl_2$. Ca^{2+} ions are shown in purple and Cl^- ions in dark blue. Lipid oxygens are shown in red, carbons in cyan, and hydrogens in white. Water is omitted. This and other snapshot figures extracted from the simulations have been created with a molecular visualization program VMD.[69]

the natural inner and outer mitochondrial membranes.[4] NaCl and $CaCl_2$ with concentrations around 0.1 M were used as salt.

To consider the effect of salt concentration on lateral diffusion, we conducted additional IM simulations with varying concentrations of $CaCl_2$. Five simulations were carried out, the $CaCl_2$ concentrations being 0.02, 0.04, 0.06, 0.08, and 0.10 M. The IM was chosen for this purpose due to the larger fraction of cardiolipins in this membrane.

Figure 2 presents a snapshot of the inner membrane model with added $CaCl_2$. The names and descriptions are summarized in Table 1 and the structures and atom numbering are depicted in Figure 1.

The final configurations of earlier salt-free simulations[33] were adopted as initial structures. After separating the bilayers from their surroundings, layers of water (~1 nm thick) containing the ions were placed on both sides of the membrane. More water was added so that one system had around 5000 water molecules. The systems were simulated for 200 ns. This was condidered as equilibration time. At this point still more water was added to confirm that hydration is sufficient. The total number of water molecules was then about 8500. Further simulations of 100 ns were carried out for all six systems. Then, the first 20 ns was considered as final equilibration and the last 80 ns were used for the analysis. All together, we simulated 10 systems for a total of more than 3 μs.

The simulations were conducted using the GROMACS version 3.3.1,[35,36] and the protocol employed followed closely the one used in ref 33. An all-atom OPLS force field[37] was employed. Partial charges of PC and PE head groups were taken from refs 38 and 39, the derivation of both sets of charges being compatible with the OPLS methodology. These were also used for phosphate and carbonyl groups of CL. Standard OPLS charges were applied for hydroxyl groups and glycerol backbone. Each methylene and methyl group in the acyl chains was regarded as one charge group. In Figure 1, the charge groups are marked with dotted lines. This parametrization has been shown to correctly reproduce the properties of lipid bilayers composed of PC, PE, and glycolipids.[40] For water, the TIP3 model compatible with OPLS parametrization was employed.[41]

The time step was 2 fs and periodic boundary conditions with the usual minimum image convention were used in all three directions. To constrain the lengths of bonds containing hydrogen, the LINCS algorithm[42] was employed. The simulations were carried out at constant temperature of 310 K and pressure of 1 bar. During the first 20 ns of the simulation, pressure and temperature were controlled with the weak-coupling methods.[43] Subsequently the Nosé−Hoover thermostat[44,45] for temperature control and semi-isotropic Parrinello−Rahman barostat[46] for the pressure were employed with coupling time constants of 0.1 and 1.0, in respective order. The temperatures of the solute and solvent were controlled independently.

The Lennard-Jones interactions were cut off at 1.0 nm. For the electrostatic interactions we employed the particle-mesh Ewald method[47] with a real space cutoff of 1.0 nm. List of nonbonded pairs was updated every 10th time step.

III. Results

A. Equilibration. Previous simulations have indicated that proper equilibration is crucial when examining lipid bilayers with salt.[9,13,48,49] Decay toward equilibrium is slow when salt ions are present. This is partly due to the binding (and unbinding) of ions to the membrane−water interface, which usually has a characteristic time scale of about 50−200 ns, the largest equilibration times corresponding to systems with divalent salt.[48] Our results were in accord with this view. Extensive considerations of radial distribution functions between salt ions and lipid head groups and the resulting coordination numbers indicated that the time scales for equilibration extended up to 100 ns and even beyond this (data not shown). Hence, the first 200 ns of the simulation data were considered for equilibration.

B. Lipid Ordering and Condensation. Addition of cardiolipins to a mixed PC−PE−membrane in the absence of salt has been observed to slightly promote membrane condensation.[33] Previous studies have shown that both monovalent and divalent salt may have a rather remarkable effect on area per lipid and lipid conformational order in membranes rich in PCs, indicating salt ions to condense lipid bilayers.[9,13,19,28] In negatively charged membranes with salt, the area either decreases or remains the same.[12,14,50]

Here we have determined the area per lipid by first dividing the area of the bilayer by the number of acyl chains in a monolayer. This yields the average area per lipid acyl chain. The average "area per lipid" is then obtained by considering the area of two acyl chains. In this manner, the contributions of different lipid types (PCs and PEs with two acyl chains, and cardiolipins with four chains) is taken into account in an appropriate manner.[33]

In models of IM and OM studied in this work, we found the influence of salt to be rather marginal. In the inner membrane, the area per lipid was 0.618 ± 0.008 nm^2 in the absence of salt, and 0.613 ± 0.005 nm^2 for NaCl and 0.610 ± 0.005 nm^2 for $CaCl_2$. In the outer membrane, the results for area per lipid were similar, yielding 0.635 ± 0.009 nm^2, 0.633 ± 0.005 nm^2, and 0.625 ± 0.005 nm^2 for OM, OM_na, and OM_ca, respectively. Further studies on lipid conformational order (characterized by the S_{CD} order parameter often studied through NMR) yielded identical conclusions. NaCl and $CaCl_2$ had only a minor effect on lipid packing. Accordingly, the effect on the bilayer thickness is also negligible (data not shown).

The salt concentrations for NaCl and $CaCl_2$ used in this study are larger than their physiological values.[51−55] Thus, given the above results, it seems obvious that in actual mitochondrial membranes the influence of salt is rather minute.

C. Ion Binding. Electron density profiles are shown in Figure 3. Notably, calcium ions prefer to reside at the same depth as

TABLE 1: Abbreviations Used for the Systems

system name	numbers of molecules	corresponding natural membrane	salt added
IM_no-salt	54 PC, 46 PE, 14 CL	inner mitochondrial membrane	
IM_na	54 PC, 46 PE, 14 CL	inner mitochondrial membrane	NaCl
IM_ca	54 PC, 46 PE, 14 CL	inner mitochondrial membrane	$CaCl_2$
OM_no-salt	64 PC, 56 PE, 4 CL	outer mitochondrial membrane	
OM_na	64 PC, 56 PE, 4 CL	outer mitochondrial membrane	NaCl
OM_ca	64 PC, 56 PE, 4 CL	outer mitochondrial membrane	$CaCl_2$

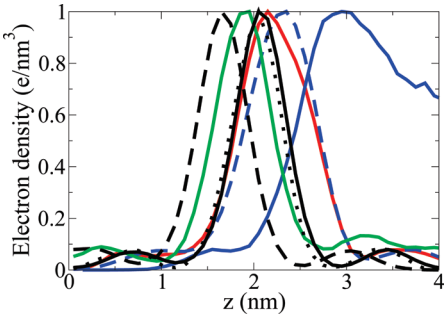

Figure 3. Electron density profiles of selected system components, namely some principal polar groups and ions. Shown are results for Ca (red line), Cl (solid blue line), Na (green line), choline and amine groups (dashed blue line), phosphate oxygens (solid black line), ester oxygens (dashed black line), and cardiolipin head groups (dotted black line). Only the inner membrane model with added Ca ions is shown. All profiles have been averaged over two leaflets, $z = 0$ corresponding to the membrane center, and the results are given in units of e/nm^3 though they have been here scaled by the maximum value of the given component.

the phosphate groups, whereas sodium ions penetrate deeper, their profile being centered between the phosphate and ester oxygens. This is in line with the observations of Miettinen et al.[13] Because of the cardiolipin molecular structure, the headgroup oxygens of CL are settled nearby the phosphate groups.

A more detailed look at the ions is given by their radial distribution functions (RDFs) with the oxygens they are supposed to interact with. For particle types A and B the radial distribution function is defined as

$$g_{AB}(r) = \frac{\langle \rho_B(r) \rangle}{\langle \rho_B \rangle_{local}} = \frac{1}{\langle \rho_B \rangle_{local} N_A} \sum_{i \in A}^{N_A} \sum_{j \in B}^{N_B} \frac{\delta(r_{ij} - r)}{4\pi r^2} \quad (1)$$

where $\langle \rho_B(r) \rangle$ denotes the density of type B particles at a distance r around type A particles, and $\langle \rho_B \rangle_{local}$ is the average density of type B particles inside a maximum radius around particles A.[56] The definition yields $g(r) = 1$ for an ideal gas. Deviation from unity implies correlations between the particle locations.

The coordination number of a given cation was calculated by counting the number of oxygen atoms inside its first hydration shell by evaluating the integral

$$N = \int_0^{r_{min}} dr 4\pi \rho g(r) r^2 \quad (2)$$

where ρ is the average number density of the given oxygens and r_{min} denotes the hydration shell radius.

We find that generally Ca^{2+} ions are more tightly bound to the interface than Na^+ ions. First shell coordination of Ca^{2+} ions with roughly 3−3.5 water oxygens and 3.5−3.7 phosphate oxygens was found. For Na^+ ions the numbers were 2.8 and 1.8, respectively. Coordination with ester oxygens was stronger for Na^+ ions, 1.1−1.4 oxygens per one Na^+ ion. The respective

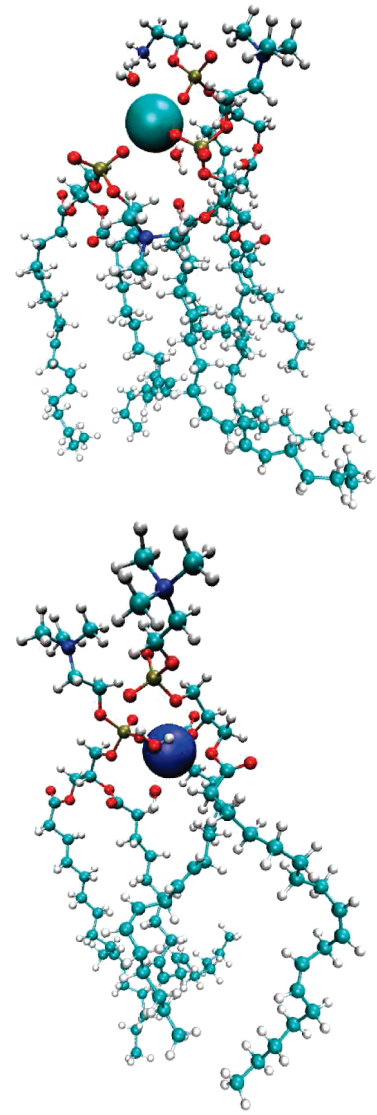

Figure 4. Complexes formed by ions interacting with oxygen atoms of lipid and water molecules. Calcium ion is surrounded by 2 water molecules, 2 PCs, and 1 PE (top), and Na^+ ion with PC and water molecules (bottom). Oxygens are marked red.

numbers for Ca^{2+} ions were 0.01 in the IM and 0.006 in the OM. Na^+ ions also preferred the headgroup oxygens of cardiolipin more than Ca^{2+} ions, consequently having an average coordination of 0.2 in the IM. The number for Ca^{2+} ions was negligible. In the OM the coordination numbers for cardiolipin headgroup oxygens are small due to only four CL molecules in the bilayer.

Single ions bind usually to more than one lipid, creating a small local lipid-ion cluster or complex. On average Na^+ binds 3.1 and Ca^{2+} 3.6 lipid molecules. Figure 4 demonstrates snapshots of such structures, where Ca^{2+} and Na^+ ions interact with water and lipid molecules. Distribution of the cluster size differs between the ions. Na^+ ions create both small and large

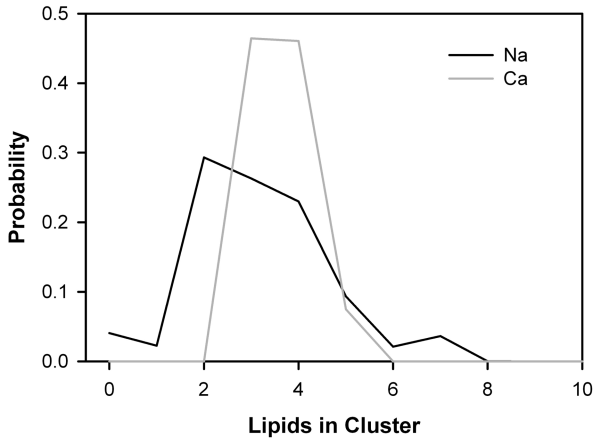

Figure 5. Distribution for the number of lipids bridged to an ion in the inner membrane. Results shown are for Na^+ and Ca^{2+} and the lipids in the cluster can be any from the lipids in the membrane; we found no preference among the lipids considered.

clusters, as Na^+ can be bonded from 1 to 7 lipid molecules (or remain unbound) while Ca^{2+} binds mainly 3−4 lipid molecules (see Figure 5). We did not find clear preferences for the studied lipids to be involved in a cluster. This observation should be taken with caution, however, since it is most likely due to insufficient statistics resulting from slow dynamics of ions exchanging between the various bonding sites at the water-membrane interface.[13,57,58]

D. Influence of Salt on Headgroup−Headgroup and Headgroup−Water Interactions. In our previous papers, we analyzed interactions at the water−membrane interface.[33,59] We considered direct hydrogen bonds, charge pairs between positively charged choline methyl group and negatively charge oxygen atoms as well as water bridges and hydration. These interactions were practically independent of ion type and thus no data is presented. The only clear effect of the Ca^{2+} ions is related to the decrease of the number of hydrogen bonded water molecules; the presence of calcium decreases hydration by about 5−15%.

E. Headgroup Orientation and Dynamics. The salt-induced effects on the lipid headgroup orientations were examined by computing the headgroup tilt angles. The angles were taken between the PN-vectors (from phosphorus to nitrogen) of PC and PE and the outward bilayer normal.

Figure 6 shows the obtained angle distributions. We find that the distributions of PC and PE head groups are pretty different. PE head groups are on average lying along the membrane plane, the distribution of angles being wide. In systems without salt, the average angle of PE gead groups is 91.2 (90.7)° in IM (OM). For PC, the corresponding angle is 74.5 (75.1) in IM (OM). Comparison with other studies is difficult to make, since the present three-component system is distinctly different from previous studies that have mainly focused on 1- or 2-component systems. However, the recent study by Zhao et al.[58] has shown PE tilt to be about 92° in a pure PE system, and other studies have indicated the PC tilt to be about 78° in pure PC systems.[60] The present results and especially their trend are therefore consistent with earlier findings.

We find that both the shape and the location of the angle distribution are influenced by the addition of salt. Because of a cloud of negatively charged chloride ions residing in the water phase near the bilayer interface, the positively charged amine and choline groups face an attractive force. Therefore, they are expected to stretch outward, that is, orient more vertically, decreasing the tilt angle. This occurs in the presence of both

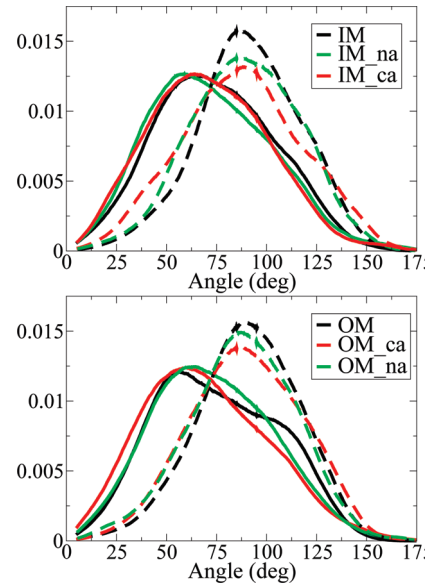

Figure 6. Tilt angle distributions of the PN-vectors of PC (solid lines) and PE (dashed lines).

ion species. Because Ca^{2+} ions are divalent whereas Na^+ ions are monovalent, there is both a stronger positive charge bound to the bilayer interface and a greater number of chloride ions in the system with $CaCl_2$. Furthermore, in these systems the negatively charged chloride ions are located closer to the bilayer interface.

Consequently, the average PN tilt angle is smaller in systems containing salt, the behavior of PC and PE headgroups being somewhat different. In IM systems the tilts of PC and PE decrease 3.1 and 3.8°, respectively, in the presence of $CaCl_2$, whereas NaCl results in a decrease of 2.4 and 1.9°. In the OM systems, the tilt of PE molecules decreases only 1° in the presence of $CaCl_2$ but that of PCs decreases 5.1°. NaCl causes a decrease of 1.7 and 2.8° for PC and PE tilts, respectively. The average tilt angle values of PC molecules in the IM systems were 74.5, 72.1, and 71.4° for salt-free, Na-containing and Ca-containing systems, respectively. For PEs, the respective numbers are 91.2, 89.3, and 87.4. In the outer membrane systems the tilt values for PCs were 75.1, 73.4, and 70° for salt-free, Na-containing and Ca-containing systems, respectively. For PEs the numbers are 90.7, 87.9 and 89.7, in respective order. In a previous study, Zhao et al.[58] found PE tilt to decrease for those head groups that were bound to Na^+ ions. Sachs et al. have found a similar effect due to Na^+ ions for PC head groups.[21] While the details vary due to the different systems studied, the trends are in line with one another.

To compare the dynamics, rotational motions of the molecules were analyzed through examining angular reorientation. For this purpose the second rank reorientational correlation functions[61] $C_2(t)$ were computed

$$C_2(t) \equiv \left\langle P_2(\hat{\mu}(0)\cdot\hat{\mu}(t))\right\rangle = \left\langle \frac{3}{2}(\hat{\mu}(0)\cdot\hat{\mu}(t))^2 - \frac{1}{2}\right\rangle \quad (3)$$

where $\hat{\mu}(t)$ is a unit molecular vector determining the rotational mode in question. The brackets denote averaging over all initial times and $P_2(x)$ is the second order Legendre polynomial. Information about the dynamics of molecules and the related relaxation times can be obtained experimentally with NMR and other relaxation experiments.

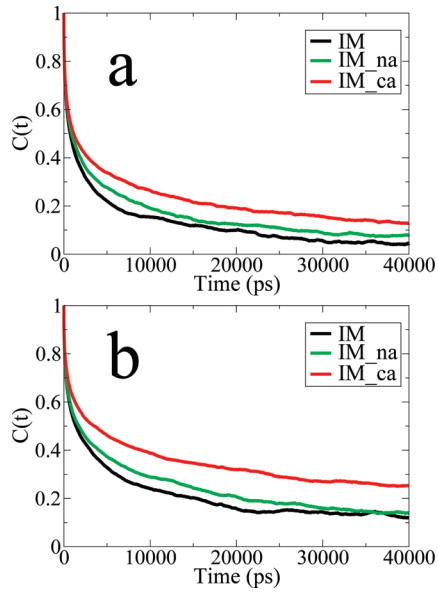

Figure 7. Rotation correlation functions of PN-vectors of (a) PC and (b) PE in the inner membrane.

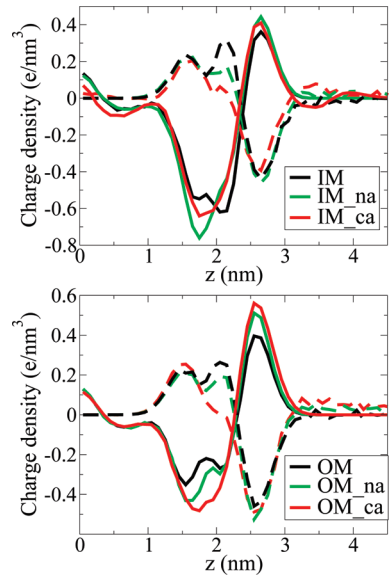

Figure 8. Bilayer (solid lines) and water (dashed lines) contributions to the charge density profile, where $z = 0$ corresponds to the membrane center.

The effect of salt on headgroup dynamics follows the pattern implied by the average tilt angles in the inner membrane systems and in the systems containing Ca^{2+} ions; see Figure 7. As the smaller average tilt angle of the PN vector implies, the rotational dynamics of the vector are restricted. This is seen as a slower decay of $C_2(t)$. Rotational dynamics is the slowest in the presence of $CaCl_2$, followed by NaCl, and the fastest in the absence of salt.

Generally, the deviation from the headgroup dynamics of the pure system upon salt inclusion is greater in the inner membrane systems. The main difference of these systems to the OM system is the greater number of CL molecules. Since cardiolipins are strongly charged, also the effects upon ion addition are expected to be greater in the cardiolipin-rich systems.

To conclude, the proximity of salt affects both the average tilt angle and the dynamics of the head groups. The mechanism supposedly involves shielding of the CL charges and also partial charges of the lipids. Moreover, salt modifies the headgroup interactions with water, such as hydrogen bonding. Indeed, the presence of salt was observed to decrease the hydrogen bonds between lipids and water (data not shown).

F. Electrostatics. Electrostatic potential across the bilayer interface plays a crucial role in the interplay between the membrane surface and a variety of charged substances, such as ions. To characterize the membrane potential, we first compute the charge density across the system by dividing the simulation box into slices and counting the number of charges in each slice. To attain the electrostatic potential, this profile was integrated twice from the water phase toward bilayer center as follows

$$\Phi(z) - \Phi(0) = \frac{-1}{\varepsilon_0} \int_0^z \int_0^{z'} \mathrm{d}z'' \mathrm{d}z' \rho(z'') \qquad (4)$$

where ε_0 is the permittivity of vacuum and ρ is the charge density. For practical aspects regarding the calculation of the membrane potential, see ref 62.

Figure 8 illustrates the individual contributions of lipids and water to the total charge density across one leaflet of the membrane. We find that these two components partially compensate each other in the interface region. The more negative charge of the lipid components in the inner membrane systems is due to the greater number of negatively charged cardiolipin molecules. Whereas the locations of ester and headgroup oxygens are represented as negative peaks around 1.5−2 nm in the lipid charge profile, the choline groups contribute to a positive peak around 2.5 nm. Notably, the charge density in the neutral hydrocarbon core of the bilayer is not zero due to the nonzero partial charges of chain carbons and hydrogens.

As expected, the effect of salt addition is seen in the interface region, whereas the charge near the bilayer center remains unaffected in all the other cases except the inner membrane system with Ca^{2+} ions. The positive and negative peaks in the choline and ester-phosphate regions are greater when salt has been added, which is mainly not compensated by changes in the water profile. Ca^{2+} ions, whose charge is double compared to Na^+ ions, induce greater changes in the charge densities, especially the water contribution profile around 2 nm is of different shape compared to the other systems.

The total electrostatic potential across one monolayer was calculated as an average of the two leaflets (see Figure 9). As here we have used an all-atom model with nonzero partial charges in the chain hydrogens and carbons, the potential in the bilayer center is positive. This is in agreement with previous findings.[63,64] In contrast, the simulations with united-atom force fields yield a flat potential in the hydrocarbon region, since the chains are uncharged.[63]

In the inner membrane models, the changes upon salt addition occur mainly inside the bilayer (0−1.5 nm) and just outside the bilayer (3 - 4 nm). Roughly the opposite happens in the outer membrane systems, where the potential becomes more positive in the interfacial region. This is in accordance with results of united-atom simulations of bilayers with added NaCl.[9,13,19] Additionally, the positive peak around 2 nm moves slightly toward the water phase. Similar observations have been seen by Miettinen et al.[13] in cationic membranes (DMPC and DMTAP) in the presence of added salt.

Both the location of the charged ions with respect to the bilayer and the orientation of the polar lipids affect the potential. As shown in the previous sections, positive ions accumulate to the bilayer interface region, monovalent Na^+ ions slightly deeper than the divalent Ca^{2+} ions. A cloud of negative chloride ions

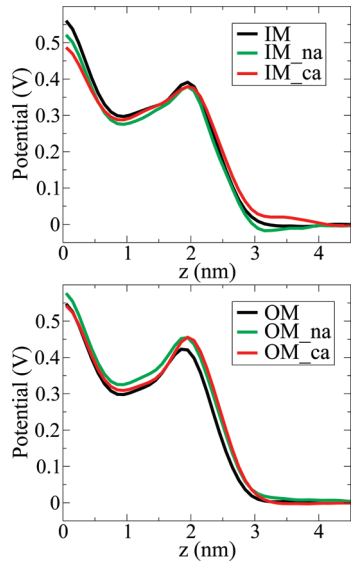

Figure 9. Electrostatic potential of all system components calculated from the membrane center ($z = 0$) toward the water phase.

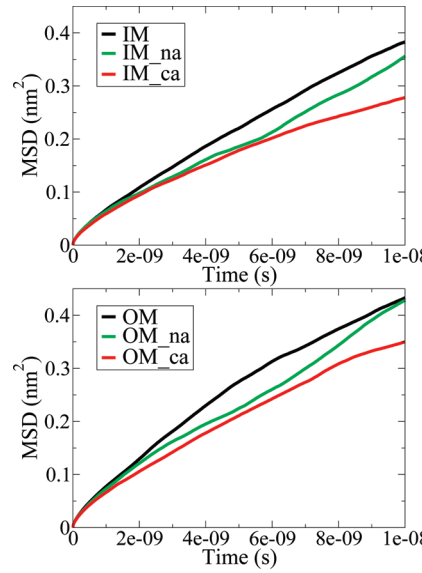

Figure 10. Mean-squared displacements of PC molecules in inner and outer membrane models.

resides just outside the bilayer, interacting with the amine and choline groups. This distribution of ions causes a more positive potential in the interface region with respect to the water phase, when compared to a pure reference system. However, the effect is largely compensated for by the reorientation of the lipid electric dipoles, particularly the head groups. The larger impact of ions on the inner membrane model is presumably due to the greater portion of cardiolipin molecules. Their head groups are very small and thus incapable to greatly compensate for the effect of added ions by conformational change. In addition, CL is strongly charged and its intramolecular movements are more restricted due to the dimeric structure. As aforementioned, the presence of CL has also been shown to limit the movements of PC and PE head groups, further exposing the bilayer to salt effects.

G. Influence of Salt on Lateral Diffusion. Because of the lipid−ion complex formation, the lateral mobility of the lipids is greatly restricted. Previous studies, both experiments and simulations, have shown that this may lead to a significant alteration of the lateral diffusion coefficient of the lipids.[9,49] However, there are also systems where lateral diffusion is only weakly affected by salt.[13]

The diffusion coefficients were calculated using the Einstein relation

$$D_T = \lim_{t\to\infty} \frac{1}{2dt}\langle|\vec{r}(t)|^2\rangle \qquad (5)$$

where $\vec{r}(t)$ is the center of mass position of a molecule at time t and $\langle|\vec{r}(t)|^2\rangle$ its mean-squared displacement (MSD). Dimensionality of the surface d equals 2. Monolayer CM movement was taken into account when calculating the coefficients.[13,65] In practice, the diffusion coefficients were extracted from the slope of the MSD over a time interval of 2−5 ns, averaging over the whole section of trajectory that was used for analysis.

Figure 10 shows the mean-squared displacement of PC molecules in the different systems. The data for other lipid species show the same trend.

The results for a salt concentration of 0.1 M are summarized in Table 2. As expected, the movement of lipids is slower in the cardiolipin-rich inner membrane systems due to the restricting nature of large cardiolipin molecules. Diffusion is also restrained by salt, as the decelerating effect of around 10−30% upon salt addition is clearly seen for all lipid species in all systems. This effect is strongest in systems containing $CaCl_2$. Lipid-wise, the large cardiolipin molecules move around slower than the smaller PC and PE molecules.

TABLE 2: Diffusion Coefficients of the Lipids in the Inner and Outer Membrane Systems for a Salt Concentration of 0.1 M in Units of 10^{-8} cm^2/s[a]

	D		
system name	PC	PE	CL
IM_no-salt	9.5	9.4	7.7
IM_na	7.6	6.7	6.8
IM_ca	6.9	6.3	5.7
OM_no-salt	12.1	9.6	
OM_na	8.4	8.2	
OM_ca	8.8	8.5	

[a] Error bars are ±7% for PC and PE, and ±12% for CL. Data for CL diffusion in the outer membrane system is ignored due to the small number of CL molecules.

TABLE 3: Diffusion Coefficients of the Lipids in the Inner Membrane Systems for Varying $CaCl_2$ Concentration of 0.02−0.1 M in Units of 10^{-8}cm^2/s[a]

	D		
concentration	PC	PE	CL
0.00 M	9.5	9.4	7.7
0.02 M	7.4	7.3	6.4
0.04 M	8.4	7.6	7.6
0.06 M	7.4	6.8	6.3
0.08 M	6.8	7.2	5.5
0.10 M	6.9	6.3	5.7

[a] Error bars are ±7% for PC and PE, and ±12% for CL.

For increasing concentration of $CaCl_2$, we find a rather substantial dependence of D on salt concentration; see Table 3. The diffusion coefficient in IM decreases by ∼30% as $CaCl_2$ concentration increases from 0 to 0.1 M. A similar trend has been observed for monovalent salt by Bockmann et al.[9] Moreover, in the so far most extensive simulation study of the effect of salt on lateral diffusion, including the diffusion of salt ions themselves, Miettinen et al.[13] found lipid diffusion to be

rather weakly affected for small concentrations of NaCl (0.1 M), while the effect for larger salt concentrations was almost negligible.[13] The effect of salt on diffusion was also found to be system specific, depending on the lipid composition. Our general findings are in line with Miettinen et al.[13]

However, while it is apparent that Ca^{2+} ions slow down the diffusion of individual lipids through ion binding and cluster formation, it is not clear whether this is significant over larger scales in the membrane plane; typical concentrations of Ca^{2+} ions on the cytosolic side of a mitochondrion are of the order of μM,[53] which is considerably smaller than the concentrations we have considered.

IV. Concluding Remarks

Because of the crucial role of mitochondria in Ca^{2+} metabolism and the proved effects of Na^+ and Ca^{2+} ions on membranes, this work has focused on the effect of salt on the inner and outer mitochondrial membranes. To this end, we have exploited atomistic simulations to consider ternary model membranes constructed of zwitterionic PC and PE lipids and anionic cardiolipin molecules, the consentrations reflecting those of natural inner and outer mitochondrial membranes.

As expected, the influence of salt is predominantly seen in the headgroup region of the bilayer. Sodium ions penetrate deeper to the bilayer interface compared to the larger, divalent calcium ions. While association of Ca^{2+} ions with the ester groups was negligible, every Na^+ ions had on average one neighboring ester oxygen. Both cations, however, preferred the phosphate oxygens to the ester groups. Notably more Na^+ compared to Ca^{2+} ions resided near the hydroxyl headgroup of CL. As a result of ion coordination with the polar lipid oxygens, aggregates of lipids and water molecules were formed. Similar complex formation has been observed in other studies involving bilayers with salt.[9,12] It has been shown to restrict the movement of lipids, thus slowing their diffusion in the plane of the membrane.[9,49]

The presence of salt alters the electrostatic potential across the membrane leaflets. However, the effect is partially compensated by reorientation of the electric dipoles of lipids and water. Consistent with the findings of a previous study,[49] a slightly more vertical orientation of the PC and PE head groups was induced by the presence of salt.

Furthermore, the dynamics of lipid head groups were restricted, more so in the cardiolipin-rich inner membrane model. This effect might be partially due to the shielding of the CL charges and also partial charges of the lipids by cations. Moreover, salt modifies the headgroup interactions with water.

The portion of cardiolipin molecules of the membrane lipids seems to influence the salt's capability to alter both the headgroup behavior and the electrostatic potential. Indeed, a more pronounced impact of ions in the inner membrane model with greater number of CL was observed. This is presumably due to many of the molecule's structural features. CL is strongly charged and its intramolecular movements are rather restricted due to the dimeric structure. Furthermore, the small headgroup is insufficient to greatly affect the electric potential by changing its orientation. The presence of CL has also been shown to confine the movements of PC and PE head groups,[33] which should make the bilayer more susceptible to salt effects.

To the authors' knowledge, the current work is the first computational study concerning mitochondrial membrane properties in the presence of salt. The main focus was on the basic modifications induced by ions to the bilayer. Because of the vital role of charge transport in ATP production, the interplay between ions and lipids as well as electrostatic properties of the bilayer are crucial in the inner mitochondrial membrane. Of particular interest are the effects on cardiolipin and its rich phase behavior, as cardiolipin has been shown to be required for the maintenance of mammalian mitochondrial structure and inner membrane potential.[66] Divalent cations are known to increase the propensity of cardiolipin to form nonlamellar structures,[1] which are found in, for example, contact sites between the inner and outer mitochondrial membranes. These are, indeed, enriched in cardiolipin and are involved in lipid transport and apoptosis.[67] Bilayer features also crucially affect the function of embedded proteins,[68] such as respiratory chain complexes and carrier proteins of the inner membrane. Along with mitochondrial membranes, the results gained are relevant for other bilayers with coupled electron transport and phosphorylation. Such membranes include among others chloroplasts and bacterial membranes.[2]

Acknowledgment. We would like to thank C. S. Oliver for careful reading of the manuscript. We acknowledge support from the Academy of Finland (T.R., I.V.) and the Natural Sciences and Engineering Research Council (NSERC) of Canada (M.K.). The Finnish IT Centre for Science and the HorseShoe Computing cluster in the University of Southern Denmark are thanked for computing resources.

References and Notes

(1) Schlame, D. R. M.; Greenberg, M. L. The biosynthesis and functional role of cardiolipin. *Prog. Lipid Res.* **2000**, *39*, 257–288.

(2) Hoch, F. L. Cardiolipins and biomembrane function. *Biochim. Biophys. Acta* **1992**, *1113*, 71–133.

(3) Deguchi, H.; Fernández, J. A.; Hackeng, T. M.; Bankadagger, C. L.; Griffin, J. H. Cardiolipin is a normal component of human plasma lipoproteins. *Proc. Natl. Acad. Sci. U.S.A.* **2000**, *97*, 1743–1748.

(4) Daum, G. Lipids of mitochondria. *Biochim. Biophys. Acta* **1985**, *822*, 1–42.

(5) Nichols-Smith, S.; Kuhl, T. Electrostatic interactions between model mitochondrial membranes. *Colloids Surf., B* **2005**, *41*, 121–127.

(6) Lewis, R. N.; Zweytick, A. H. D.; Pabst, G.; Lohner, K.; McElhaney, R. N. Calorimetric, X-ray diffraction, and spectroscopic studies of the thermotropic phase behavior and organization of tetramyristoyl cardiolipin membranes. *Biophys. J.* **2007**, *92*, 3166–3177.

(7) Zhang, M.; Mileykovskaya, E.; Dowhan, W. Gluing the respiratory chain together. *J. Biol. Chem.* **2002**, *277*, 43553–43556.

(8) Haines, T. H.; Dencher, N. A. Cardiolipin: a proton trap for oxidative phosphorylation. *FEBS Lett.* **2002**, *26508*, 1–5.

(9) Bockmann, R. A.; Hac, A.; Heimburg, T.; Grubmuller, H. Effect of sodium chloride on a lipid bilayer. *Biophys. J.* **2003**, *85*, 1647–1655.

(10) Sammalkorpi, M.; Karttunen, M.; Haataja, M. Sodium dodecyl sulphate (SDS) in the presence of excess NaCl and CaCl2. *J. Phys. Chem. B* **2009**, *113*, 5863–5870.

(11) Cevc, G. Membrane electrostatics. *Biochim. Biophys. Acta* **1990**, *1031*, 311–382.

(12) Mukhopadhyay, P.; Monticelli, L.; Tieleman, D. P. Molecular dynamics simulation of a palmitoyl-oleoyl phosphatidylserine bilayer with Na+ counterions and NaCl. *Biophys. J.* **2004**, *86*, 1601–1609.

(13) Miettinen, M. S.; Gurtovenko, A. A.; Vattulainen, I.; Karttunen, M. Ion Dynamics in Cationic Lipid Bilayer Systems in Saline Solutions *J. Phys. Chem. B*, in press.

(14) Pandit, S. A.; Berkowitz, M. L. Molecular dynamics simulation of dipalmitoylphosphatidylserine bilayer with Na+ counterions. *Biophys. J.* **2002**, *82*, 1818–1827.

(15) Cascales, J. J. L.; de la Torre, J. G.; Marrink, S. J.; Berendsen, H. J. C. Molecular dynamics simulation of a charged biological membrane. *J. Chem. Phys.* **1996**, *104*, 2713–2720.

(16) Parsegian, V. A.; Rand, R. P. Interactions in Membrane Assemblies In *Structure and Dynamics of Membranes*, 1st ed.; Lipowsky, R., Sackmann, E., Eds.; Elsevier, North-Holland: Amsterdam, 1995.

(17) Rydall, J. R.; Macdonald, P. M. Investigation of anion binding to neutral lipid membranes using ^{2}H NMR. *Biochemistry* **1992**, *31*, 1092–1099.

(18) Pabst, G.; Hodzic, A.; Strancar, J.; Danner, S.; Rappolt, M.; Laggner, P. Rigidification of neutral lipid bilayers in the presence of salts. *Biophys. J.* **2007**, *93*, 2688–2696.

(19) Pandit, S. A.; dagger, D. B.; Berkowitz, M. L. Molecular dynamics simulation of a dipalmitoylphosphatidylcholine bilayer with NaCl. *Biophys. J.* **2003**, *84*, 3743–3750.

(20) Petrache, H. I.; Tristram-Nagle, S.; Harries, D.; Kucerka, N.; Nagle, J. F.; Parsegian, V. A. Swelling of phospholipids by monovalent salt. *J. Lipid Res.* **2006**, *47*, 302–309.

(21) Sachs, J. N.; Nanda, H.; Petrache, H. I.; Woolf, T. B. Changes in phosphatidylcholine headgroup tilt and water order induced by monovalent salts: molecular dynamics simulations. *Biophys. J.* **2004**, *86*, 3772–3782.

(22) Brown, M. F.; Seelig, J. Ion-induced changes in head group conformation of lecithin bilayers. *Nature* **1977**, *269*, 721–723.

(23) Loosley-Millman, M. E.; Rand, R. P.; Parsegian, V. A. Effects of monovalent ion binding and screening on measured electrostatic forces between charged phospholipid bilayers. *Biophys. J.* **1982**, *40*, 221–232.

(24) Macdonald, P. M.; Seelig, J. Anion binding to neutral and positively charged lipid membranes. *Biochemistry* **1988**, *27*, 6769–75.

(25) Clarke, R. J.; Lüpfert, C. Influence of anions and cations on the dipole potential of phosphatidylcholine vesicles: a basis for the Hofmeister effect. *Biophys. J.* **1999**, *76*, 2614–2624.

(26) Roux, M.; Bloom, M. Ca2+, Mg2+, Li+, Na+, and K+ distributions in the headgroup region of binary membranes of phosphatidylcholine and phosphatidylserine as seen by deuterium NMR. *Biochemistry* **1990**, *29*, 7077–7089.

(27) Sachs, J. N.; Woolf, T. B. Understanding the Hofmeister effect in interactions between chaotropic anions and lipid bilayers: molecular dynamics simulations. *J. Am. Chem. Soc.* **2003**, *125*, 8742–8743.

(28) Gurtovenko, A. A.; Vattulainen, I. Effect of NaCl and KCL on phosphatidylcholine and phosphatidylethanolamine lipid membranes: Insight from atomic-scale simulations for understanding salt-induced effects in the plasma membrane. *J. Chem. Phys.* **2008**, *112*, 1953–1962.

(29) Niemela, P.; Hyvönen, M. T.; Vattulainen, I. Atom-scale molecular interactions in lipid raft mixtures. *Biochim. Biophys. Acta* **2009**, *1788*, 122–135.

(30) Rog, T.; Pasenkiewicz-Gierula, M.; Vattulainen, I.; Karttunen, M. Ordering effects of cholesterol and its analogues. *Biochim. Biophys. Acta* **2009**, *1788*, 97–121.

(31) Marrink, S. J.; de Vries, A. H.; Tieleman, D. Lipids on the move: simulations of membrane pores, domains, stalks, and curves. *Biochim. Biophys. Acta* **2009**, *1788*, 149–168.

(32) Dahlberg, M.; Maliniak, A. Molecular dynamics simulations of cardiolipin bilayers. *J. Phys. Chem. B.* **2008**, *112*, 11655–11663.

(33) Róg, T.; Martinez-Seara, H.; Reigada, R.; Munck, N.; Oresic, M.; Karttunen, M.; Vattulainen, I. Role of cardiolipins in lipid bilayer structure - properties of water membrane interface. *J. Phys. Chem. B* **2009**, *113*, 3413–3422.

(34) Dahlberg, M. Polymorphic phase behavior of cardiolipin derivatives studied by coarse-grained molecular dynamics. *J. Phys. Chem. B* **2007**, *111*, 7194–7200.

(35) Berendsen, H. J. C.; va derSpoel, D.; van Drunen, R. GROMACS: A message-passing parallel molecular dynamics implementation. *Comput. Phys. Commun.* **1995**, *91*, 43–56.

(36) Lindahl, E.; Hess, B.; van der Spoel, D. Gromacs 3.0: A package for molecular simulation and trajectory analysis. *J. Mol. Model.* **2001**, *7*, 306–317.

(37) Jorgensen, W. L.; Tirado-Rives, J. The OPLS potential functions for proteins. Energy minimizations for crystals of cyclic peptides and crambin. *J. Am. Chem. Soc.* **1988**, *110*, 1657–1666.

(38) Takaoka, Y.; Pasenkiewicz-Gierula, M.; Miyagawa, H.; Kitamura, K.; Tamura, Y.; Kusumi, A. Molecular dynamics generation of non-arbitrary membrane models reveals lipid orientational correlations. *Biophys. J.* **2000**, *79*, 3118–3138.

(39) Murzyn, K.; Pasenkiewicz-Gierula, M. Construction and optimization of a computer model for a bacterial membrane. *Acta Biochim. Pol.* **1999**, *46*, 631–639.

(40) Róg, T.; Vattulainen, I.; Bunker, A.; Karttunen, M. Glycolipid membranes through atomistic simulations: effect of glucose and galactose head groups on lipid bilayer properties. *J. Phys. Chem. B* **2007**, *111*, 10146–10154.

(41) Jorgensen, W. L.; Chandrasekhar, J.; Madura, J. D.; Impey, R.; Klein, M. L. Comparison of simple potential functions for simulating liquid water. *J. Chem. Phys.* **1983**, *79*, 926–935.

(42) Hess, B.; Bekker, H.; Berendsen, H. J. C.; Fraaije, J. G. E. M. LINCS: A linear constraint solver for molecular simulations. *J. Comput. Chem.* **1997**, *18*, 1463–1472.

(43) Berendsen, H. J. C.; Postma, J. P. M.; DiNola, A.; Haak, J. R. Molecular dynamics with coupling to an external bath. *J. Chem. Phys.* **1984**, *81*, 3684–3690.

(44) Nóse, S. A unified formulation of the constant temperature molecular dynamics methods. *J. Chem. Phys.* **1984**, *81*, 511–519.

(45) Hoover, W. G. Canonical dynamics: equilibrium phase-space distributions. *Phys. Rev. A* **1985**, *31*, 1695–1697.

(46) Parrinello, M.; Rahman, A. Polymorphic transitions in single crystals: A new molecular dynamics method. *J. Appl. Phys.* **1981**, *52*, 7182–7190.

(47) Essman, U.; Perera, L.; Berkowitz, M. L.; Darden, H. L. T.; Pedersen, L. G. A smooth particle mesh Ewald method. *J. Chem. Phys.* **1995**, *103*, 8577–8592.

(48) Bockmann, R. A.; Grubmuller, H. Multistep binding of divalent cations to phospholipid bilayers: A molecular dynamics study. *Angew. Chem., Int. Ed.* **2004**, *43*, 1021–1024.

(49) Gurtovenko, A. A. Asymmetry of lipid bilayers induced by monovalent salt: Atomistic molecular-dynamics study. *J. Chem. Phys.* **2005**, *122*, 244902.

(50) Pedersen, U. R.; Leidy, C.; Westh, P.; Peters, G. H. The effect of calcium on the properties of charged phospholipid bilayers. *Biochim. Biophys. Acta* **2006**, *1758*, 573–582.

(51) Donoso, P.; Mill, J. G.; O'Neill, S. C.; Eisner, D. A. Fluorescence measurements of cytoplasmic and mitochondrial sodium concentration in rat ventricular myocytes. *J. Physiol.* **1992**, *448*, 493–509.

(52) Baron, S.; van de Ven, M.; Radu, M.; Despa, S.; Lambrichts, I.; Ameloot, M.; Steels, P.; Smets, I. Role of mitochondrial Na+ concentration, measured by corona red, in the protection of metabolically inhibited MDCK cells. *J. Am. Soc. Nephrol.* **2005**, *16*, 3490–3497.

(53) Chalmers, S.; Nicholls, D. The relationship between free and total calcium concentrations in the matrix of liver and brain mitochondria. *J. Biol. Chem.* **2002**, *278*, 19062–19070.

(54) Bernardi, P. Mitochondrial transport of cations: channels, exhangers and permeability transition. *Physiol. Rev.* **1999**, *79*, 1127–1155.

(55) Miyata, H.; Silverman, H. S.; Sollot, S. J.; Lakatta, E. G.; Stern, M. D.; Hansford, R. G. Measurement of mitochondrial free Ca2+ concentration in living single rat cardiac myocytes. *Am. J. Physiol. Heart Circ. Physiol.* **1991**, *261*, 1123–1134.

(56) van der Spoel, D. Lindahl, E. Hess, B. van Buuren, A. R. Apol, E. Meulenhoff, P. J. Tieleman, D. P. Sijbers, A. L. T. M. Feenstra, K. A. van Drunen, R., Berendsen, H. J. C. Gromacs user manual version 3.2. www.gromacs.org; 2004.

(57) Zhao, W.; Rog, T.; Gurtovenko, A.; Vattulainen, I.; Karttunen, M. Atomic-scale structure and electrostatics of anionic POPG lipid bilayers with Na+ counterions. *Biophys. J.* **2007**, *92*, 1114–1124.

(58) Zhao, W.; Rog, T.; Gurtovenko, A.; Vattulainen, I.; Karttunen, M. Role of phosphatidylglycerols in the stability of bacterial membranes. *Biochimie* **2008**, *90*, 930–938.

(59) Murzyn, K.; Zhao, W.; Karttunen, M.; Kurdziel, M.; Rog, T. Dynamics of water at membrane surfaces: effect of headgroup structure. *Biointerphases* **2006**, *1*, 98–105.

(60) Ollila, S.; Hyvonen, M. T.; Vattulainen, I. Polyunsaturation in Lipid Membranes: Dynamic Properties and Lateral Pressure Profiles. *J. Phys. Chem. B* **2007**, *111*, 3139–3150.

(61) *Biological Membranes*; Merz, K.; Roux, B., Eds.; Birkhauser: Boston, MA, 1996.

(62) Gurtovenko, A. A.; Vattulainen, I. Calculation of the electrostatic potential of lipid bilayers from molecular dynamics simulations: Methodological issues *J. Chem. Phys.*, in press.

(63) Siu, S. W. I.; Vacha, R.; Jungwirth, P.; Bockmann, R. A. Biomolecular simulations of membranes: Physical properties from different force fields. *J. Chem. Phys.* **2008**, *128*, 125103.

(64) Gawrisch, K.; Ruston, D.; Zimmerberg, J.; Parsegian, V. A.; Rand, R. P.; Fuller, N. Membrane dipole potentials, hydration forces, and the ordering of water at membrane surfaces. *Biophys. J.* **1992**, *61*, 1213–1223.

(65) Patra, M.; Karttunen, M.; Hyvönen, M. T.; Falck, E.; Lindqvist, P.; Vattulainen, I. Molecular dynamics simulations of lipid bilayers: major artifacts due to truncating electrostatic interactions. *Biophys. J.* **2003**, *84*, 3636–3645.

(66) Choi, S. Y.; Gonzalvez, F.; Jenkins, G. M.; Slomianny, C.; Chretien, D.; Arnoult, D.; Petit, P. X.; Frohman, M. A. Cardiolipin deficiency releases cytochrome c from the inner mitochondrial membrane and accelerates stimuli-elicited apoptosis. *Cell Death Differ.* **2007**, *14*, 597–606.

(67) Epand, R. F.; Schlattner, U.; Wallimann, T.; Lacombe, M.-L.; Epand, R. M. Novel lipid transfer property of two mitochondrial proteins that bridge the inner and outer membranes. *Biophys. J.* **2007**, *92*, 126–137.

(68) Alberts, B.; Lewis, D. B. J.; Raff, M.; Roberts, K.; Watson, J. D. *Molecular Biology of the Cell*, 3rd ed.; Garland: New York, 1994.

(69) Humphrey, W.; Dalke, A.; Schulten, K. VMD - Visual Molecular Dynamics. *J. Mol. Graphics* **1996**, *14.1*, 33–38.

JP905915M

Paper III

S. Pöyry, O. Cramariuc, P. Postila, K. Kaszuba, M. Sarewicz, A. Osyczka, I. Vattulainen and T. Róg. Atomistic simulations indicate cardiolipin to have an integral role in the structure of the cytochrome bc1 complex. Submitted to BBA Bioenergetics (2012).

Atomistic simulations indicate cardiolipin to have an integral role in the structure of the cytochrome bc_1 complex

Sanja Pöyry[a], Oana Cramariuc[a], Pekka A. Postila[a], Karol Kaszuba[a], Marcin Sarewicz[b], Artur Osyczka[b], Ilpo Vattulainen[a,c], and Tomasz Róg[a*]

[a]Department of Physics, Tampere University of Technology, P.O. Box 692, FI-33101 Tampere, Finland
[b]Department of Biophysics, Jagiellonian University, Kraków, Poland
[c]MEMPHYS Center for Biomembrane Physics, University of Southern Denmark, Odense, Denmark

E-mail: Ilpo.Vattulainen@tut.fi, tomasz.rog@gmail.com

Abstract

The reaction mechanism of the cytochrome (*cyt*) bc_1 complex relies on proton and electron transfer to/from the substrate quinone/quinol, which in turn generate a proton gradient across the mitochondrial membrane used in the ATP synthesis. Cardiolipin (CL) lipids have been suggested to play an important role in *cyt* bc_1 function by both ensuring the structural integrity of the protein complex and also by taking part in the proton uptake. Yet, the atom-scale understanding of these highly charged four-tail lipids in the *cyt* bc_1 function has remained quite unclear. We consider this issue through atomistic molecular dynamics simulations that are applied to the entire *cyt* bc_1 dimer of the purple photosynthetic bacterium *Rhodobacter capsulatus* embedded in a lipid bilayer. We find CLs to spontaneously diffuse to the dimer interface to the immediate vicinity of the higher potential heme groups of the complex's catalytic (quinone reduction) Q_i-sites. This observation is in full agreement with earlier predictions based on crystallographic studies of the complex, and supports the view that CLs are key players in the proton uptake. The simulation results also allow us to present a refined picture for the dimer arrangement in the *cyt* bc_1 complex, the novelty of our work being the description of the role of the surrounding lipid environment: in addition to the specific CL-protein interactions, we observe the protein domains on the positive side of the membrane to settle against the lipids. This conformational shift was furthermore found to be more evident when the Q_o-site (the hydroquinone oxidation site) lacked a bound substrate. Altogether, the simulations discussed in this article provide novel views into the dynamics of *cyt* bc_1 with lipids, complementing previous experimental findings.

Keywords: cardiolipin, cytochrome bc_1, membrane protein, molecular dynamics simulations, proton transfer

1. Introduction

The role of lipids in biological membranes and their function has earlier been undervalued, though the situation has changed quite recently [1]. Nowadays it is known that the lipids surrounding membrane proteins may have a role in proteins' stability, membrane partitioning, folding, assembly, and dynamics [2,3]. It has also been realized that lipids can modulate or even govern the function of membrane proteins [4]. For instance, there is ample evidence that generic membrane properties such as hydrophobic thickness, phase behavior, surface charge, and membrane elasticity [2,4] can influence conformations of membrane-embedded proteins. Besides these membrane-mediated interactions, individual lipids may also play a crucial role in protein function through specific binding and interaction patterns. The latter possibility is a very timely topic since recent studies by Contreras et al. have shown concretely how sphingomyelin, one of the abundant lipid types in e.g. plasma membranes, interacts specifically with certain transmembrane protein domains [5].

Further, X-ray crystallographic studies have suggested that several membrane proteins include specific phospholipid species as integral parts of their structures [6]. Some of these lipids bind to well-defined binding pockets and are a prerequisite for the structural integrity and proper function of the proteins [6]. The underlying reasons to the lipid specificity and the detailed role of the lipids in the protein function have, however, remained largely

elusive. To a large extent, this is due to practical issues that limit the chances of experiments to clarify atomistic-scale phenomena associated with dynamic lipid-protein interactions.

One of the appropriate means to complement experiments is to consider complex membrane-protein systems in a purely atomistic manner through molecular dynamics (MD) simulations. This approach not only provides structural information of lipid-protein complexes but it also generates knowledge on the dynamic properties of proteins in membranes.

In this spirit, here we study the effects of lipids on the cytochrome (*cyt*) bc_1 complex (or complex III, see Fig. 1) of the purple photosynthetic bacterium *Rhodobacter capsulatus* using atomistic MD simulations. The bacterial *cyt* bc_1 complex is a 6-subunit dimer, composed of *cyt b*, *cyt* c_1, and iron sulfur protein (ISP) subunits (Fig. 1A). It functions as a redox carrier in the electron transport chain, a key part of bacterial and eukaryotic energy metabolism, embedded in a cardiolipin-rich membrane (Fig. 1B). During the catalytic reaction of the *cyt* bc_1 complex (also called the Q-cycle) one quinol molecule is oxidized at the Q_o-site (that is thereby known as the oxidation site) and two electrons and protons are released. One of the electrons is delivered *via* the 2-iron 2-sulfur cluster (see Fig. 1B for Fe_2S_2 as part of the ISP subunit) to the heme c_1 redox center (Fig. 1B describing also part of the *cyt* c_1 subunit). Meanwhile, the other electron is routed *via* the low potential heme (b_L in Fig. 1B) and the high potential heme (b_H in Fig. 1B) redox centers at the Q_i-site (quinone reduction site) to reduce a non-protonated substrate quinone. Because the reaction is bifurcated, two Q-cycles are needed to produce a fully protonated substrate quinol at the Q_i-site (quinone + e^-/H^+ → semiquinone + e^-/H^+ → quinol). The proton/electron transfers to/from the substrate quinone/quinol contribute to maintaining a proton gradient across the membrane where the complex is embedded.

The presence of phospholipids has been shown to be essential for the catalytic activity and the native structure of the *cyt* bc_1 complex [7,8]. Also, the complex has been crystallized together with tightly bound cardiolipins (CLs), phosphatidylcholines (PCs), phosphatidylethanolamines (PEs), and phosphatidylinositols (PIs) [9–14]. The structural analysis of these lipid-bound complexes has been complemented by studies of lipid-dependent enzymatic activity, revealing the vital role played by the lipids [7,15,16]. Removal of the lipids has been shown to inactivate the complex, and especially CL has been found to be essential for the restoration of the enzymatic function [17,18].

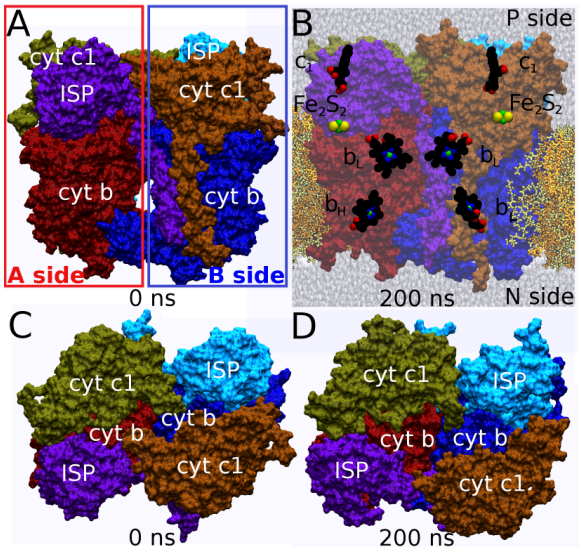

Fig. 1. The cytochrome bc_1 complex. A) The protein dimer includes cytochrome *b* (*cyt b*; red and blue), cytochrome c_1 (*cyt* c_1; yellow and orange), and iron sulfur protein (ISP; cyan and magenta) subunits shown using water-accessible surface at 0 ns. The A side of the dimer (red box) is composed of chains C (*cyt b*), D (*cyt* c_1), and R (ISP), while the B side (blue box) includes chains P (*cyt b*), Q (*cyt* c_1), and E (ISP) in the crystal structure (PDB: 1ZRT). B) The protein complex embedded in a lipid bilayer at 200 ns in the $conf_3$ simulation (Table 1) has a different conformation if compared to the state at 0 ns. The redox centers heme c_1, 2-iron 2-sulfur (Fe_2S_2) cluster, low potential heme (b_L), and high potential heme (heme b_H) are illustrated as CPK models on top of the protein. For clarity, water molecules are only shown in the background and the membrane has been clipped to reveal the protein subunits. The positive (P) side and the negative (N) sides separated by the membrane have been labeled. The Q_o site, close to the b_L heme, is located on the P side of the membrane and the Q_i-site near the heme b_H is closer to the N side of the membrane. Comparison of the top view of the complex from the P side shows that the dimer interface opens considerably between C) 0 ns and D) 200 ns. Note that most of the opening happens between the extracellular domains of *cyt* c_1 subunits.

With a total of four acyl chains and two negatively charged phosphate groups connected by a central glycerol group, CL has a unique double lipid structure. It is a vital component in membranes with

coupled electron transport and phosphorylation, namely bacterial plasma membranes, chromatophores, chloroplasts, and mitochondria [19]. While affecting the barrier properties of the membranes, CL has also been suggested to operate at the interface between membrane proteins and their surroundings, or between the subunits of protein complexes, possibly inducing conformational changes thereby affecting their activity [20]. CL may also have a pivotal role in the higher order organization of respiratory chain's components, literally gluing the chain together [21].

Importantly, in addition to insuring the structural integrity of the *cyt* bc_1 complex, CLs have also been proposed to take part in the proton uptake at the enzyme's Q_i-site [22] and act as a proton sink [23]. More precisely, a CL molecule on the periphery of the negative (N) side of the *cyt* bc_1 complex has been proposed to function as an anionic antenna for proton uptake at the Q_i-site [22,24]. As the low potential chain (quinol → heme b_L → heme b_H → quinone/semiquinone) provides electrons to the substrate at the Q_i-site, the proposed picture says that the closely positioned CLs would in concert deliver protons for the non-reduced substrate forms. This theory is backed up by the facts that the acidic head groups of CL are able to carry out intramembrane proton transfer [20], and in several X-ray crystal structures of the complex (see, for example, [10,25]) CLs are positioned in the close vicinity of the Q_i-sites. Due to the difficulties in determining its charge, which depends on pH and environmental factors such as the concentration of CLs, the charge state of CL has been debated and both single and double charged cardiolipins have been proposed [23,26,27].

The objective of this work is to unravel how strongly and specifically CL interacts with *cyt* bc_1, and how these interactions are manifested in the function of the protein complex. In this context, there are only a few computational studies that have examined the properties of CL-rich bilayers [27-30]. The present work is, to the authors' knowledge, the first simulation study focusing on CL-protein interactions. To this end, we discuss the results of four 200-ns atomistic simulations of *cyt* bc_1 in a many-component membrane comprised of CL, PC, and PE lipids.

We find lipids to play a role in a number of intriguing processes. We first find CLs to spontaneously diffuse to the protein-dimer interface to the immediate vicinity of the higher potential heme groups of the complex's catalytic (quinone reduction) Q_i-sites. This suggests that the specific CL positioning with the *cyt* bc_1 complex is highly conserved between different species. The CL positioning in the simulations close to the Q_i-sites is similar to that seen in the X-ray crystal structures of several higher level organisms such as yeast, chicken, and bovine [9–14,22,25].

The agreement of the present simulations with experiments is very promising for a number of reasons. From experimental point of view, our data provide support for the experimental approaches used to crystallize proteins of this type, since in the simulations we readily circumvent the detrimental effects caused by delipidation, crystal lattice packing, and other potential artifacts. Further, our simulation results allow us to present a refined picture for the dimer arrangement in the *cyt* bc_1 complex. The novelty of our work is the description of the role of the surrounding lipid environment: in addition to the specific CL-protein interactions, we also observe a conformational shift due to the general lipid environment, as the domains on the positive (P) side of the *cyt* bc_1 complex (see Fig. 1B) settle against the membrane. Altogether, this study represents the first atom-level perspective into the bacterial *cyt* bc_1 complex dynamics, exploring the full effect of lipids in a many-component lipid bilayer for the enzyme's structure and function.

2. Methods

2.1 System set-up

We consider four configurations ($conf_1$ – $conf_4$) of the *cyt* bc_1 complex, corresponding to different states in the Q-cycle functional mechanism of the cytochrome (Table 1). Each configuration differs from the others by the redox states of the prosthetic groups and by the occupancy of the Q_o- and Q_i-sites. In the $conf_1$ simulation, the Q_o-site is not occupied by a substrate or an inhibitor (*apo*), but the Q_i-site contained antimycin as an inhibitor. In the $conf_2$ simulation the Q_o-site is unoccupied while antimycin, an inhibitor, is present at the Q_i-site. The first Q-cycle turnover is captured in $conf_3$, while $conf_4$ represents the state of the complex following immediately quinol oxidation at the Q_o-site. The details of the $conf_2$-$conf_4$ set-ups are discussed more thoroughly in our previous studies [31,32].

In each system set-up (Table 1), the *cyt* bc_1 protein dimer (PDB: 1ZRT; [33]) is embedded in a

lipid bilayer, which was done using VMD [34] (Fig. 1B). In all simulation set-ups the lipid bilayer consists of three components: 102 cardiolipin (CL 18:2/18:2/18:2/18:2), 406 phosphatidylcholine (PC 18:2/18:2), and 342 phosphatidylethanolamine (PE 18:2/18:2) lipids (850 lipid molecules in total, see Fig. S1), all equilibrated in our previous studies [28,35]. This choice of lipids is particularly abundant in mitochondrial membranes [28] and is often used in experimental studies where protein complexes are reconstituted in artificial membranes. The system is fully solvated with TIP3P water molecules. For neutralizing the negative charge of the system, 246 Na^+ ions were added randomly to the water phase. The resulted systems comprise about 500,000 atoms each.

2.2 Molecular dynamics simulations

The 200 ns molecular dynamics (MD) simulations were performed with NAMD2.7 [36] using CHARMM 22 parameters for the protein with the CMAP [37] correction map for main chain dihedrals, and CHARMM 27 parameters for lipids with later modification [38]. The MD simulation set-up is described in detail in our previous work [39]. Atomic point charges for the prosthetic redox centers and ligands were fitted using the RESP methodology for both reduced and oxidized states based on extensive quantum mechanical calculations [31]. The time step was 1 fs and short-range non-bonded forces were calculated at 2 fs interval. The smooth particle mesh Ewald method was used to calculate long-range electrostatic interactions [40]. A periodic boundary box was used with dimensions of 162 Å x 142 Å x 132 Å. The protein-protein distance in the neighboring images was as a minimum two times larger than the 12 Å cut-off distance for van der Waals interactions. The target temperature was 310 K and target pressure 1 atm.

2.3 Trajectory analysis and figure preparation

The superimpositions of the protein structures were done using either VMD 1.9 or VERTAA in BODIL 0.8.1 [41]. The distance, hydrogen bonding (H-bonding), solvent accessible surface area (SASA), and electrostatic potential calculations were also performed with VMD. The distance of 3.25 Å between polar groups was used as the upper limit for H-bond formation with an angle criterion of 30 degrees. The contacting surface area (in units of $Å^2$) between the *cyt b* and ISP subunits was assessed by performing SASA calculations. The electrostatic potential was calculated in VMD with the PMEPot plugin [42]. The figures were generated using VMD, BODIL, MOLSCRIPT 2.1.2 [43], and RASTER3D [44].

2.4 Equilibrating system configurations

As mentioned above, the starting configurations for lipid bilayers were based on our previous studies [28,35] and were thus equilibrated. When the protein was embedded to these bilayers, the lipid arrangements around the protein were therefore based on simulations of a protein-free membrane, meaning that cardiolipins and other lipids were not positioned close to the previously proposed binding sites of the protein. Important to stress is that the distance between the central binding cavity of the *cyt* bc_1 dimer (that is at the interface between the proteins, see discussion below) and the cardiolipin that was the closest to it was about 20-25 Å in the initial starting configuration (see Supplementary Material (SM)). As the below data show, this

Table 1. The atomistic molecular dynamics simulation set-ups of the cytochrome *bc*$_1$ complex.

MD simulation configuration	Q_i-site inhibitor or substrate	Q_o-site substrate	Heme b_L [3]	Heme b_H [3]	Heme c_1 [3]	Fe_2S_2 cluster [3]
$conf_1$ [1]	quinol	*apo*	-1 ox	-2 red	-2 red	-2 red
$conf_2$ [2]	antimycin	*apo*	-1 ox	-1 ox	-2 red	-1 red
$conf_3$ [2]	quinone	quinol	-1 ox	-1 ox	-1 ox	0 ox
$conf_4$ [2]	semiquinone	quinone	-2 red	-1 ox	-1 ox	-1 red

[1] First 100 ns of the simulation presented in Kaszuba et al. [31].
[2] Presented in Postila et al. [32].
[3] The formal charge of the redox centers: "red" stands for reduced, and "ox" stands for oxidized.

distance decreased rapidly as the simulations were started (see Section 3.2). Further, immediately in the beginning of the simulation, the cavity at the dimer interface was filled with water molecules from the negative (N) side, but they were subsequently replaced by lipids which entered the cavity. Further discussion on equilibration is given in SM (S.1).

3. Results

3.1 Key results in a nutshell

Below we describe the results that we have found through extensive atomistic simulations. Yet, since the new knowledge we have observed is quite detailed, we consider it useful to first outline the main findings and conclusions in advance. Given this view, our four key results (in order of importance) are as follows:

1. We observed spontaneous diffusion of CL lipids to similar locations as have been earlier predicted by X-ray crystallographic experiments (Fig. 2). This is positive news for the experimental community, providing support for the protocols used in membrane protein structure determination.
2. As the role of CLs bound to the specific sites was elucidated in detail, it turned out that they were positioned very close to the active sites of the protein and indeed could participate in the proton transfer to the active sites *via* hydrogen-bonded networks of water and lysine.
3. The space between the two protein monomers became filled up with phospholipids, thereby likely affecting the stability of the complex's structure and possibly participating in its dimer formation and quinone/quinol diffusion.
4. We also observed a conformational shift due to the general lipid environment in the *cyt* bc_1 dimer's quaternary structure, as the P side domains of the complex settled against the membrane.

We next discuss these aspects in more detail.

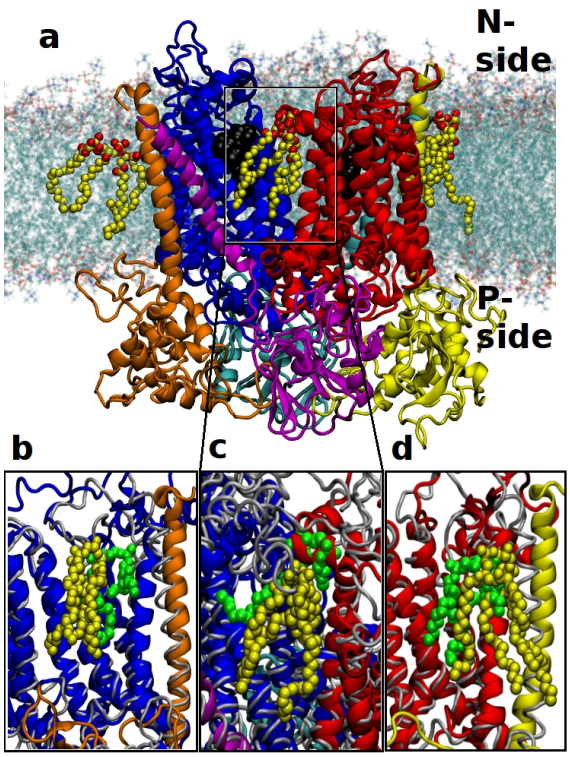

Fig. 2. Cardiolipin diffuses spontaneously to similar binding sites as observed in X-ray crystal structures. A) An example of the final locations of three cardiolipin molecules in the *cyt* bc_1 structure, as observed in our simulations ($conf_4$, cardiolipins yellow with red oxygens). Other lipids are shown only in the background for clarity. In panels B-D are shown close-up snapshots of the CL locations versus the locations observed in the crystal structure by Solmaz et al. ([25], PDB: 3CX5). The yellow CL is the one observed in our MD simulations and the green one is from the crystal structure. The positions were obtained by superimposing the protein structures from MD simulations (colored ribbons) with the crystal structure (gray tubes). Panel C corresponds to simulation $conf_4$, and panels B and D to simulation $conf_1$.

3.2 Cardiolipins diffuse to be an integral part of the protein complex

3.2.1 Cardiolipins bind close to the Q_i-site

When the simulations were started, we readily observed that a CL molecule diffused spontaneously to a particular position in the complex: to the surface of the protein, located on both sides of the protein dimer in the vicinity of the Q_i-site (see Fig. 2 (top)).

The double negatively charged head group of the CL molecule pointed towards the N side leaflet (see Fig. 1B), while its hydrophobic acyl tails aligned

towards the P side. Importantly, a similar binding location for CL has also been reported in the yeast *cyt* bc_1 crystal structures (PDB: 1KB9; [22]; PDB: 3CX5; [25]), see Fig. 2 (panels B and D). While the yeast and bacterial complexes differ markedly in their amino acid sequence and subunit composition, the CL molecule acquired quite the same positioning near the Q_i-site in both the yeast X-ray structure and in our simulations with the bacterial complex. This is demonstrated in Fig. 2 (panels B and D), which provides compelling evidence for the agreement between simulations and experiments: it is clear that in the simulation model the CLs diffuse spontaneously to the same spots as observed in the crystal structure. All four simulations yielded essentially the same conclusion. The minor difference between the simulations and experiments (Fig. 2) is expected due to, e.g., crystallization conditions and the differences between the yeast and bacterial complexes.

The conserved positioning of CL can largely be explained by electrostatic effects, *i.e.,* the lipid's anionic head group is attracted by the positively charged residues such as lysines and arginines on the protein surface. Nonetheless, since the head group of CL is very small and charged, the conserved positioning can also in part be driven by the so-called umbrella effect, where the head groups of other lipids and the residues of the protein shield the CL head group from contact with water. This possibility would deserve further attention in future studies.

Although the CL positioning was very similar on both sides of the dimer, there were differences between the monomers. On the A side, the CL molecule stayed close to the *cyt b* subunit and H-bonded only with TRP44 (Table S1). Closer association of the CL molecule with the *cyt* c_1 subunit on the B side was induced by a number of stable H-bonding interactions: the CL's phosphate groups formed H-bonds with the side chains of ASN246, TYR243 and LYS254 of the *cyt* c_1 subunit (Table S1). It is also noteworthy that in the yeast structures the CL head group resides in a clearly visible niche on the protein surface – an equally tight fit could not happen with the bacterial complex that consists of a minimal *cyt* bc_1 core.

In addition, we found that one CL molecule always occupied a central position close to the Q_i-site(s) between the heme b_H groups of the *cyt b* subunits, the head group pointing towards the N side leaflet. The distance diffused by CL varied between the four simulated system configurations but was typically ~20-25 Å after which its movement became more confined as demonstrated by the small variations in the distance plots (Fig. S2). Altogether, this diffusion process took typically about 20-40 ns.

A similar binding location for CL has also been reported in the yeast *cyt* bc_1 crystal structure (PDB: 3CX5; [25]), see Fig. 2 (panel C). Although the CL entered the dimer interface in all four simulations (Fig. S2), in two simulations the lipid molecule approached the heme b_H groups in particular ($conf_2$ and $conf_4$, see Fig. S2). Interestingly, despite several similarities, the binding residues differ in the four simulations (Fig. 3). In the $conf_1$ (Fig. 3A, Fig. 3B) and $conf_3$ simulations (Fig. 3D), the CL molecule binds first to LYS12 of the *cyt b* subunit at the side of the cavity. For the $conf_1$ in particular (Fig. 3A, Fig. 3B), the occupancy of this H-bond was 75% over the entire simulation. In the $conf_2$ and $conf_4$ simulations (Fig. 3C and Fig. 3E, respectively), where CL reached deeper inside the dimer interface than in the other two simulations, CL first bonded to ARG22 at the A side and then also to TRP214 at the B side. This linked the two dimer sides together for 69-200 ns of the $conf_2$ simulation and for 113-129 ns of the $conf_4$ trajectory. Later on, the interactions to the A side residues were broken and simultaneously a local conformational shift occurred, widening the dimer interface near the Q_i-site. Figs. 3B-E show parts of the *cyt b* secondary structures from the A (light blue) and B (light red) sides of the dimer (Fig. 1A), represented as transparent cartoon models.

Next we measured the distance of the above-mentioned CL molecules to the b_H hemes to quantitatively estimate their positioning with respect to the Q_i-site (Fig. S3). At the end of the simulations, the distance from the surface-bound CLs to the heme b_H ranged around 22-26 Å for the CL on the B-side of the dimer and around 19-21 Å (somewhat larger in two simulations) for the CL on the A-side. Notably, because the distance was measured between the centers of mass of the CL head group (phosphorus atoms) and the heme b_H, the effective distance could be occasionally even smaller. These distances are equivalent to the values of 19.4-19.5 Å measured

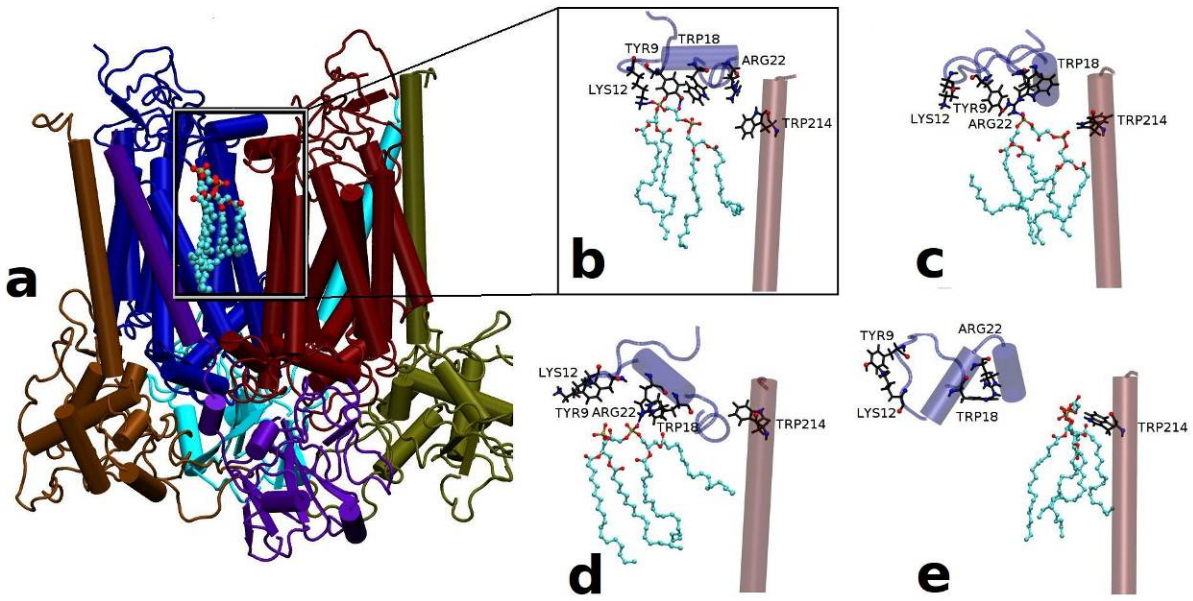

Fig. 3. Cardiolipin binding in the cytochrome bc_1 dimer interface at 200 ns. A) The final positioning of a CL molecule (CPK model with cyan carbons) that entered the dimer interface (cartoon model) from the lipid bilayer (see Fig. 2) during the $conf_1$ simulation (Table 1). B-E) Close-ups of CLs (ball-and stick models with cyan backbone) and their main interacting partners (ball-and-stick models with black backbone) at the dimer interface in the $conf_1$-$conf_4$ simulations. In panels B-E are shown parts of the *cyt b* secondary structures from A (light blue) and B (light red) sides of the dimer (Fig. 1A), shown as transparent cartoon models.

from the yeast *cyt* bc_1 complex X-ray crystal structures (PDB: 1KB9 [22], PDB: 3CX5 [25]). For the centrally-located CL, the final CL-*heme* b_H (B side) distances fluctuated around ~22-24 Å in the $conf_1$ and $conf_2$ simulations. The shortest final distance (~18 Å) was observed in the $conf_4$ simulation. The distance of CL head group to the A side heme b_H was somewhat larger in all simulations. However, the arrangement was almost symmetric between the monomers in the $conf_2$ simulation. The final distances (Fig. S2) are well in line with the crystallographic results calculated from the yeast *cyt* bc_1 structure (PDB: 3CX5; [25]), which have been determined to be 19.7-20.0 Å from the central CL to each of the hemes.

Despite strenuous efforts we did not find any major secondary structure changes such as helix unwinding around the protein complex that would have correlated with CL-protein interactions. Only minor changes in the dimer arrangement at the inner leaflet were observed as a result of CL binding, likely related to the CL entry to the dimer interface.

3.2.2 Conserved cardiolipin binding on the protein surface

To determine the possible conserved CL binding sites on the protein surface, we searched for long-lived CL-protein H-bonds. A limiting value for the occupancy of a long-lived H-bond was calculated based on two criteria: 1) the area per lipid and 2) CL diffusion speed. A preceding computational study [28] suggested that it takes roughly 60 ns (corresponding to H-bond occupancy of 30 %) for a CL molecule to move across its own area in the membrane plane. This value was used as a rough estimate for the time it would take for a CL to move a distance of its own size in the bilayer plane. While the time would be longer if the diffusion were considered in the immediate vicinity of the protein [3], we expect this value to adequately describe the average lipid diffusion process.

In line with experimental results [45], the majority of the tightly bound CLs were bound on the N side of the protein and only one CL bound strongly on the positive P side. All CL-protein H-bonds with occupancies over 30% are listed in Table S1, including the CLs near the active sites (discussed

above). Of the listed binding locations, the one acquired by CL on the surface of the *cyt* c_1 on the A side (bound in all simulations, binding residues LYS247, ARG248, HIS256 and LYS257) was particularly long-lived, lasting for a major part of all of the 200 ns simulations. This location of CL also induced minor conformational changes (helix reorientation) in two of the simulations. In one simulation, the CL in question formed an H-bond also with the ISP subunit on the B side. Meanwhile, on the A side, there was also a CL molecule close to the equivalent place near the ISP subunit in the starting configuration. It formed an H-bond with the *cyt b* subunit (with residues LYS362 and TRP366) that lasted for a major period of three simulations.

3.2.3 No specific binding pattern for cardiolipin

A specific CL-protein binding pattern, designated as XXY, where one molecule would bind to two positively charged residues (XX) and one polar residue Y, was suggested by Palsdottir et al. [45]. Accordingly, there is one bound CL molecule in every simulation that follows this pattern, where CL binds to two positive lysine residues (LYS247 and LYS254 of *cyt* c_1 or LYS251 of *cyt b*) and a polar asparagine residue (ASN42 of *cyt b*) for part of the simulation. The occupancies varied a lot between simulations, ranging from 6 to 75% for individual H-bonds. Simultaneous binding to two lysines and one asparagine was observed to happen only momentarily in the $conf_1$, $conf_2$, and $conf_4$ simulations. This binding pattern did not occur with the other CL molecules in any of the simulations, which implies that this suggested arrangement is not generally favored with the membrane-embedded *cyt* bc_1 complex. Altogether, it is fair to say that we did not find a universal binding pattern for CL.

To further examine the CL-protein contacts, we analyzed the H-bonding between CLs and protein residues (Table S2). *Via* their hydroxyl groups, CLs were observed to H-bond with the protein both as donors and acceptors. Only the H-bonds with occupancies over 1% were considered (as determined in terms of percentage of trajectory frames when the bond exists). The negatively charged CL molecules H-bonded preferentially with positively charged lysine residues (~26% in $conf_1$, $conf_2$, and $conf_4$, see Table S2). This strong preference was evident in all of the simulations except in $conf_3$ where tryptophan residues had a slightly stronger preference (26% in $conf_3$, Table S2). The second favored binding partners were the tryptophan residues forming 18% of all H-bonds on average.

3.3 Cardiolipin positioning close to the Q_i-site suggests a role in proton uptake

The anionic head groups of CL molecules have been proposed to act as proton traps or buffers, supplying protons for the *cyt* bc_1 complex [23]. The idea is that CL would pass a new proton to a nearby lysine side chain from which it would detach during the reduction of ubiquinone [24]. The CL molecules positioned near the Q_i-sites in various *cyt* bc_1 X-ray crystal structures [9–14,22,25,46] indeed support the idea that they could serve as the entry point for the proton uptake process [22,24]. As there is no direct opening between the enzyme's Q_i-site and the bulk solvent, this short proton 'wire' or a hydrogen-bonded network is needed [22,24]. Such a network, called the CL/K pathway, was described in [24] to consist of CL bound to the *cyt b* surface, a lysine residue (LYS228 in yeast *cyt* bc_1 crystal structure; PDB: 1KB9), and three water molecules (Fig. 4A).

Notably, the CL arrangement at the site in the yeast bc_1 crystal structure (Fig. 4A, [24]) is very similar to the one seen for the bacterial complex at the end stage of our simulations (Fig. 4A, Fig. 4B). In line with this proton uptake hypothesis, the positioning of water molecules and the LYS251 side chain in our simulations indeed suggest a possible proton uptake pathway between the CL molecule and the bound quinone/semiquinone at the Q_i-site (Fig. 4B). Even though all the H-bonds comprising this network did not generally exist precisely at the same time, the similar chain-like arrangement existed in the different simulations. Qualitatively, the described arrangement is seen during 80-200 ns ($conf_1$) and 110-200 ns ($conf_1$ and $conf_2$, where for part of the time CL is bound straight to LYS251). In the $conf_3$ simulation the CLs are located slightly further away from the lysine, accommodating at least two water molecules between the head group and the lysine side chain. We wish to note that even though the discussion above only concerns the surface-bound CLs, it is possible that the centrally-located CL, also positioned close to the active sites, may also form a proton-uptake pathway with water molecules between its binding site and the active site.

The proximity of the CL head group affected the local electrostatic potential near the proposed entrance to the proton conduction pathway (Fig. 5). The electrostatic potential differs between the

beginning of the simulation, when the lipid molecules have not yet bound to the protein surface, and the end stage when the system is equilibrated. There was a general shift towards neutral/negative potential values on the N side during the simulation, but also a specific effect by the bound CL molecules at the Q_i-site (circled areas in Fig. 5). However, this is not always the case since other factors such as the orientation of protein residues and the binding of counter ions also contribute. Fig. 4C gives a qualitative look at the potential of the proposed proton conduction pathway, where the potential of the whole system is reflected on the molecular surfaces of the suggested proton transfer partners. Notably, the CL head group, which has been suggested to act as a proton trap, concentrating protons to the bilayer surface and passing them further to the protein [24], reflects a clearly negative potential.

3.4 Behavior of other phospholipids

Like CLs with their hydroxyl groups, PEs are also able to participate in H-bonding as proton donors *via* their ammonium groups, whereas PCs can act only as acceptors (Fig. S1). In the simulations PCs and PEs formed a greater number of shorter-lived H-bonds than the more negatively charged CLs. During the last 10 ns of the simulations, CLs formed on average seven H-bonds with protein residues at each time step, as PCs form 23 and PEs 24. Thus, CL-protein H-bonding accounts for 13% of all H-bonds at a given time step, while PCs account for 42%, and PEs for 45% of the H-bonds. The corresponding molar concentrations for CL, PC, and PE in the membrane are 12, 48, and 40%, respectively. The H-bonds of PCs and PEs had shorter lifetimes compared to those formed by CL, the average occupancies being 20, 9, and 14% for CL, PC, and PE, respectively. A slight preference for lysine residues is seen also for PC and PE. However, it is not as clear as in the case of CL, see Table S3. Other favored H-bonding partners were tryptophan, asparagine, and tyrosine for PCs, and arginine, serine, and aspartic acid for PEs. The conserved binding sites of PC and PE were analyzed similarly as those of CL (Table S3). Due to the great number of these bonds, the selection was further refined to include only H-bonds that were found in at least three out of the four simulations. Interestingly, half of the H-bonds found were those of lipids from the P side rather than from the N side, as was the case with the tightly bound CLs.

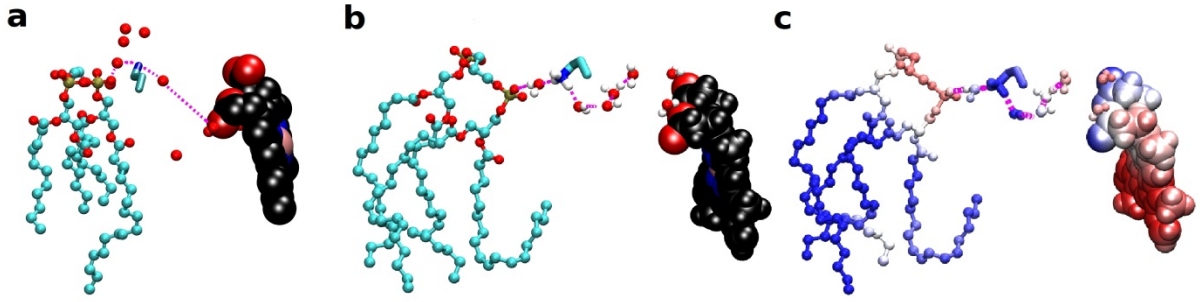

Fig. 4. Possible water-mediated proton-uptake pathway involving cardiolipin near the Q_i-site. A) A water bridge between a CL molecule (ball-and-stick model with cyan carbons, red oxygens and brown phosphates) and heme b_H (CPK model with black backbone) close to the Q_i-site (see Fig. 1A) in the yeast *cyt* bc_1 complex crystal structure (PDB:1KB9; [22]. The protein is omitted for clarity and only the side chain of the lysine (LYS228) taking part in the conduction pathway is shown (stick-model, carbons cyan, nitrogen blue). The proposed hydrogen-bonded proton transfer pathway from cardiolipin to the water molecule in the Q_i-site is shown with magenta dotted lines. B) Similar arrangement of water was reproduced for example in the end of the $conf_1$ simulation (snapshot taken at 199.25 ns). Water hydrogens (white) are only shown in the MD simulation snapshot (panel B). H-bonds existing at this time step are shown with dotted magenta lines. The side chain of LYS251 is shown as a stick model (hydrogens white). C) The same arrangement as in panel B but colored according to the electrostatic potential of the system. The potential values were calculated based on all atoms in the system and averaged over the last 1 ns of the simulation. Red color indicates negative potential values, blue indicates positive, and white corresponds to neutral.

PEs and PCs, in addition to CL (Fig. 3), also entered the dimer interface during the simulations. In the starting configuration, a PC molecule (head group pointing to the N side) lied straight between CL and the protein and consequently the two lipids moved together to the cavity. As opposed to the CL molecule, PC formed hardly any H-bonds on its way inside. The head group of PC ended up closer to the monomer B than to the monomer A in all simulations (Fig. S4, Fig. 1A). Steric interactions are expected to play a role in this arrangement of the lipids rather than the electrostatic ones. On the other side, there were PE molecules (head groups pointing to the N side), which were initially located closer to the protein than either CL or PC. These PEs (shown for the B side in Fig. S5) H-bonded with the residues lining the cavity near the protein surface, while their acyl chains penetrated deep into the protein (Fig. S5B). This is evidenced by a smaller PE tails–heme b_H distance as compared to the PE head–heme b_H distance (Fig. S5A), resulting in some cases in an almost horizontal orientation of the lipid (Fig. S5B).

The lipids entering the dimer interface from the two opposite sides of the membrane and enclosing the *cyt* bc_1 complex moved deep into the protein complex and ended up being very close to each other. The distance between the central glycerol atoms of CL and PE changed from 70 Å in the initial configuration to ~20 Å in the end of the simulations, and the tails of lipids from the opposite sides were touching in the $conf_2$ and $conf_4$ set-ups. The head groups of all phospholipids were positioned on the N side. Since these lipids interacted with both monomers of *cyt* bc_1, they should substantially affect the stability of the dimer interface and could also be involved in dimer formation. An interesting feature of this lipid network is the acyl chain disorder which has been previously suggested to provide a pathway for quinone/quinol diffusion and exchange between the lipid bilayer and the inter-monomer cavity in the bc_1 complex [47].

3.5 The dimer complex opens on the P side of the membrane

The *cyt* bc_1 complex was observed to undergo rearrangement at the dimer interface on the P side in all of the 200 ns simulations. The P side parts of the *cyt* c_1 subunits moved the most (Fig. S8D). This view was supported by both a visual inspection of the simulation trajectories (Fig. 1C *vs.* D) and calculation of the prosthetic redox center distances (Fig. S6A-D, Table S4). The distances between the equivalent heme c_1 groups across the dimer interface also increased (Fig. S6D, Table S4). The conformational shift took place due to non-specific electrostatic lipid-protein interactions that were not present in the initial crystal structure, *i.e.,* the positively charged residues aligned favorably towards the hydrophilic head groups of the lipid membrane (Fig. 1B). Despite these changes, the core of the enzyme remained fairly immobile as shown by the moderate ~1-2 Å increase in the heme b_L distance across the dimer interface (Fig. S6A, Table S4). Furthermore, the calculations on the solvent accessible surface area (SASA) showed that the contact area between the *cyt b* subunits increased markedly in most of the simulations.

Moreover, the opening of the dimer interface on the P side was more pronounced in the Q_o-site simulations lacking a bound substrate ($conf_1$, $conf_{12}$, Table S4) than what was seen in the substrate-occupied simulations ($conf_3$, $conf_4$, Table S4). This widening was accompanied by narrowing of the dimer interface close to the Q_i-site or the N side in the *apo*-Q_o simulations (Fig. 1B). This was shown by the heme b_H distance across the dimer interface (Table S4). Accordingly, the results suggest that the substrate binding at the Q_o-site could weaken the extent of the movements of the extracellular domain, as the spreading on the P side was most prominent in the *apo*-Q_o simulations (Fig. 1B). A plausible mechanism behind the increased widening in the *apo* simulations could be the lack of a bound substrate to mediate specific *cyt b*-ISP subunit interactions, as was the case in the substrate-occupied simulations [32].

A close association of *cyt b* and ISP subunits is needed for the successful reaction cycle at the Q_o-site [9]. However, the transfer of electrons from the Fe_2S_2 cluster to the heme c_1 is equally important. To facilitate the transfer, the ISP and *cyt* c_1 subunits have to stay close to each other. In our case, on average, the Fe_2S_2 cluster-heme c_1 distances did not change within the dimer sides or across the dimer interface (Table S5). However, a closer inspection showed that the redox center distance fluctuated above and below the initial crystal structure value on the A and B sides, respectively (Fig. S7, Table S5). Similarly, the contact surface area between ISP and *cyt* c_1 subunits on either dimer side was raised only slightly and differed widely between simulations and dimer sides (Table S5). Because these domain movements did

not seem to follow a similar pattern on the dimer sides in any of the simulations, it seems unlikely that substrate-occupancy at the Q_o-site could be the governing factor behind the extracellular ISP-*cyt* c_1 association.

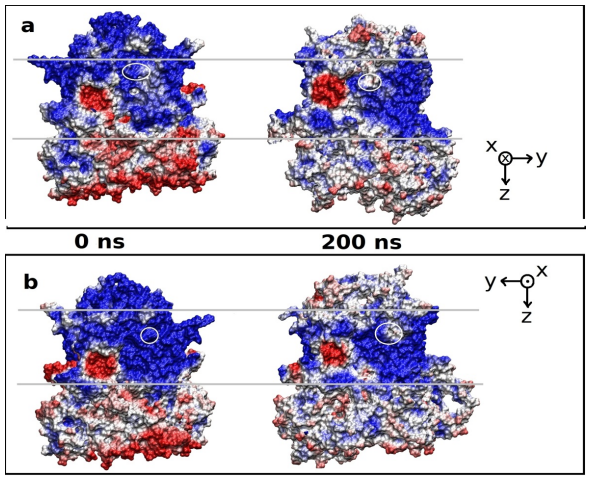

Fig. 5. Electrostatic potential on protein surface. Comparison of snapshots from the beginning and end of the simulation, two sides (on panels A and B) of the protein shown. The phospholipid membrane (level of head group phosphates) is indicated by the gray lines. The N side of the membrane points up, as indicated by the axes on the right. The protein is shown as a van der Waals-surface (probe radius 1.4 Å). The white circles mark the sites of given cardiolipin molecules on the A side of $conf_1$ (A) and on the B side of $conf_2$ (B) of the dimer (see Fig. 1B). The values of the electrostatic potential on the protein surface are shown with the blue color indicating positive values and red color indicating negative. White color indicates the zero potential. The shown potentials are averages over 1 ns time slices, e.g. the first snapshot shows the average potential during 0-1 ns of the simulation and the second shows the average potential during 199-200 ns. All atoms in the system were taken into account when calculating the potential.

4. Discussion

From structural point of view, the simulation results stress the membrane protein nature of the *cyt* bc_1 complex and consequently one should remain wary when examining it out of this context. Although several experimental studies have successfully demonstrated that specific lipids are an integral part of the dimer complex [10,25,45], the X-ray crystal structures have been unable to depict the full effect of the surrounding lipid bilayer on the enzyme's quaternary structure. The existing structures are likely accurate in describing the enzyme's protein fold at the monomer level [31], but due to the lack of large-scale lipid-protein contacts the solved dimer assemblies have been somewhat distorted. When the bc_1 dimer was simulated in a lipid bilayer, the dimer interface opened considerably on the P side leaflet immediately in all of our simulations (Fig. 1C vs. 1D). The driving force behind the conformational shift was the electrostatic effect of the bilayer: the positively charged residues of the P side domains spread out to acquire more favorable alignment against the negatively charged phosphate groups of the phospholipids.

Prior to this work, we have already demonstrated through atomistic simulations that quinol binding accompanied by coordinated water arrangement at the Q_o-site assures exceptionally close association of the extracellular domains of the *cyt b* and ISP subunits [32]. This arrangement is a prerequisite for the electron transfer to the Fe_2S_2 cluster during the oxidation of quinol [9]. However, the electron transfer should also continue towards the heme c_1 on the high-potential chain (quinol → Fe_2S_2 cluster → heme c_1 → *cyt* c_1). None of our simulations recreated the full range of ISP movement in relation to the *cyt b* subunit seen in the crystal structures. Yet also the Fe_2S_2 cluster-heme c_1 distance fluctuated above and below the initial crystal structure value (Fig. S4, Table S5). This suggests that the *cyt* c_1 subunits might move randomly back and forth in relation to the ISP subunits independent of the Q_o-site interactions. On the other hand, the final dimer assembly at the P side (Figs. 1C, 1D) differed considerably between the substrate-occupied and ligand-free Q_o simulations. Without a bound ligand at the Q_o-site, the dimer interface widened more at the P side than in the Q_o-occupied simulations. In other words, the monomer parts approached each other a little bit near the N side leaflet. Thus, it seems that the substrate binding at the Q_o-site not only controls directly the *cyt b*-ISP dynamics but it also affects inter-monomer dynamics.

The dimer interface on the N side leaflet, covering the vicinity of the Q_i-site, became filled by a variety of phospholipids during the first 50 ns of our simulations. Previous X-ray crystallization studies have already suggested that the cavity contains phospholipids [25,45]. However, the atomistic simulations show conclusively that the entire space is filled with lipids. Although more lipids entered the

dimer interface in the simulations than is seen in the available structures, it is possible that the cavity could contain a few more phospholipids *in situ*. Because of the delayed entry of phospholipids, solvent molecules also entered the area of the cavity, where presumably only lipids should reside. This solvation prevented unwanted vacuum effects inside the dimer interface in the very beginning of the simulations. On the other hand, the inflowing lipids were mostly able to displace the water molecules in the cavity. Even though the entered lipids must have a structural role keeping the dimer sides of the *cyt* bc_1 complex apart (Fig. 1A), no hefty movements (only local changes) between the dimer sides (*e.g.,* redox center distance changes) could be attributed directly to specific lipid effects.

We detected two specific CL binding sites for the *cyt* bc_1 complex of *Rhodobacter capsulatus* in our MD simulations: 1) in the dimer interface and 2) on the surface of the protein outside the interface. Both positions are close enough to the Q_i-site to possibly affect its function. Notably, the CL binding site(s) outside the dimer interface has (have) been suggested to function in the proton uptake [22,24]. In general, the entry of the lipid molecules into the dimer interface seemed to be directed by hydrophobic or steric interactions, but with CL the negatively charged head group also affected its final positioning. Initially the electrostatic potential of the dimer interface was neutral, favoring the entry of hydrophobic acyl tails of phospholipids. However, the later changes in the cavity implied that the potential became more positive, thus attracting especially the doubly negative CL head group. Although there were minor differences in the composition and positioning of the lipids that entered the dimer interface during the simulations, CLs consistently acquired these conserved positions close to the Q_i-site.

The consistency in the CL positioning both in our simulations and in previous structural studies supports the hypothesis of CLs participating in the proton uptake from the N side to the redox reactions at the Q_i-sites [45]. The positioning of CL at the dimer interface was first reported by Palsdottir et al. [45] based on X-ray density data, followed by another study showing CL at the same site [25]. Thus, our simulations support previous experimental results indicating the CL's central positioning in the *cyt* bc_1 dimer interface. The simulations were also able to reproduce the X-ray crystallization results regarding CL positioning outside the dimer interface. That is to say, a CL molecule bound close to the heme b_H on both monomers in almost all of our simulations, in line with several crystallization studies for different species. Our simulation results therefore provide quite compelling evidence that these CL binding sites are conserved regardless of the origin of the *cyt* bc_1 complex inspected. The next logical question is whether the preference for CLs at these sites has direct effects on the Q-cycle, or if CLs only affect the *cyt* bc_1 complex integrity or dimer arrangement.

The negatively charged head groups of CLs, positioned on the sides of the monomers, are connected by a lysine residue and a water meshwork to the Q_i-site (Fig. 4). This arrangement could render water-mediated proton tunneling possible between the CL molecules and the non-protonated substrates. Unfortunately, the simulations cannot conclusively confirm the role of either central or peripheral CL molecules in the proton transfer. We analyzed exhaustively the effect of CLs on the electrostatic potential of the *cyt* bc_1 complex, and especially concentrated on the vicinity of the Q_i-site. It is clear that the CL molecules that acquired these conserved positions can in some cases shift the electrostatic potential to more negative values, in principle therefore attracting protons from the N side (Fig. 5). It is possible that the real differences in the electrostatic potential did not show in our simulations because the dimer interface lacked some lipids, and, thus, the Q_i-site was not isolated enough from the water phase. However, the fact that both MD simulations and crystallographic studies positioned CL molecules in these particular sites (at the periphery and at the dimer interface of the *cyt* bc_1 complex) provides a strong indication that these CL-protein interactions close to the Q_i-site are universally conserved.

5. Conclusions

The atomistic molecular dynamics simulations reported here provide a great deal of insight into understanding the role of cardiolipin (CL) in *cyt* bc_1 complexes. It provides one with an alternative refined dimer arrangement for the *cyt* bc_1 dimer at the P side leaflet of the membrane (see Fig. 1B). The picture suggested here differs somewhat from the previous X-ray crystallographic data. The new tertiary assembly of the protein dimer is caused by non-specific lipid-protein interactions such as

hydrophobic and electrostatic effects. The simulations also provide clear-cut evidence that phospholipids and in particular CLs are an integral part of the *cyt* bc_1 complex at the dimer interface. The simulations demonstrated that CLs as well as the other phospholipids enter the dimer interface and position themselves in the close vicinity of the heme b_H groups in the Q_i-site. Although the composition and alignment of the entered lipids varied slightly between the simulations, each time there was a CL molecule, which spontaneously diffused to a central location inside the cavity. Importantly, the observed central positioning of CL inside the dimer is consistent with the previous X-ray crystallographic data [25,45]. Also, outside the dimer interface CLs were able to acquire close positions to the heme b_H groups on the protein surface as reported in several crystal structures. The consistency in the CL positioning in the close vicinity of the Q_i-site in our simulations and in previous X-ray crystallographic studies suggests that the negatively charged phospholipid species could indeed function as a proton source during substrate quinone/semiquinone reduction [22,23]. Overall, the conserved CL positioning near the Q_i-site suggests that the lipid has a central role in the *cyt* bc_1 complex structure and possibly in the redox reactions too.

Acknowledgments

Computational resources were provided by the Finnish IT Centre for Science (CSC). For financial support, we wish to thank the Academy of Finland (TR, IV, PAP), Finnish Doctoral Programme in Computational Sciences (SP, KK) and Vilho, Yrjö and Kalle Väisälä foundation (SP) for financial support, and the European Research Council through the Advanced Grant (CROWDED-PRO-LIPIDS). AO acknowledges The Welcome Trust International Senior Research Fellowship.

References

[1] D. Lingwood, K. Simons, Lipid rafts as a membrane-organizing principle, Science 327 (2010) 46–50.

[2] A.G. Lee, How lipids affect the activities of integral membrane proteins, Biochim. Biophys. Acta 1666 (2004) 62–87.

[3] P.S. Niemelä, M.S. Miettinen, L. Monticelli, H. Hammaren, P. Bjelkmar, T. Murtola, E. Lindahl, I. Vattulainen, Membrane proteins diffuse as dynamic complexes with lipids, J. Am. Chem. Soc. 132 (2010) 7574–7575.

[4] R. Phillips, T. Ursell, P. Wiggins, P. Sens, Emerging roles for lipids in shaping membrane-protein function, Nature 459 (2009) 379–385.

[5] F.-X. Contreras, A.M. Ernst, P. Haberkant, P. Björkholm, E. Lindahl, B. Gönen, C. Tischer, A. Elofsson, G. von Heijne, C. Thiele, R. Pepperkok, F. Wieland, B. Brügger, Molecular recognition of a single sphingolipid species by a protein's transmembrane domain, Nature 481 (2012) 525–529.

[6] C. Hunte, S. Richers, Lipids and membrane protein structures, Curr. Opin. Struct. Biol. 18 (2008) 406–411.

[7] H. Schägger, T. Hagen, B. Roth, U. Brandt, T.A. Link, G. von Jagow, Phospholipid specificity of bovine heart bc1 complex, Eur. J. Biochem. 190 (1990) 123–130.

[8] C.A. Yu, L. Yu, Structural role of phospholipids in ubiquinol-cytochrome c reductase, Biochemistry 19 (1980) 5715–5720.

[9] Z. Zhang, L. Huang, V.M. Shulmeister, Y.I. Chi, K.K. Kim, L.W. Hung, A.R. Crofts, E.A. Berry, S.H. Kim, Electron transfer by domain movement in cytochrome bc1, Nature 392 (1998) 677–684.

[10] H. Palsdottir, C.G. Lojero, B.L. Trumpower, C. Hunte, Structure of the yeast cytochrome bc1 complex with a hydroxyquinone anion Qo site inhibitor bound, J. Biol. Chem. 278 (2003) 31303–31311.

[11] L.-S. Huang, D. Cobessi, E.Y. Tung, E.A. Berry, Binding of the respiratory chain inhibitor antimycin to the mitochondrial bc1 complex: a new crystal structure reveals an altered intramolecular hydrogen-bonding pattern, J. Mol. Biol. 351 (2005) 573–597.

[12] E.A. Berry, L.-S. Huang, D.-W. Lee, F. Daldal, K. Nagai, N. Minagawa, Ascochlorin is a novel, specific inhibitor of the mitochondrial cytochrome bc1 complex, Biochim. Biophys. Acta 1797 (2010) 360–370.

[13] E.A. Berry, Z. Zhang, H.D. Bellamy, L. Huang, Crystallographic location of two Zn(2+)-binding sites in the avian cytochrome bc(1) complex, Biochim. Biophys. Acta 1459 (2000) 440–448.

[14] L. Esser, B. Quinn, Y.-F. Li, M. Zhang, M. Elberry, L. Yu, C.-A. Yu, Di Xia, Crystallographic studies of quinol oxidation site inhibitors: a modified classification of inhibitors for the cytochrome bc(1) complex, J. Mol. Biol. 341 (2004) 281–302.

[15] T. Wenz, R. Covian, P. Hellwig, F. Macmillan, B. Meunier, B.L. Trumpower, C. Hunte, Mutational analysis of cytochrome b at the ubiquinol oxidation site of yeast complex III, J. Biol. Chem. 282 (2007) 3977–3988.

[16] T. Wenz, R. Hielscher, P. Hellwig, H. Schägger, S. Richers, C. Hunte, Role of phospholipids in respiratory cytochrome bc(1) complex catalysis and supercomplex formation, Biochim. Biophys. Acta 1787 (2009) 609–616.

[17] M. Fry, D.E. Green, Cardiolipin requirement for electron transfer in complex I and III of the mitochondrial respiratory chain, J. Biol. Chem. 256 (1981) 1874–1880.

[18] B. Gomez, N.C. Robinson, Phospholipase digestion of bound cardiolipin reversibly inactivates bovine cytochrome bc1, Biochemistry 38 (1999) 9031–9038.

[19] F. Hoch, Cardiolipins and biomembrane function, Biochim. Biophys. Acta (BBA)/Reviews on Biomembranes 1113 (1992) 71–133.

[20] M. Schlame, D. Rua, M.L. Greenberg, The biosynthesis and functional role of cardiolipin, Prog. Lipid Res. 39 (2000) 257–288.

[21] M. Zhang, E. Mileykovskaya, W. Dowhan, Gluing the respiratory chain together. Cardiolipin is required for supercomplex formation in the inner mitochondrial membrane, J. Biol. Chem. 277 (2002) 43553–43556.

[22] C. Lange, J.H. Nett, B.L. Trumpower, C. Hunte, Specific roles of protein-phospholipid interactions in the yeast cytochrome bc1 complex structure, EMBO J. 20 (2001) 6591–6600.

[23] T.H. Haines, N.A. Dencher, Cardiolipin: a proton trap for oxidative phosphorylation, FEBS Lett. 528 (2002) 35–39.

[24] C. Hunte, H. Palsdottir, B.L. Trumpower, Protonmotive pathways and mechanisms in the cytochrome bc1 complex, FEBS Lett. 545 (2003) 39–46.

[25] S.R.N. Solmaz, C. Hunte, Structure of complex III with bound cytochrome c in reduced state and definition of a minimal core interface for electron transfer, J. Biol. Chem. 283 (2008) 17542–17549.

[26] S. Nichols-Smith, T. Kuhl, Electrostatic interactions between model mitochondrial membranes, Colloids Surf. B Biointerfaces 41 (2005) 121–127.

[27] M. Dahlberg, A. Marini, B. Mennucci, A. Maliniak, Quantum chemical modeling of the cardiolipin headgroup, J. Phys. Chem. A 114 (2010) 4375–4387.

[28] S. Pöyry, T. Róg, M. Karttunen, I. Vattulainen, Mitochondrial membranes with mono- and divalent salt: changes induced by salt ions on structure and dynamics, J. Phys. Chem. B 113 (2009) 15513–15521.

[29] M. Dahlberg, A. Maliniak, Molecular dynamics simulations of cardiolipin bilayers, J. Phys. Chem. B 112 (2008) 11655–11663.

[30] D. Aguayo, F.D. González-Nilo, C. Chipot, Insight into the Properties of Cardiolipin Containing Bilayers from Molecular Dynamics Simulations, Using a Hybrid All-Atom/United-Atom Force Field, J. Chem. Theory Comput. 8 (2012) 1765–1773.

[31] K. Kaszuba, P.A. Postila, O. Cramariuc, M. Sarewicz, A. Osyczka, I. Vattulainen, T. Róg, Parameterization of the prosthetic redox centers of the bacterial cytochrome bc1 complex for atomistic molecular dynamics simulations. *Submitted*.

[32] P.A. Postila, K. Kaszuba, M. Sarewicz, A. Osyczka, I. Vattulainen, T. Róg, Key role of water in proton transfer at the Qo-site of the cytochrome bc1 complex predicted by atomistic molecular dynamics simulations. *Submitted*.

[33] E.A. Berry, L.-S. Huang, L.K. Saechao, N.G. Pon, M. Valkova-Valchanova, F. Daldal, X-Ray Structure of Rhodobacter Capsulatus Cytochrome bc (1): Comparison with its Mitochondrial and Chloroplast Counterparts, Photosyn. Res. 81 (2004) 251–275.

[34] W. Humphrey, A. Dalke, K. Schulten, VMD: visual molecular dynamics, J. Mol. Graph. 14 (1996) 33-8, 27-8.

[35] T. Róg, H. Martinez-Seara, N. Munck, M. Oresic, M. Karttunen, I. Vattulainen, Role of cardiolipins in the inner mitochondrial membrane: insight gained through atom-scale simulations, J. Phys. Chem. B 113 (2009) 3413–3422.

[36] J.C. Phillips, R. Braun, W. Wang, J. Gumbart, E. Tajkhorshid, E. Villa, C. Chipot, R.D. Skeel, L. Kalé, K. Schulten, Scalable molecular dynamics with NAMD, J. Comput. Chem. 26 (2005) 1781–1802.

[37] A.D. Mackerell, M. Feig, C.L. Brooks, Extending the treatment of backbone energetics in protein force fields: limitations of gas-phase quantum mechanics in reproducing protein conformational distributions in molecular dynamics simulations, J. Comput. Chem. 25 (2004) 1400–1415.

[38] J. Taylor, N.E. Whiteford, G. Bradley, G.W. Watson, Validation of all-atom phosphatidylcholine lipid force fields in the tensionless NPT ensemble, Biochim. Biophys. Acta 1788 (2009) 638–649.

[39] K. Kaszuba, T. Róg, K. Bryl, I. Vattulainen, M. Karttunen, Molecular dynamics simulations reveal fundamental role of water as factor determining affinity of binding of beta-blocker nebivolol to beta(2)-adrenergic receptor, J. Phys. Chem. B 114 (2010) 8374–8386.

[40] U. Essmann, L. Perera, M.L. Berkowitz, T. Darden, H. Lee, L.G. Pedersen, A smooth particle mesh Ewald method, J. Chem. Phys. 103 (1995) 8577.

[41] J.V. Lehtonen, D.-J. Still, V.-V. Rantanen, J. Ekholm, D. Björklund, Z. Iftikhar, M. Huhtala, S. Repo, A. Jussila, J. Jaakkola, O. Pentikäinen, T. Nyrönen, T. Salminen, M. Gyllenberg, M.S. Johnson, BODIL: a molecular modeling environment for structure-function analysis and drug design, J. Comput. Aided Mol. Des. 18 (2004) 401–419.

[42] A. Aksimentiev, K. Schulten, Imaging alpha-hemolysin with molecular dynamics: ionic conductance, osmotic permeability, and the electrostatic potential map, Biophys. J. 88 (2005) 3745–3761.

[43] P.J. Kraulis, MOLSCRIPT: a program to produce both detailed and schematic plots of protein structures, J. Appl. Crystallogr. 24 (1991) 946–950.

[44] E.A. Merritt, M.E.P. Murphy, Raster3D Version 2.0. A program for photorealistic molecular graphics, Acta Crystallogr. D Biol. Crystallogr. 50 (1994) 869–873.

[45] H. Palsdottir, C. Hunte, Lipids in membrane protein structures, Biochim. Biophys. Acta 1666 (2004) 2–18.

[46] P.J. Crowley, E.A. Berry, T. Cromartie, F. Daldal, C.R.A. Godfrey, D.-W. Lee, J.E. Phillips, A. Taylor, R. Viner, The role of molecular modeling in the design of analogues of the fungicidal natural products crocacins A and D, Bioorg. Med. Chem. 16 (2008) 10345–10355.

[47] C. Hunte, Specific protein-lipid interactions in membrane proteins, Biochem. Soc. Trans. 33 (2005) 938–942.

Paper IV

S. Pöyry, A. Mark and I. Vattulainen. Cardiolipin protects charged membranes against the antimicrobial peptide aurein. Submitted to BBA Biomembranes (2012).

Cardiolipin protects charged membranes against the antimicrobial peptide aurein

Sanja Pöyry[1], Alan E. Mark[2] and Ilpo Vattulainen[1,3]

[1]*Department of Physics, Tampere University of Technology, Finland*

[2]*School of Chemistry and Molecular Biosciences,*

The University of Queensland, Australia

[3]*MEMPHYS-Center for Biomembrane Physics, University of Southern Denmark*

(Dated: September 6, 2012; E–mail: Ilpo.Vattulainen@tut.fi)

Abstract

Atomistic molecular dynamics simulation techniques have been used to investigate the interaction of the antimicrobial peptide aurein 1.2 with highly negatively charged membranes in order to shed light on a) the mechanism by which aurein 1.2 disrupts membranes and b) the factors that give rise to membrane selectivity. Aurein is positively charged and selective against membranes containing anionic lipids. In this work the effect of the presence of two alternative anionic lipids phosphatidylglycerol (PG) and cardiolipin (CL) were examined. We find that despite its anionic nature, CL may be protective against the disruptive effects of aurein 1.2. The unique double-lipid structure of CL appears to increase the structural integrity of the bilayer and help counteract the tendency of peptides to induce positive curvature. The high concentration of CL in many bacterial membranes may thus be an adaption to the presence of pore forming antimicrobial peptides.

INTRODUCTION

Whenever pathogens are exposed to antibiotic agents the development of resistance is always a possibility. Indeed, resistance to conventional antibiotic agents used clinically has become a global public-health problem. One class of antibiotic agent that has remained effective against bacteria on an evolutionary timescale and thus have the potential to be developed into a new class of therapeutics, are membrane disrupting antimicrobial peptides (1, 2). These relatively small peptides are found throughout the animal and plant kingdoms and are vital components of the defence systems of complex multicellular organisms (2).

Membrane disrupting antimicrobial peptides bind to the surface of microbial membranes and beyond a threshold concentration induce the formation of transmembrane pores or otherwise destabilize the membrane. While in general peptides that are able to span the bacterial membrane are believed to act by inserting into the membrane and forming pores, short peptides (less than 20 amino acids), assemble at the membrane surface without inserting into the bilayer. These peptides then lyse the membrane in a detergent-like manner. This is generally referred to as the carpet model (3). While this model is often invoked in order to account for the general features observed experimentally, the molecular details of how the binding of peptide leads to membrane disruption via the carpet mechanism have not been fully elucidated.

One proposal is that the peptides induce the formation of non-lamellar lipid phases (4). According to this model the peptides induce local changes in the phase of the lipids by altering either membrane packing, the distribution of lipids, or by neutralization of negative lipid charges leading to destabilization (4). An alternative proposal is that the disruption of the membrane results from the wedge-like insertion of the peptides into the bilayer interface (5).

Another aspect of membrane disrupting antimicrobial peptides that is poorly understood are the factors that give rise to membrane selectivity, specifically the ability to disrupt bacterial as opposed to mammalian membranes. Surface charge is clearly one factor. Most membrane disrupting antimicrobial peptides are cationic and bacterial membranes in general contain a high proportion of anionic lipids (6). However, the different charge alone is not, however, sufficient to explain the selectivity in all cases. For example, SMAP-28 (sheep myeloid antimicrobial peptide-28) is haemolytic towards human erythrocytes but not towards closely related sheep erythrocytes (7).

In addition to charge, a range of chemical and physical properties of the membranes such as their thickness, fluidity, bending modulus, and phase could in principle also contribute to selectiv-

ity. These will be affected by both the nature of the head group and the nature of the lipid tails which differ significantly between organisms. Differences in the length, degree of (un)saturation, and branching of the tails will affect for example the phase of the membrane and thus the ease with which the peptides might induce strain within the membrane. In addition, membranes are not homogeneous. The distribution of lipids within the membrane may vary, both within a given leaflet and between the two leaflets.

One hypothesis aiming to explain selectivity is based on matching the intrinsic curvature of the peptide and that of the membrane. In this model the location of residues that orientate and anchor the peptide to the membrane also play a role. Indeed, it has been shown in a previous simulation study that four antimicrobial peptides (aurein 1.2, citropin 1.1, maculatin 1.1, and caerin 1.1) were largely disordered when bound to a planar DMPC bilayer whereas the peptides adopted a more helical conformation when bound to a toroidal pore within a POPC bilayer, a region of high local positive curvature (8). This effect was most evident in the longer peptides maculatin and caerin with the shortest peptide aurein 1.2 being least affected.

The specific peptide considered in this study is aurein 1.2. Aurein 1.2 is one of a series of pore forming or membrane disrupting antimicrobial peptides found in the skin secretions of the Australian tree frog Litoria aurea (9). With only 13 amino acids and charge of +1e, aurein is the smallest amphibian peptide to show antibiotic and anticancer activity (10) (see Fig. 1). As aurein is too short to span a membrane it is generally considered to act via the carpet mechanism (11–13).

The interaction of aurein 1.2 with a wide range of zwitterionic and anionic bilayers have been examined (11, 12). Aurein is cationic and interacts selectively with anionic lipids (14, 15), such as phosphatidylglycerol (PG) and cardiolipin (CL), which are characteristic of both bacterial and cancer cells. For example the affinity of aurein for anionic PG lipids as opposed to neutral lipids has been demonstrated experimentally by Seto et al. (14) who used differential scanning calorimetry (DSC) to examine the effects of peptides on the thermotropic phase behavior of DMPC, DMPG, and DMPE membranes. In the same study Fourier transform infrared spectroscopy (FTIR) was used to probe the location of the peptides in membranes. It was shown that the peptides are unstructured in water but adopt an alpha-helical form when bound to membranes. The data suggests that aurein 1.2 most probably binds within the polar/apolar interfacial regions of bilayers (14).

A lower lysis threshold concentration of aurein 1.2 for DMPC/DMPG as opposed to DMPC was also observed with quartz crystal microbalance (QCM) (16), with the data obtained being consistent with the carpet model (17). Surface plasmon resonance spectroscopy (SPR) and solid-

state nuclear magnetic resonance (NMR) studies conducted in ref. (18) also supported the carpet mechanism, however, aurein appeared to interact with the membranes with little discrimination between neutral (DMPC) and anionic (DMPC/DMPG mixture) bilayers. Destruction of vesicles by aurein 1.2 was visualized by fluorescent microscopy in ref. (19), which also supported the carpet mechanism and indicated that a high concentration of aurein was needed to destroy the membrane.

Dual polarization interferometry (DPI) has also been used to analyze the aurein-induced destabilization of supported lipid bilayers (13). DPI is a technique that can be used to probe adsorbed layers of biomolecules on a sensor chip of a dual slab waveguide by analyzing the interference patterns produced by laser light (20, 21). The bilayers were comprised of DMPC, DMPE, DMPG, cholesterol and an *E. coli* lipid extract (13). Changes in membrane molecular ordering were observed with increasing peptide concentration. At first the changes were reversible (except for DMPE/DMPG) but eventually the presence of the peptide resulted in the removal of lipids, which would correspond to cell lysis. The rate of lipid loss in the case of DMPC/DMPG was nearly double that of DMPC. No loss of lipid was observed for when using DMPC/DMPG/cholesterol, DMPE/DMPC, and *E. coli* extract, which contains cardiolipins (13). The effect of aurein 1.2 on membrane order was also examined in (22).

The structure and membrane interactions of related peptides (aurein 2.2, aurein 2.3, and their variants) with POPC/POPG, CL/POPG, and POPE/POPG membranes have been studied by solution circular dichroism (CD) and ^{31}P NMR (23). It should be noted, however, that these peptides are somewhat longer compared to aurein 1.2 and have been suggested to disorder the bilayer head groups by forming toroidal pores or disordered pores (23), as opposed to the carpet mechanism suggested for aurein 1.2.

Membranes rich in cardiolipin seem to be more resistant to the effects of some antimicrobial peptides as compared to membranes containing other negatively charged lipids (24, 25). Cardiolipin is a vital component of membranes in which electron transport and phosphorylation are coupled, namely bacterial plasma membranes, chromatophores, chloroplasts, and mitochondria (26). Cardiolipin has a unique double lipid structure in which a total of four acyl chains and two negatively charged phosphate groups are connected by a central glycerol group. Considering its prevalence in mitochondria and various different eubacteria, it is likely that cardiolipin either developed at an early stage in evolution or it confers a significant selective advantage (27). Given the geometry of the CL molecule and its double lipid structure it has been proposed that CL leads to

a greater degree of cohesion in the interfacial region of CL containing membranes, which in turn would lead to an increase in the structural integrity of the bilayer (28). These properties might explain why cardiolipin-containing membranes appear to be more resistant to the effects of some antimicrobial peptides than are membranes containing other negatively charged lipids (24, 25, 28).

In this study the behaviour of aurein 1.2 in solution and when interacting with a range of strongly anionic membranes has been investigated . The primary aim was to shed light on the mechanism by which aurein 1.2 disrupts membranes at an atomic level. In particular, our goal was to examine the role that cardiolipin plays, if any, in maintaining the structure of the bilayer. A series of atomistic molecular dynamics simulations of different model membrane systems with varying amounts of peptide over a range of temperatures have been performed. Molecular dynamics simulations are a powerful approach for analysing membrane-peptide interactions in detail and have been previously used to provided insight into how other antimicrobial peptides lead to membrane disruption, see e. g. (29–31).

MODEL DESCRIPTION AND SIMULATION DETAILS

Aurein 1.2 has 13 residues. In this study the C-terminus of aurein 1.2 was assumed to be amidated leading a cationic peptide with a net charge of +1e (see Fig. 1). The parameters for aurein 1.2 were taken from the GROMOS96 53a7 force field (32). Aurein 1.2 was simulated both in water and in the presence of a bilayer comprised of a mixture of CL and PG.

Force field parameters for POPG were obtained by adapting the parameters from GROMOS96 53a6 parameters in (33) to GROMOS96 53a7 atom types (32). CL was built as a symmetric double PG with four oleic tails. The initial bilayer configurations were constructed with Packmol (34) and equilibrated for 56 ns. A highly anionic membrane composition was chosen so as to make an ideal target for the cationic peptides. The bilayers contained 25 mol% CL, meaning that 40 % of all lipid tails present in the membrane belong to CL. The rest of the bilayer comprised a racemic mixture of LPOPG and DPOPG. Na^+ counter ions described using the GROMOS96 53a6 force field parameters were included to neutralize the bilayer. The simple point charge model (SPC) was used to describe water (35).

In total 16 independent simulations were performed. These are grouped into 4 classes depending on the initial configuration used and simulation conditions (see Table I). The first class of simulations were performed to investigate the conformational preferences of an isolated aurein 1.2

molecule free in solution and when bound to a membrane. In simulations A1 the initial structure of the aurein 1.2 was that of an ideal alpha helix generated using PyMOL (36). In A1, which comprised of a set of 3 independent simulations with different starting velocities the peptide was placed in a rectangular periodic box filled with water. No counter ions were included. Each system was simulated for 100 ns. A2 comprised a set of 3 independent simulation simulations in which an aurein molecule was allowed to bind spontaneously to a bilayer comprised of 102-lipids, 26 CL and 76 PG. The 3 simulations were performed using different initial configurations for aurein. These configurations were generated by extracting alternative configuration of the peptide from the simulations performed in A1 and placing these in the water layer. This was done to ensure that position and orientation of the peptide with respect to the membrane varied. Each simulation was run for 100 ns. As in all membrane simulations presented here, Na^+ counter ions were included to neutralize the bilayer charge. No counter ions were included to neutralize the peptide charge in class A simulations.

The simulations in class B and C were performed to investigate the effect of multiple aurein 1.2 molecules binding simultaneously to a membrane consisting of 104 GL molecules and 304 PG molecules. This system was generated by replicating the membrane used in A2 in both dimensions in the plane of the membrane. In class B a total of 20 peptides initially placed in solution were allowed to associate spontaneously with either side of the membrane. In class C 10 peptides were allowed to interact with the membrane but these were restrained to bind only to one side of the membrane. Again the peptides were placed initially in the water phase. To restrict the binding of the peptides to one side of the membrane weak harmonic position restraints using a force constant of $100\,kJ\,mol^{-1}\mathrm{nm}^{-2}$ were applied to a layer of water molecules above the peptides preventing the peptides from diffusing toward and interacting with the periodic image of the membrane. It should be noted that the applied force is rather weak so it does not completely fix the water molecules in place but allows slow diffusion of the restrained waters. The restraints were removed approximately when all the peptides had bound to the bilayer surface. It should also be stressed that we did not use any position restraints on the peptides themselves. The simulations in classes B and C were performed at three different temperatures. Sufficient Cl^- and Na^+ counter ions were added to each system to neutralize the peptide and lipid charges, respectively. Consequently, the overall charge of the system was neutral.

The simulations in class D were performed to investigate the effect of increasing peptide concentration on the structure of the membrane. Initially, 10 aurein molecules were allowed to as-

sociate with the membrane and equilibrate for 20 ns (D1). Five additional aurein molecules were then added to the system (D2) and equilibrated for 55 ns. A further 5 aurein molecules were then added to obtain system D3 (30 peptides) and a further 10 to obtain system D4 (40 peptides). In each case the final configuration after equilibration of one system was used as the starting configuration for the next. Every time more peptides were added, their diffusion towards the periodic image of the membrane was prevented by applying position restraints to a thin layer of water molecules above the peptides, as described above. The restraints were removed approximately when the peptides were bound to the bilayer surface, meaning that for example during 110 ns to 160 ns (system D4) there are no position restraints in the system at all. Also, every time that more peptides and water were added, the number of water molecules to which the position restraints were applied was approximately the same. Consequently, the ratio of restrained to non-restrained components in the system actually becomes smaller with increasing peptide and water amount, before all position restraints are removed altogether. Moreover, it should again be stressed that we did not use any position restraints on the peptides themselves at any point. In these simulations the initial conformation of the peptide was non-helical. In addition the amount of water in the system was progressively increased from 70 to 100 water molecules per lipid in line with the increasing concentration of peptide. Again sufficient Cl^- and Na^+ counter ions were added to each system to neutralize the overall charge.

All simulations were performed using the GROMACS simulation package version 3.3.3, (37). The time step was 2 fs in single-peptide and 4 fs in other simulations, where we used dummy atoms for hydrogens, according to the scheme described in (38). Periodic boundary conditions and a minimum image convention were used in all three directions. The lengths of all covalent bonds were constrained using the LINCS algorithm (39). Lennard-Jones and electrostatic non-bonded interactions were described using a twin-range method. Interactions within the short-range cutoff of 0.8 nm were calculated every step whereas interactions within the longer range cutoff of 1.4 nm were updated every second time step together with the generation of the short range neighbour list. To correct for the truncation of interactions beyond the 1.4 nm long-range cutoff, a reaction field correction was applied (40). This approach has been used successfully in numerous simulations studies (see, e.g., (41)).

The temperature and pressure were held constant in all simulations using the weak-coupling method of Berendsen with time constants of 0.1 ps and 4 ps, for the temperature and pressure, respectively. The simulations of the isolated peptides in water were performed at a constant tem-

perature of 310 K. The simulations of the membrane systems were performed either at 298 K, 318 K or 338 K (see Table I). The temperatures of the solute and solvent were independently coupled to the temperature bath. A reference pressure of 1 bar was used. The pressure coupling was isotropic in the case of the isolated peptide in water but semi-isotropic in the case of the membrane systems.

Analysis

The secondary structure of the peptides was determined using the program DSSP (42). The average helicities were calculated as the number of amino acids in a peptide in alpha-helical conformation divided by the total number of amino acid residues in the peptide. The preference for certain peptide residues to interact with the membrane was examined by counting the number of each peptide residue within 0.3 nm of any lipid every nanosecond in the 10-aurein simulation in 298 K (system C1 in Table I). A program modified from GridMAT-MD (43) was used to calculate membrane thickness. The thickness was defined as the average distance between lipid head group phosphorus atoms in the opposing leaflets. Further details of the used analysis techniques are given below, where appropriate.

RESULTS

Aurein secondary structure

Aurein has been shown by NMR spectroscopy to adopt an amphipathic alpha-helical structure in a solution system containing 70 percent d_3-trifluoroethanol (v/v in water) (10). FTIR spectroscopy indicates that aurein 1.2 is unstructured in aqueous solution but adopts an alpha-helical structure when incorporated into a DMPC bilayer (14). As indicated by the CD results in (23), related peptides (aurein 2.2, aurein 2.3, and aurein 2.3-COOH) adopt close to 100% helical conformations at high peptide concentrations (peptide to lipid molar ratio up to 1:15) in POPC/POPG, POPE/POPG, and CL/POPG membranes. In contrast, at low peptide concentrations (peptide to lipid molar ratio 1:100) there were differences between the different lipid compositions. In POPC/POPG and POPE/POPG the peptides adopted ca. 64-74% and 60-73% helical structure, respectively. In CL/POPG, the helical content was somewhat lower, 34-54 % (23).

Three 100 ns simulations of a single aurein 1.2 molecule in water were performed (system A1 in Table I), starting from an ideal alpha helix. The secondary structure was highly dynamic with the peptide alternating between being completely unstructured to being partly helical multiple times during each of the simulations. The structure of a single aurein 1.2 molecule bound to membrane consisting of a mixture of CL and PG was then examined. Fig. 2 shows the average helicity of the single aurein molecule in one of the 3 simulations of system A2 (Table I). In this case the peptide bound spontaneously to the membrane within 4 ns and remained in bound to the membrane for the majority of the rest of the simulation. The peptide briefly returned to solution during the period between 60-80 ns. As can be seen from Fig. 2 the initial conformation of the peptide was non-helical but upon binding to the membrane the helicity became as high as 55 %. The helicity averaged close to 30 % for the period the peptide was bound to the membrane. The helicity of related peptides (aurein 2.2, aurein 2.3, and aurein 2.3-COOH) has been observed to be in the same range (34-54 %) when associated with a CL/POPG membrane at low peptide concentrations (peptide to lipid ratio 1:100, roughly the same as here)(23).

A similar helical percentage was also observed when multiple copies of aurein 1.2 were allowed to bind simultaneously to the membrane. Fig. 3 shows the average helicity during the 80 ns simulation of system C1 (see Table I). In C1 10 copies of aurein 1.2 were allowed to spontaneously interact with one side of a membrane. The initial conformation of the peptide was non-helical. After around 10-20 nanoseconds all the peptides had bound to the surface of the bilayer. As can be seen from Fig. 3 the average helicity of the peptides increases steadily as more peptides bind, reaching a plateau values of around 25-30 % after 20-30 ns. Experimentally, the helical content of related peptides (aurein 2.2, aurein 2.3, and aurein 2.3-COOH) has been observed to increase with increasing peptide:lipid ratio, up close to 100 % in high peptide concentration (23). This trend is not observed in this study, however, it should be noted that these peptides are somewhat longer compared to aurein 1.2, the lipid concentrations were somewhat different in the studies and the peptides studied in (23) have been suggested to disorder the bilayer with a different mechanism than aurein 1.2 (23).

Fig. 4 shows an Edmundson projection of aurein 1.2 in an alpha-helical conformation. As seen, in the helical conformation the peptide is amphipathic with well-defined hydrophilic and hydrophobic regions. Fig. 5, displays a snapshot of a partly helical aurein molecule on the membrane surface taken from one of the 3 simulations of system A2 in which the hydrophilic regions can be seen embedded within the membrane as commonly proposed for amphipathic peptides. This was,

however, not the only binding mode observed in the simulations. In fact in most configurations examined, the hydrophobic and hydrophilic residues were not aligned such that the peptide conformation was clearly amphipathic and, as noted above, in most configurations the peptides were only partly helical. The peptides do, nevertheless, show a marked increase in helicity on binding to the membrane in agreement with experiment (14).

Hydrogen bonding between the lipids and protein residues was defined by geometric criteria, using a cut-off distance of 3.25 Å between the donor and acceptor and a cut-off angle (acceptor-donor-hydrogen) of 30 degrees, using VMD (44). Of all hydrogen bonds found between protein and lipid residues during the simulation C1, 21 % were formed by lysine residues and 20 % by glysine residues. Other favoured residues were phenylalanine (15 % of all hydrogen bonds) and serine (11 %) and the terminal amine group (11 %). Of all hydrogen bonds, lipid hydroxyl oxygens were involved in 54 %, lipid phosphate oxygens in 30 %, and lipid ester oxygens in 17 %. After (approximately) all of the peptides had bound to the bilayer surface (after 20 ns), each peptide was bound to the lipids through 3.3 hydrogen bonds on average (averaged over time and number of peptides).

Membrane disruption due to aurein adsorption

Simulations of systems B1 to B3 involved the spontaneous interaction of 20 aurein 1.2 molecules interacting in an unrestricted manner with a membrane comprised of 104 CL and 304 PG lipids. In this case the peptides bound to both membrane leaflets and resulted in little if any disruption of the membrane irrespective of the temperature (data not shown). Antimicrobial peptides act, however, by binding to the outside of the cell and thus accumulate only on one side of the membrane. Fig. 6 shows snapshots from simulations C1, C2 and C3 after either 80 or 100ns. Class C correspond to a system containing 10 aurein 1.2 molecules bound to one side of the membrane simulated at three different temperatures (see block C in Table I). Disruption of the membrane is very clear. In each case once the peptides had bound to the surface of the bilayer they neither moved back into the water phase nor into to the core of the membrane. In addition, the peptides did not show a clear preference between CL and PG. What is clear from Fig. 6 is that 10 copies of aurein 1.2 lead to a major disruption of the membrane especially at higher temperature. These findings are in general agreement with the available experimental data (13, 14, 17, 18). For example, Lee et al (13) studied the effect of aurein 1.2 on a range of supported lipid bilayers using

dual polarization interferometry (DPI) (20, 21). The extent of the changes in birefringence as a function of bound peptide suggested that aurein 1.2 bound primarily to the surface of the membrane surface without inserting. Visualization of the destruction of vesicles by aurein 1.2 using fluorescent microscopy also suggests that the peptides would be primarilay associated with the interfacial region of the bilayer (19). SPR and NMR spectroscopy measurements are also consistent aurein interacting primarily with the surface of the membrane (18).

Increasing asymmetric binding of aureins at the membrane induces increasing curvature

As is evident from Fig. 6 aurein 1.2 induced strong curvature of the membrane at peptide to lipid ratios of approximately 1:40 especially at 338 K when the membrane in in the fluid phase. The effect at 298 K was, however, less well pronounced. A series of simulations were thus performed in which the concentration of aurein was gradually increased. Fig. 7 shows how the degree of curvature depends on the peptide to lipid ratio at 298 K. As the peptide to lipid ratio was increased from approximately 1:40 (D1) to approximately 1:10 (D4) curvature of the membrane increased systematically. The degree of curvature was similar along all directions in the plane of the membrane. However, while high concentrations of the peptide induced a very high degree of curvature within the membrane, the membrane bilayer itself remained intact. Note, the induction of curvature was reversible. When the amount of bound peptide was progressively reduced the membrane became progressively flatter (data not shown).

The changes in bilayer thickness upon the addition of peptide were surprisingly small. The thickness was 3.4 nm in the absence of peptide. This decreased to 3.0 nm at a peptide to lipid ratio of approximately 1:10, suggesting increased disorder in the bilayer. Fig. 8 shows water molecules surrounding the bilayer at the end of the simulation. Despite the high curvature, no clear leakage of water molecules through the membrane was observed. There was a marked reduction in the value of the order parameters calculated for carbons in the acyl chains of all of the lipids (data not shown). However, this decrease is likely to primarily reflects an increase in membrane curvature as opposed to an increase in the local disorder. Nevertheless a decrease on the order parameters is in line with the findings in (13), where changes in molecular ordering as a function of membrane-bound peptide mass where proposed based on dual polarization interferometry (DPI) (20), and with (22) where ^{2}H NMR suggested that the addition of aurein 1.2 increased disorder within the membrane.

The change in peptide helicity as a function of peptide concentration and thus membrane curvature was also examined. The average percentage helicity of the initial 10 peptides was monitored during the combined 160 ns of simulation corresponding to D1, D2 D3 and D4 (see Fig. 9. As can be seen if one compares Fig. 9 to Fig. 3, the degree of helicity does not change significantly with either increasing peptide concentration or membrane curvature. Note, the first 20 nanoseconds of the two figures are identical as they correspond to the same simulation. As noted earlier, the helical content of related peptides (aurein 2.2, aurein 2.3, and aurein 2.3-COOH) has been observed experimentally to increase with increasing peptide:lipid ratio, up close to 100 % in high peptide concentration (23). Our simulations do not produce a similar trend. This might be due to these peptides being somewhat longer compared to aurein 1.2, they have indeed been suggested to disorder the bilayer with a different mechanism than aurein 1.2 (23). Also the lipid concentrations were somewhat different in the two studies.

A critical question is the extent to which the peptide to lipid ratios and the associated induction of curvature used in the simulations are experimentally relevant. Comparing the peptide to lipid ratios used in the simulations to those used experimentally is problematic as in many experimental studies only the concentration of peptide in water is given, not the proportion of peptide bound to the membrane. In addition it is evident from the simulations that the peptides bind strongly to the surface of the membrane and below the level of complete saturation there will be very little peptide remaining in the water phase. Nevertheless, the work of Lee et al (13) suggested that the lysis of DMPC/DMPG membrane could be achieved with an aurein:lipid ratio of 1:9.8 similar to that achieved in system D4. However, they found no evidence of the lysis of an *E. coli* membrane using similar aurein concentrations a difference that was attributed to the presence of cardiolipins (13).

DISCUSSION AND CONCLUDING REMARKS

Because of their potential as future antibiotics, antimicrobial peptides have attracted much interest in recent years. Despite this the precise molecular details by which antimicrobial peptides disrupt membranes and which give rise to cell specificity remain unclear. In this work atomistic molecular dynamics simulations have been used to study the interaction of one of the smallest active antimicrobial peptides, aurein 1.2 with a highly anionic membrane comprised of two anionic lipid species, PG and CL.

At the concentrations used in this study with a maximum peptide to lipid ratio of 1:10 aurein 1.2 was not able to destroy the bilayer structure within 160 ns. Instead, aurein 1.2 was found to induce a very high degree of membrane curvature. The failure of aurein 1.2 to completely disrupt the membrane under the conditions examined may seem surprising. It might be simply due to either the peptide concentration or the timescale examined being insufficient. Experimentally a peptide to lipid ratio of 1:10 is sufficient to lead to the destruction of bilayers consisting of DMPC and DMPG. It was, however, insufficient to lead to the disruption of bilayers containing CL.

A combination of two factors could explain how aurein 1.2 might induce high curvature but not lead to the destruction of the membrane in this case. The first is due to the properties of aurein 1.2 itself and the second due to the properties of cardiolipin. In a previous simulation study (8) aurein 1.2 and three other antimicrobial peptides were observed to lose helical structure when bound to a planar DMPC membrane. However, the peptides were able to become fully helical when bound to a toroidal pore formed in a POPC membrane, that is a region of a membrane with high positive curvature. It was concluded that the peptides would stabilize membrane structures with a curvature that matched the intrinsic curvature of the peptides. It was suggested that aurein 1.2 would act via a detergent-like mechanism as it can induce high local but not long-range curvature (8).

Cardiolipins have a large hydrocarbon volume but small head group. Thus CL promotes the formation of inverted hexagonal phases when neutralized by divalent cations, such as Ca^{2+} and Mg^{2+} (26). Moreover, it has been shown that CL microdomains form regions of high intrinsic negative curvature (45). Fig. 10 shows the distribution of cardiolipin molecules in the highly curved membranes obtained in this study. From Fig. 10 it can be seen that CL has accumulated in region of high negative curvature (circled). The concentration of CL in this region is nearly 40 % as compared to the overall concentration of 25 %. Charge neutralization alone, however, could not fully explain the curvature induced. The peptides are monovalent and before the addition of the 40 aurein 1.2 molecules the bilayer was stable despite the presence of a sufficient number of Na^{+} counterions to ensure the neutrality of the system.

The physical characteristics of pure cardiolipin bilayers can largely be explained by the relative rigidity and limited mobility of the head group which results from the binding of both of the phosphate groups to the same glycerol (28). It has been proposed that this impairs the capacity of the phosphates to participate in intermolecular interactions with other phosphate groups, diminishing the shielding of the two negative charges (28). As a consequence, the phosphate groups interact more strongly with water and any counter ions (28). Together with the geometry of the

CL molecule, this has been proposed to lead to a high degree of cohesion within the interfacial region of CL membranes, enhancing the structural integrity of the bilayer (28). This could explain why some organisms increase the CL content of their membranes in case of resource depletion and halophilic stress (28). In addition, this could explain why membranes containing CL are more resistant to the effects of some antimicrobial peptides than are membranes containing other negatively charged lipids (24), (13).

The antimicrobial peptide magainin is believed to act by imposing positive curvature strain (24) and thus its effects on a membrane could be diminished by the presence of lipids, such as CL, that induce negative curvature. Our results suggest that aurein 1.2 also induces positive curvature, and consequently the presence of CL would likely inhibit its action. This hypothesis is also supported by the observations in the simulations that on average aurein 1.2 adopted a conformation that was only partly helical despite regions of high curvature. In fact almost no aurein 1.2 molecules were found in those regions that had the highest positive curvature. This is likely due to these regions having the smallest lipid surface charge density. Thus there is a competition between the binding of aurein to regions of high positive curvature but low charge density or high charge density but negative curvature..

In this study atom-scale molecular dynamics simulations of several model systems have been used to examine the interaction of the antimicrobial peptide aurein 1.2 with PG-CL membranes. We find that at peptide to lipid ratios of up to 1:10 the aurein 1.2 was not able to completely destroy the structure of the membrane despite inducing high positive curvature. It is suggested that this is due to the high proportion of cardiolipin molecules in the membrane. Overall the work is in broad agreement with a range of experimental studies which suggest that the presence of CL provides protection against antimicrobial peptides compared to other negatively charged lipids (24). Many organisms increase the CL content of their membranes during periods of resource depletion and/or halophilic stress (28). As bacteria also release membrane disrupting antimicrobial peptides when starved for resources this increase in CL might represent and evolutionary adaption to the presence of antimicrobial peptides.

Acknowledgements. We would like to thank R. Chen and D. Poger for helpful discussions during this work. The work was supported by the FICS graduate school, the Finnish Cultural Foundation, European Research Council (CROWDED-PRO-LIPIDS), and Vilho, Yrjo and Kalle Väisalä Foundation. The computational resources were provided by the Australian National Facil-

ity (NCI), the HorseShoe supercluster computing facility at the University of Southern Denmark, and CSC – IT Centre for Science Ltd (Espoo, Finland).

1. A. Giuliani, G. Pirri, S. F. Nicoletto, Antimicrobial peptides: an overview of a promising class of therapeutics, Cent. Eur. J. Biol. 2 (2007) 1–33.
2. M. Zasloff, Antimicrobial peptides of multicellular organisms, Nature 415 (2002) 389–395.
3. Y. Pouny, D. Rapaport, A. Mor, P. Nicolas, Y. Shai, Interaction of antimicrobial dermaseptin and its fluorescently labeled analogues with phospholipid membranes, Biochemistry 31 (1992) 12416–12423.
4. E. F. Haney, S. Nathoo, H. J. Vogel, E. J. Prenner, Induction of non-lamellar lipid phases by antimicrobial peptides: a potential link to mode of action, Chemistry and Physics of Lipids 163 (2010) 82–93.
5. B. Bechinger, Rationalizing the membrane interactions of cationic amphipathic antimicrobial peptides by their molecular shape, Curr. Opin. Colloid Interface Sci. 14 (2009) 349–355.
6. R. E. W. Hancock, R. Lehrer, Cationic peptides: a new source of antibiotics, Trends in Biotechnology 16 (1998) 82–88.
7. R. M. Dawson, C. Q. Liu, Cathelicidin peptide smap-29: Comprehensive review of its properties and potential as a novel class of antibiotics, Drug Dev. Res. 70 (2009) 481–498.
8. R. Chen, A. E. Mark, The effect of membrane curvature on the conformation of antimicrobial peptides: implications for binding and the mechanism of action, Eur. Biophys. J. 40 (2011) 545–553.
9. M. A. Apponyi, T. L. Pukala, C. S. Brinkworth, V. M. Maselli, J. H. Bowie, M. J. Tyler, G. W. Booker, J. C. Wallace, J. A. Carver, F. Separovic, J. Doyle, L. E. Llewellyn, Host-defence peptides of australian anurans: structure, mechanism of action and evolutionary significance, Peptides 25 (2004) 1035–1054.
10. T. Rozek, K. L. Wegener, J. H. Bowie, I. N. Olver, J. A. Carver, J. C. Wallace, M. J. Tyler, The antibiotic and anticancer active aurein peptides from the australian bell frogs litoria aurea and litoria raniformis, Eur. Biophys. J. 267 (2000) 5330–5341.
11. M. P. Boland, F. Separovic, Membrane interactions of antimicrobial peptides from australian tree frogs, Biochim. Biophys. Acta 1758 (2006) 1178–1183.
12. D. I. Fernandez, J. D. Gehman, F. Separovic, Membrane interactions of antimicrobial peptides from australian frogs, Biochim. Biophys. Acta 1788 (2009) 1630–1638.
13. T. Lee, C. Heng, M. J. Swann, J. D. Gehman, F. Separovic, M. Aguilar, Real-time quantitative analysis of lipid disordering by aurein 1.2 during membrane adsorption, destabilisation and lysis, Biochim.

Biophys. Acta 1798 (2010) 1977–1986.

14. G. W. Seto, S. Marwaha, D. M. Kobewka, R. N. Lewis, F. Separovic, R. N. McElhaney, Interactions of the australian tree frog antimicrobial peptides aurein 1.2, citropin 1.1 and maculatin 1.1 with lipid model membranes: Differential scanning calorimetric and fourier transform infrared spectroscopic studies, Biochim. Biophys. Acta 1768 (2007) 2787–2800.
15. S. R. Dennison, F. Harris, D. A. Phoenix, The interactions of aurein 1.2 with cancer cell membranes, Biophys. Chem. 127 (2007) 78–83.
16. K. A. Marx, Quartz crystal microbalance: a useful tool for studying thin polymer films and complex biomolecular systems at the solution-surface interface, Biomacromolecules 4 (2003) 1099–120.
17. A. Mechler, S. Praporski, K. Atmuri, M. Boland, F. Separovic, L. L. Martin, Specific and selective peptide-membrane interactions revealed using quartz crystal microbalance, Biophys. J. 93 (2007) 3907–3916.
18. J. D. Gehman, F. Luc, K. Hall, T.-H. Lee, M. P. Boland, T. L. Pukala, J. H. Bowie, M.-I. Aguilar, F. Separovic, Effect of antimicrobial peptides from australian tree frogs on anionic phospholipid membranes, Biochemistry 47 (2008) 8557–8565.
19. E. E. Ambroggio, F. Separovic, J. H. Bowie, G. D. Fidelio, L. A. Bagatolli, Direct visualization of membrane leakage induced by the antibiotic peptides: Maculatin, citropin, and aurein, Biophys. J. 89 (2005) 1874–1881.
20. M. J. Swann, L. L. Peel, S. Carrington, N. J. Freeman, Dual-polarization interferometry: An analytical technique to measure changes in protein structure in real time, to determine the stoichiometry of binding events, and to differentiate between specific and nonspecific interactions.
21. C. J. Terry, J. F. Popplewell, M. J. Swann, N. J. Freeman, D. G. Fernig, Characterisation of membrane mimetics on a dual polarisation interferometer, Biosensors and Bioelectronics 22 (5) (2006) 627 – 632.
22. I. Marcotte, K. L. Wegener, Y.-H. Lam, B. C. S. Chia, M. R. R. de Planque, J. H. Bowie, M. Auger, F. Separovic, Interaction of antimicrobial peptides from australian amphibians with lipid membranes, Chem. Phys. Lipids 122 (2003) 107–120.
23. J. T. Cheng, J. D. Hale, M. Elliott, R. E. Hancock, S. K. Straus, The importance of bacterial membrane composition in the structure and function of aurein 2.2 and selected variants, Biochim. Biophys. Acta 1808 (2011) 622–633.
24. K. Matsuzaki, K. Sugishita, N. Ishibe, M. Ueha, S. Nakata, K. Miyajima, R. M. Epand, Relationship of membrane curvature to the formation of pores by magainin 2, Biochemistry 37 (1998) 11856–11863.

25. C. Giffard, S. Ladha, A. Mackie, D. Clark, D. Sanders, Interaction of nisin with planar lipid bilayers monitored by fluorescence recovery after photobleaching, The Journal of Membrane Biology 151 (1996) 293–300.
26. F. L. Hoch, Cardiolipins and biomembrane function, Biochim. Biophys. Acta 1113 (1992) 71–133.
27. D. R. M. Schlame, M. L. Greenberg, The biosynthesis and functional role of cardiolipin, Prog. Lipid Res. 39 (2000) 257–288.
28. R. N. A. H. Lewis, D. Zweytick, G. Pabst, K. Lohner, R. N. McElhaney, Calorimetric, x-ray diffraction, and spectroscopic studies of the thermotropic phase behavior and organization of tetramyristoyl cardiolipin membranes, Biophys. J. 92 (2007) 3166–3177.
29. A. A. Gurtovenko, J. Anwar, I. Vattulainen, Defect-mediated trafficking across cell membranes: Insights from in silico modeling, Chemical Reviews 110 (2010) 6077–6103.
30. H. Leontiadou, A. E. Mark, S. J. Marrink, Antimicrobial peptides in action, J. Am. Chem. Soc. 128 (2006) 12156–61.
31. P. L. Rocca, P. C. Biggin, P. Tieleman, M. S. P. Sansom, Simulation studies of the interaction of antimicrobial peptides and lipid bilayers, Biochim. Biophys. Acta 1462 (1999) 185–200.
32. N. S. A. P. E. A. C. S. R. M. W. A. E. M. W. F. van Gunsteren, Definition and testing of the gromos force-field versions 54a7 and 54b7, Eur. Biophys. J. 40 (2011) 843–856.
33. A. Kukol, Lipid models for united-atom molecular dynamics simulations of proteins, J. Chem. Theo. Comp. 5 (2009) 615–626.
34. L. Martinez, R. Andrade, E. G. Birgin, J. M. Martnez, A package for building initial configurations for molecular dynamics simulations, J. Comp. Chem. 30 (2009) 2157–2164.
35. B. Pullman (Ed.), In Intermolecular Forces, Reidl, Dordrecht, 1981.
36. Schrödinger, LLC, The PyMOL molecular graphics system, version 1.3r1 (August 2010).
37. D. van der Spoel, E. Lindahl, B. Hess, G. Groenhof, A. E. Mark, H. J. C. Berendsen, Gromacs: Fast, flexible, and free, J. Comp. Chem. 26 (2005) 1701–1718.
38. K. A. Feenstra, B. Hess, H. J. C. Berendsen, Improving efficiency of large time-scale molecular dynamics simulations of hydrogen-rich systems, J. Comput. Chem. 20 (1999) 786–798.
39. B. Hess, H. Bekker, H. J. C. Berendsen, J. G. E. M. Fraaije, Lincs: A linear constraint solver for molecular simulations, J. Comp. Chem. 18 (1997) 1463–1472.
40. I. G. Tironi, R. Sperb, P. E. Smith, W. F. van Gunsteren, A generalized reaction field method for molecular dynamics simulations, J. Phys. Chem. Phys. 102 (1995) 5451.

41. P. Niemela, S. Ollila, M. T. Hyvonen, M. Karttunen, I. Vattulainen, Assessing the nature of lipid raft membranes, PLoS Comput. Biol. 3 (2007) 304–312.

42. W. Kabsch, C. Sander, Dictionary of protein secondary structure: pattern recognition of hydrogen-bonded and geometrical features, Biopolymers 22 (1983) 2577–2637.

43. W. J. Allen, J. A. Lemkul, , D. R. Bevan, Gridmat-md: A grid-based membrane analysis tool for use with molecular dynamics, J. Comput. Chem. 30 (2009) 1952–1958.

44. W. Humphrey, A. Dalke, K. Schulten, Vmd - visual molecular dynamics, J. Molec. Graphics 14.1 (1996) 33–38.

45. L. D. Renner, D. B. Weibel, Cardiolipin microdomains localize to negatively curved regions of escherichia coli membranes, Proc. Natl. Acad. Sci. U.S.A. 108 (2011) 6264–6269.

TABLE I:

Label	No. of simulations	No. of peptides	No. of lipids	No. of waters	Time (ns)	Temperature (K)	Starting structure of aurein
A1	3	1	-	1700	100	310	α-helical
A2	3	1	26 CL, 76 PG	6500	100	298	partly helical
B1	1	20	104 CL, 304 PG	24000	20	298	non-helical
B2	1	20	104 CL, 304 PG	24000	20	318	non-helical
B3	1	20	104 CL, 304 PG	24000	20	338	non-helical
C1	1	10	104 CL, 304 PG	28200	80	298	non-helical
C2	1	10	104 CL, 304 PG	28200	80	318	non-helical
C3	1	10	104 CL, 304 PG	28200	100	338	non-helical
D1	1	10	104 CL, 304 PG	28200	0-20	298	non-helical
D2	1	15	104 CL, 304 PG	36200	20-75	298	non-helical
D3	1	30	104 CL, 304 PG	46200	75-100	298	non-helical
D4	1	40	104 CL, 304 PG	51400	100-160	298	non-helical

TABLE II: Simulations performed in this work. The numbers of water molecules are rounded to the closest hundred.

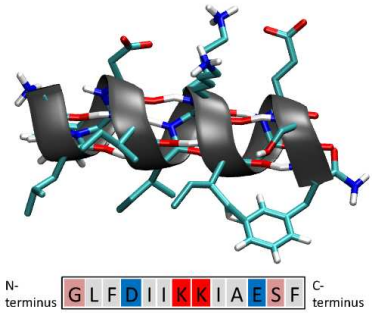

FIG. 1

Primary linear sequence (below) and secondary (top) representations of aurein. Aurein 1.2 is a cationic peptide having 13 residues, with the positive lysine residues at positions 7-8 (shown in red). Negative residues are shown in blue, polar in light red, and hydrophobic in grey. The C-terminus is amidated. This figure and all simulation snapshots in this work have been prepared using VMD (44).

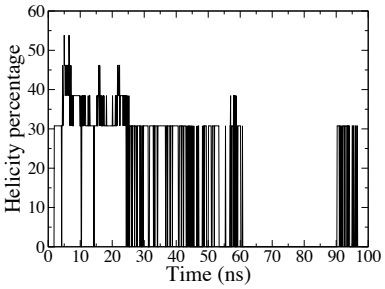

FIG. 2

Helicity percentage of aurein in a single peptide simulation with a membrane (system A2). Aurein binds to the membrane surface around 4 ns. During approximately 60-80ns, the peptide is more loosely bound than during the rest of the simulation.

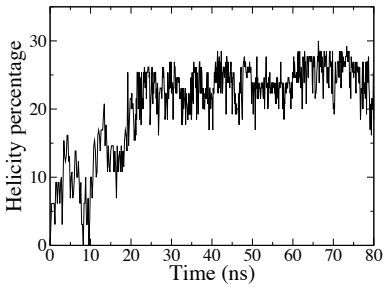

FIG. 3

Helicity percentage of aurein in the 298 K simulation of 10 aureins with a membrane (system C1). Aureins bind to the membrane surface during the first 10-20 nanoseconds.

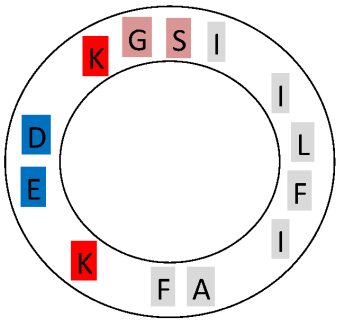

FIG. 4

Helical wheel representation of aurein.

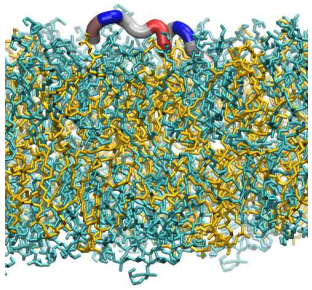

FIG. 5: A snapshot of one aurein molecule on the bilayer surface in system A2. Positive protein residues are shown in red, negative in blue, polar in light red, and hydrophobic in grey. All lipid atoms are shown without any special highlighting for head groups etc.

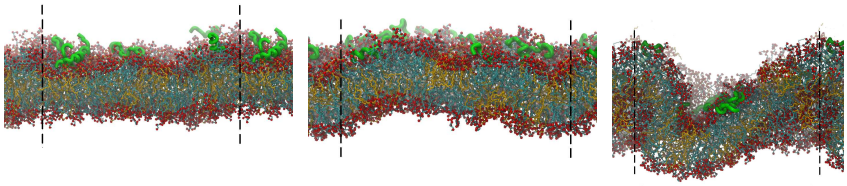

FIG. 6: 10 aureins restricted to one side of the bilayer (systems C1-C3) at 298, 318, and 338 K, from left to right. Dashed lines mark the borders of the periodic box. Peptides are shown in green, CL in orange, PG in cyan, and lipid oxygens in red. Water and ions are not shown for clarity.

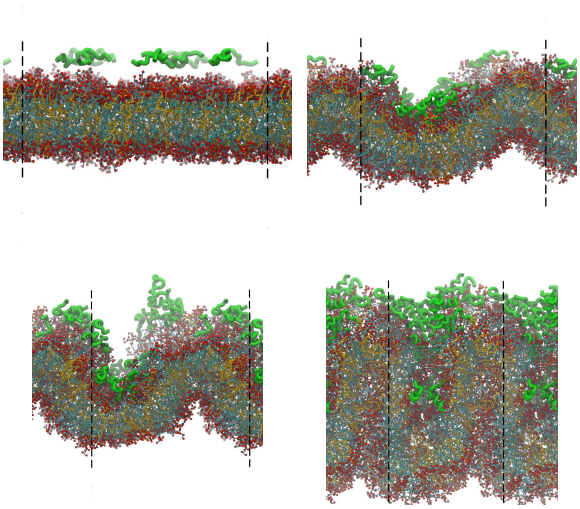

FIG. 7: The effect of increasing peptide concentration on the bilayer. Snaphots show the system D1 (10 aureins), D2 (15 aureins), D3 (30 aureins), and D4 (40 aureins), in normal reading order. In Table I these stand for simulation times 0 ns (D1), 50 ns (D2), 100 ns (D3), and 160 ns (D4). Dashed lines mark the borders of the periodic box. Peptides are colored green, CL orange, PG cyan, and lipid oxygens red. Water and ions are not shown for clarity.

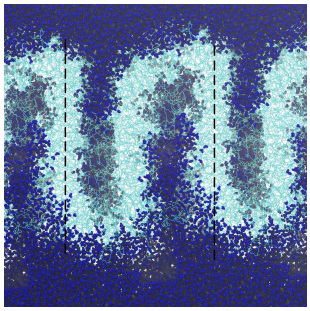

FIG. 8

A snapshot of water surrounding the membrane at 160 ns (system D4). Water is shown in blue and lipids in cyan. Peptides and ions are not shown. Dashed lines mark the borders of the periodic box.

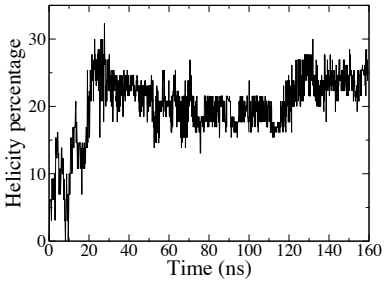

FIG. 9

Helicity percentage as a function of time for the first 10 aureins added into the system D1 at 0 ns. Additional aurein molecules were added to the water phase at 20 ns, 75 ns, and 100 ns (systems D2-D4, see Table I). The first aureins bind to the membrane surface during the first 10-20 nanoseconds, and as the number of aureins increases, the bilayer curvature increases dramatically during the rest of the simulation (see Fig. 7.

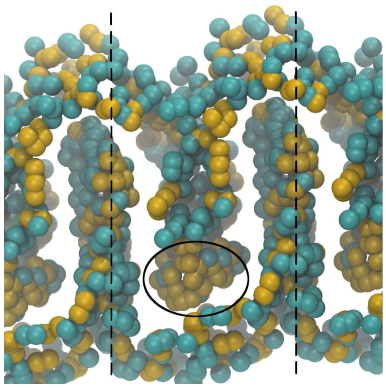

FIG. 10

A snapshot of the phosphorus atoms at 160 ns (system D4). CL atoms are shown in orange and PG atoms in cyan. Note the distribution of CL atoms between areas of different curvature, especially in the circled region of high negative curvature. The difference in membrane integrity between the upper leaflet where the peptides are bound and the lower one without peptides is also clearly visible. Dashed lines mark the borders of the periodic box.

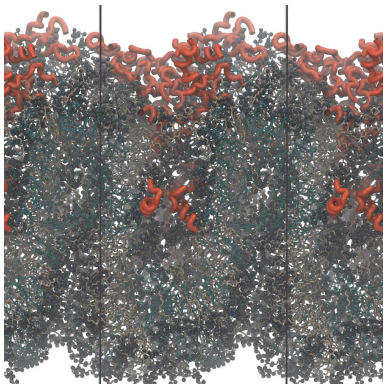

FIG. 11

Table of Contents graphic.

Tampereen teknillinen yliopisto
PL 527
33101 Tampere

Tampere University of Technology
P.O.B. 527
FI-33101 Tampere, Finland

ISBN 978-952-15-3006-7
ISSN 1459-2045